ANALYSIS OF KOCH FRACTAL ANTENNAS

A THESIS SUBMITTED TO
THE GRADUATE SCHOOL OF NATURAL AND APPLIED SCIENCES
OF
MIDDLE EAST TECHNICAL UNIVERSITY

BY

ÜMİT İRGİN

IN PARTIAL FULFILLMENT OF THE REQUIREMENTS
FOR
THE DEGREE OF MASTER OF SCIENCE
IN
ELECTRICAL AND ELECTRONICS ENGINEERING

JUNE 2009

Approval of the thesis:

ANALYSIS OF KOCH FRACTAL ANTENNA

submitted by **ÜMİT İRGİN** in partial fulfillment of the requirements for the degree of **Master of Science in Electrical and Electronics Engineering Department, Middle East Technical University** by,

Prof. Dr. Canan Özgen _____
Dean, Graduate School of **Natural and Applied Sciences**

Prof. Dr. İsmet Erkmen _____
Head of Department, **Electrical and Electronics Engineering**

Prof. Dr. M. Tuncay Birand
Supervisor, **Electrical and Electronics Engineering Dept., METU** _____

Examining Committee Members:

Prof. Dr. Altunkan Hızal _____
Electrical and Electronics Engineering Dept., METU

Prof. Dr. M. Tuncay Birand _____
Electrical and Electronics Engineering Dept., METU

Prof. Dr. Gülbin Dural _____
Electrical and Electronics Engineering Dept., METU

Assist. Prof. Dr. Lale Alatan _____
Electrical and Electronics Engineering Dept., METU

Gökhun Selçuk _____
HC SEDTMM, ASELSAN A.Ş.

Date: **23.06.2009**

I hereby declare that all information in this document has been obtained and presented in accordance with academic rules and ethical conduct. I also declare that, as required by these rules and conduct, I have fully cited and referenced all material and results that are not original to this work.

Name, Surname: Ümit İRGİN

Signature **:**

ABSTRACT

ANALYSIS OF KOCH FRACTAL ANTENNAS

İrgin, Ümit

M.Sc., Department of Electrical and Electronics Engineering

Supervisor: Prof. Dr. M. Tuncay Birand

June 2009, 89 pages

Fractal is a recursively-generated object describing a family of complex shapes that possess an inherent self-similarity in their geometrical structure. When used in antenna engineering, fractal geometries provide multi-band characteristics and lowering resonance frequencies by enhancing the space filling property. Moreover, utilizing fractal arrays, controlling side lobe-levels and radiation patterns can be realized.

In this thesis, the performance of Koch curve as antenna is investigated. Since fractals are complex shapes, there is no well–established for mathematical formulation to obtain the radiation properties and frequency response of Koch Curve antennas directly. The Koch curve antennas became famous since they exhibit better frequency response than their Euclidean counterparts. The effect of the parameters of Koch geometry to antenna performance is studied in this thesis. Moreover, modified Koch geometries are generated to obtain the relation between fractal properties and antenna radiation and frequency characteristics.

Keywords: Fractal Antennas, Self Similarity, Space Filling Antennas, Koch Curve, Modified Koch Antenna,

ÖZ

KOCH FRAKTAL ANTENLERİN ANALİZİ

İrgin, Ümit
Yüksek Lisans, Elektrik ve Elektronik Mühendisliği Bölümü
Tez Yöneticisi: Prof. Dr. M. Tuncay Birand

Haziran 2009, 89 sayfa

Fraktal kendini yineleyen bir obje olup kendi geometrisinde öz benzerliğe sahip bütün complex şekil ailelerini tanımlar. Fraktallar, anten mühendisliğinde kullanıldığında, çoklu bantlı karakter ve uzay kaplayıcılığı arttırarak resonans frekanslarını daha aşağılara çekebilme özellikleri sağlar. Ayrıca, fraktal dizileri kullanılarak, yan lopların seviyesinin ve ışıma örüntüsünün kontrolü gerçekleştirilebilir.

Bu tezde, Koch Eğrisi geometrisinin anten olarak kullanım performansı incelenmektedir. Fraktallar, kompleks yapılar olduklarından, Koch Eğrisi antenlerinin ışıma özellikleri ve frekans tepkilerini direkt olarak veren köklü bir matematiksel bir formül bulınmamaktadır. Koch Eğrisi antenleri Öklid geometrisinden türemiş muadillerine göre daha iyi freakans tepkisi gösterdikleri için ün kazanmışalrdır. Koch geometrisinin parametrelerinin anten performansına olan etki incelenmektedir bu tezde. Ayrıca, fraktal özellikleri ile anten ışıma ve frekans tepkilerinin arasındaki ilişkiyi detaylı incelemek için tadil edilmiş Koch geometrili antenler oluşturulmuştur.

Anahtar Kelimeler: Fraktal Antenler, Öz Benzerlik, Uzay Kaplayan (dolduran) Antenler, Koch Eğrisi, Tadil edilmiş Koch Anten

To My Family

ACKNOWLEDGEMENTS

I would like to thank Prof. Dr. M. Tuncay BİRAND for his valuable supervision, support and tolerance throughout the development and improvement of this thesis.

I am grateful to Ercan POLAT, Mehmet ÖNDER, M. Erim İNAL, Nihan GÖKALP, Gökhan ÜÇÜNCÜ, Can Barış TOP and Erdinç ERÇİL for their contribution for the improvement of this thesis and their support throughout the measurements performed in this thesis.

I would like to extend my special appreciation and gratitude to my family for their encouragement and understanding of my spending lots of time on this work.

I am also grateful to Aselsan Electronics Industries Inc. for the resources and facilities that I have used throughout the thesis.

I would also like to thank Turkish Scientific and Technological Research Council (TÜBİTAK) for their financial assistance during my graduate study.

Thanks a lot to all my friends for their great encouragement and their valuable help to accomplish this work

TABLE OF CONTENTS

LIST OF TABLES

LIST OF FIGURES

CHAPTER 1

INTRODUCTION

The cellular phones first appeared in 1970s. In first generation analog technology was used with Frequency Division Multiple Access (FDMA), which would only transmit voice, even with the lack of the security. In next generation, with the advances in wireless technology, digital techniques, (Time Division Multiple Access (TDMA) and Code Division Multiple Access (CDMA)) took part in communication, enhancing sending a low rate data as well as voice. In 3G, it is planned that over than 2 Mbps rate capacity can be enhanced transmitting video in addition to voice in the expense of using multiple bands.

In new era of communications, in 3G wireless communication systems, data, voice, and video must be transmitted; on the other hand the device is to be designed low profile. As a result, the antenna used in this system must be low profile and small sized. These requirements indicate using electrically small but efficient antennas and antennas providing multiband frequency operation to realize 3G wireless communication.

Studies on fractal shaped antennas showed that the fractal geometries succeeded in improving antenna radiation and frequency response characteristics. Utilizing geometries like Koch Curve, Hilbert Curve, Minkowski Loop and Koch Snowflake overcome the performance limited small antennas. The small antennas tend to posses low radiation resistance and highly reactive part of the antenna input impedance. However, having same maximum dimension (Dmax), the space filling property of the fractals enhances increase in the radiation resistance and decrease in the resonance frequency comparing to antennas utilizing Euclidean geometries.

In this thesis, properties of Koch Curve fractal geometry and performance of Koch fractal antennas are studied. In chapter 2, the well known fractal geometries are mentioned with their fractal dimensions. Since the fractals are complex shapes and can not be classified in the realms of Euclidean geometry, the concept, fractal dimension, D, is introduced.

In chapter 3, the Koch Curve geometry is defined with mathematical expressions. Afterwards, the properties of electrically small Koch antennas are analyzed as well as mentioning the limits of the electrically small antennas.

In chapter 4, the performances of the strictly self similar Koch Curve antennas are studied by assessing the results of the simulations that are performed by using CST MWS® software tool. The radiation properties and frequency response of the antennas are observed by varying the fractal parameters, indention angle (θ) and the iteration number (n).

In chapter 5, modified (not strictly self similar) Koch geometries are generated to find out the effect of spatial distribution of the geometry (which is also function of indention angle) to antenna performance. Both simulation and experimental results are compared at the end of the section.

In chapter 6, a geometry which is a combination of Koch curve and Sierpinski Triangle Gasket is utilized as antenna geometry. Sierpinski Triangle Gasket antennas are famous with their multiband frequency characteristics and log periodicity in their resonance frequencies. It was tried to obtain an antenna having close resonance frequencies and similar radiation patterns in resonance frequencies by superimposing Koch geometry to Sierpinski Triangle Gasket.

As a final remark, it should be recalled that term "*fractal*" stands for infinitely iterated geometry in mathematics, and finitely iterated geometries are named as "*prefractal*" geometries. However, in engineering literature, since infinitely iteration is impossible for implementations, prefractal geometries are regarded and named as fractal geometries.

CHAPTER 2

FRACTAL GEOMETRIES AND FRACTAL ANTENNAS

2.1 Fractals in Nature

Fractal geometries can be observed easily in the nature such as coastlines, mountains, clouds, snow flakes, leaves and trees. The term fractal was first coined by the French mathematician B.B. Mandelbrot in 1970s after his breakthrough findings on irregular and fragmented geometric topologies found in the nature that can not be explained in the realms of Euclidean geometry. The term fractal has its origins from the Latin word *fractus* which is also related to verb *fangere*, which means *to break* [1].

Mandelbrot defined the fractals as "the shapes made of parts similar to the whole in some way" [1]. In [1] measuring the coastline of England was given as an example to understand the term fractal. The results heavily depended on the scale of the map used with the same measuring tools [3]. In Figure 2.1, West coastlines of Britain in different scales are illustrated. As seen in Figure 2.1, the total length of the coastline increases, when scale(a) is used instead of scale (d) , since more details are considered in the measurement. For scale (d) the coastline of Britain seems to be rough and consisted of continuous and differentiable curve segments. However when one of these segments are observed in a larger scale, it is encountered that the segment indeed consisted of smaller sub-segments possessing non-differentiable points in it. For infinitely large magnifying scales, the coastline exhibits a continuous but nowhere differentiable curve.

The fractals can also be restated "as rough of fragmented geometric shapes that can be sub-divided in parts, each of which is approximately a reduced-size copy of

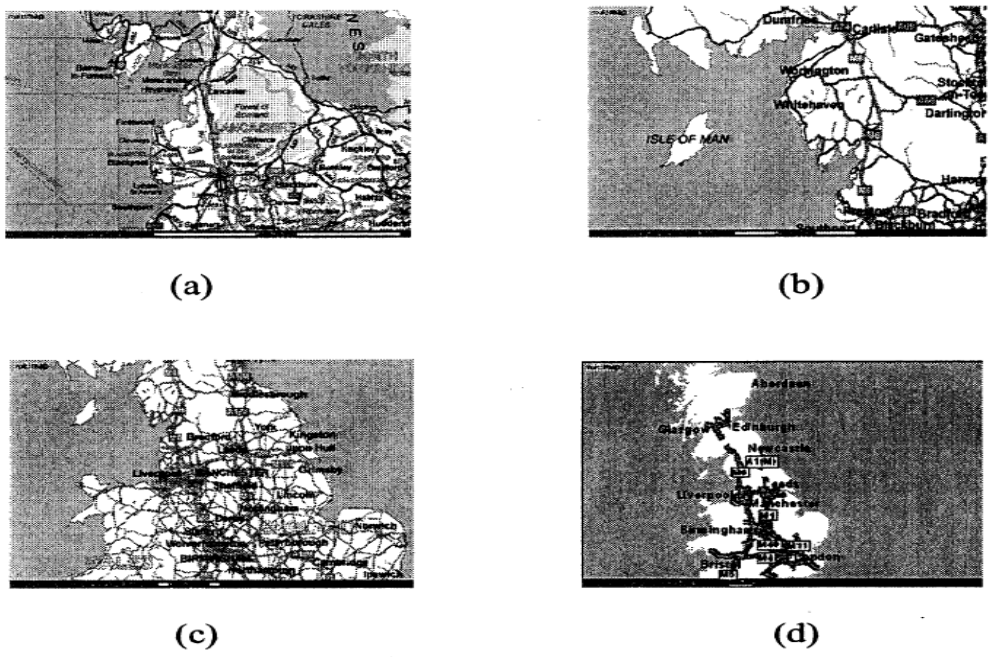

Figure 2.1 Britain's west coastline with different scales. (a) Scale 1:1,000,000 (b) Scale 1:2,000,000, (c) Scale 1:4,000,000 and (d) Scale 1:10,000,000 [2]

the whole" [1]. The fractals are generally self similar; the segments of the fractal curves are scaled versions of the parent curve. If all the segments of a fractal curve are same scaled versions of parent curve, this type of fractal is called *strictly self-similar*. However, there exist randomly scaled fractals that are found frequently in the nature.

Self-similarity is the one of the most appealing characteristics of the fractals. The fractals illustrated in Figure 2.2, shows the self-similarity of some well known fractals.

2.2 Fractal Dimension

Since the fractals can not be explained simply in Euclidean geometry, the fractals are described by the concept of fractal dimension, D. "A fractal is a set for which the Hausdorff Besicovich dimension strictly exceeds its topological dimension" [1]. Fractals can also have integer dimensions. Dimension of the geometry was defined in several ways for various studies on fractals. Self similarity dimension

and Hausdorff dimension are the most widely used definitions. Hausdorff Besicovich dimension can be rewritten as;

$$k_1\left(\frac{1}{h_1}\right)^D + k_2\left(\frac{1}{h_2}\right)^D + \ldots\ldots\ldots + k_m\left(\frac{1}{h_m}\right)^D = 1 \qquad (2.1)$$

Where, $k_{m,}$ is the number of copies of the initiator scaled by h_m and m is the number of different scale that fractal contains. [31], [35]. Self–similarity dimension is simpler than Hausdorff Besicovich dimension. Calculation of the self similarity dimension is obtained as follows; the geometry is divided into scaled down, but identical copies of itself. For n copies of the original geometry (parent) that are scaled down by a factor of m, self-similarity dimension, D can be calculated as;

$$D = -\frac{\log n}{\log m} \qquad (2.2)$$

Indeed self similarity dimension can be also calculated by Hausdorff Besicovich dimension, which can be applied to any fractal geometry. The detailed definitions and applications of fractal dimension can be found in [36].

Table 2.1 Fractal dimensions of the fractals illustrated in Figure 2.2

Fractal Curve	**Fractal Dimension (D)**
Koch Curve	1.26186
Sierpinski Carpet	1.89279
Cantor Set	0.6389
Minkowski Loop	1.46498
Sierpinski (Triangle) Gasket	1.58496
Hilbert Curve (infinitely iterated)	2
Koch Snowflake	1.26186

2.3 Fractals in Antenna Engineering

Antennas with fractal geometry become popular after the studies of N. Cohen [4]. He studied the improvements of antenna radiation properties by utilizing Koch curves, Sierpinski carpets, Meander line and Minkowski loop.

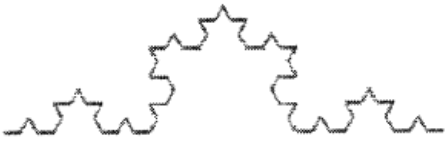

a) Koch Curve

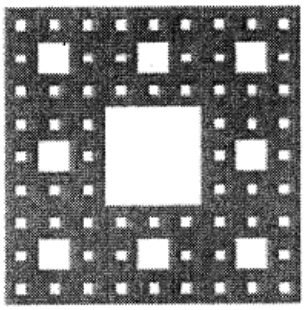

b) Sierpinski Carpet

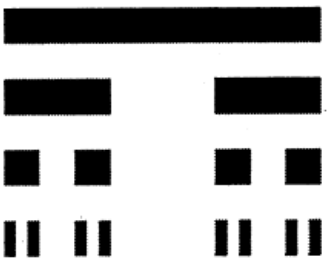

c) Cantor Set

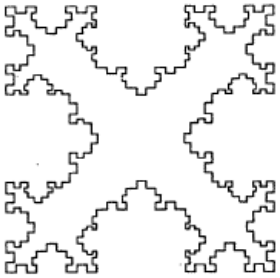

d) Minkowski Loop

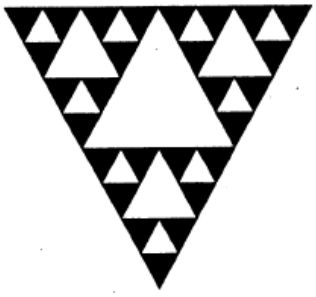

e) Sierpinski Gasket

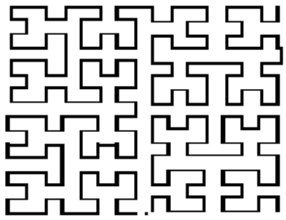

f) Hilbert Curve

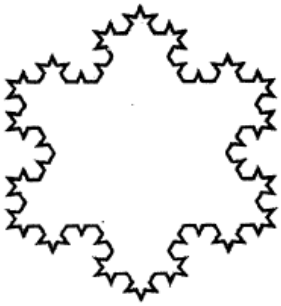

g) Koch Snowflake

Figure 2.2 Self similar well known fractal geometries [5, 6]

Koch curves are generally studied in monopole configuration. Puente et al [7] studied the shift of resonance frequencies of Koch monopole antenna as a function of iteration. By more detailed research in [8], Puente showed that there exists a limit of shift of resonance frequency even if the physical length increases. Vinoy [9] studied generalized Koch curve in dipole configuration to relate self similarity dimension to the shift in resonance frequency. The main aim these studies were to explore space filling properties of the antennas. Miniaturization of fractal antennas were investigated in [10], [11].

S. Best studied the effectiveness of space-filling properties of fractal antennas [12]. Moreover, in [13] the superiority of the performance of less complex shapes over fractal antennas were brought out.

Puente in [14], found out that fractal tree fractal antenna exhibits multiband characteristics and the reason for that was associated to self similarity of the antenna. Several other self-similar geometries, especially Sierpinski (triangle) gaskets and Sierpinski carpets have also been explored to observe the self-similarity effect of fractals on multiband characteristics in references [15], [16] and [17]. The multiband properties of these antennas were attributed to self-similar current distributions over these antennas [18]. It was also shown that multiband property of self similar fractal antennas can be controlled by perturbing the geometry [19].

A stacked antenna configuration with multiple layers of fractal geometries was utilized to increase bandwidth in [20].

Werner [21] studied on fractal arrays to achieve desired radiation pattern. In [22] it was observed that for controlling side lobe levels, multiband operation and wide bandwidth, fractal arrays yielded promising results.

CHAPTER 3

KOCH CURVES AS ELECTRICALLY SMALL ANTENNAS

The Koch curves are proposed by Swedish mathematician Helge von Koch in 1904. The Koch curves are composed of bent linear curves, yielding geometry with undefined derivative after infinitely many iterations. In Figure 3.1, a standard Koch curve derived from a straight line is illustrated.

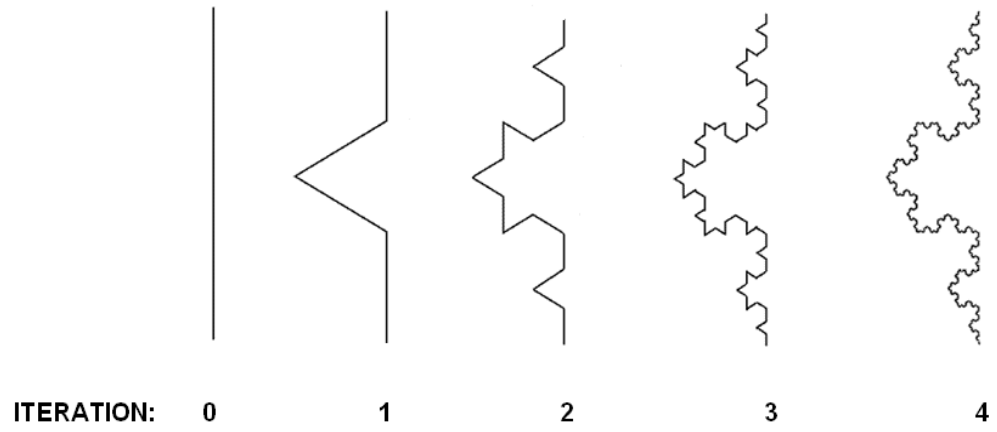

Figure 3.1 Iteratively construction of standard Koch geometric curves

The generation of Koch curves starts with bending an initial straight line, called initiator, from determined regions. To obtain the first iteration of a standard Koch curve, initiator is portioned into three equal segments and the middle segment is replaced by a equilateral triangle without base, while two other segment remain unchanged. For the next iteration the same procedure is applied to all individual

segments and the iterations continue until ideal Koch geometry, nowhere differentiable geometry is produced.

As seen in Figure 3.1, as the iteration number increases, the total length of the geometry increases meanwhile the height of the curve remains its initial value. Each segment of previous iteration curve is scaled by 1/3 and new iterated curve consists of four of those scaled segments. The length of the curve is $(4/3)^k$, where k is the iteration number.

3.1 Generation of Strictly Self-Similar Generalized Koch Curves

The generation of Koch curves can be explained by using an iterative function system (IFS). In order to express a general formulation, the scaling ratio of the segments, *s*, and the indention angle, *θ,* are defined as function parameters.

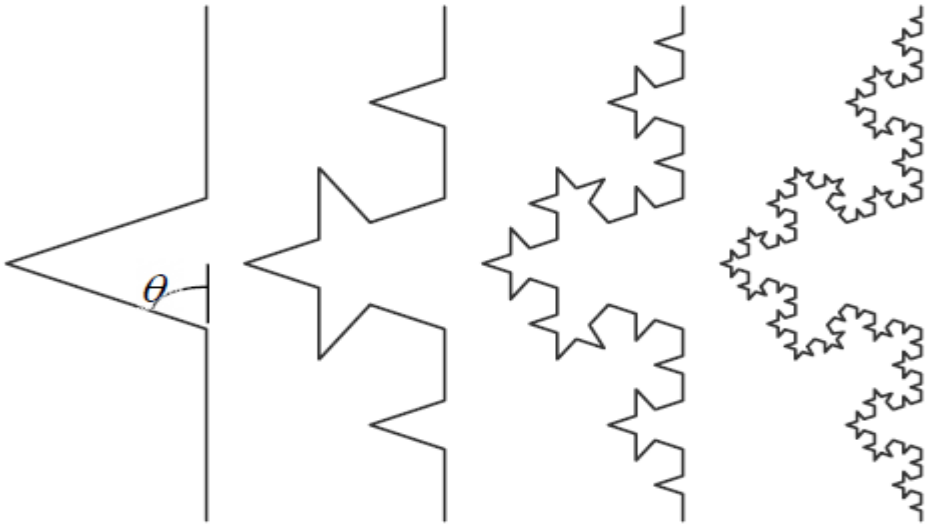

Figure 3.2 The strictly self similar generalized Koch curve as a function of indention angle, θ [9]

IFS uses affine transformation of the geometry in the coordinate system. In a 2D coordinate system, assuming that the initiator exists as straight line from (0,0) to (1,0) coordinates, the transformations can be done as in [9] ;

$$W_1\begin{pmatrix} x \\ y \end{pmatrix} = \begin{bmatrix} \frac{1}{s} & 0 \\ 0 & \frac{1}{s} \end{bmatrix} \begin{pmatrix} x \\ y \end{pmatrix} \tag{3.1}$$

$$W_2\begin{pmatrix} x \\ y \end{pmatrix} = \begin{bmatrix} \frac{1}{s}\cos\theta & -\frac{1}{s}\sin\theta \\ \frac{1}{s}\sin\theta & \frac{1}{s}\cos\theta \end{bmatrix} \begin{pmatrix} x \\ y \end{pmatrix} + \begin{pmatrix} \frac{1}{s} \\ 0 \end{pmatrix} \tag{3.2}$$

$$W_3\begin{pmatrix} x \\ y \end{pmatrix} = \begin{bmatrix} \frac{1}{s}\cos\theta & \frac{1}{s}\sin\theta \\ -\frac{1}{s}\sin\theta & \frac{1}{s}\cos\theta \end{bmatrix} \begin{pmatrix} x \\ y \end{pmatrix} + \begin{pmatrix} \frac{1}{s}(1+\cos\theta) \\ \frac{1}{s}\sin\theta \end{pmatrix} \tag{3.3}$$

$$W_4\begin{pmatrix} x \\ y \end{pmatrix} = \begin{bmatrix} \frac{1}{s} & 0 \\ 0 & \frac{1}{s} \end{bmatrix} \begin{pmatrix} x \\ y \end{pmatrix} + \begin{pmatrix} \frac{s-1}{s} \\ 0 \end{pmatrix} \tag{3.4}$$

The iterated the curve is obtained by

$$W(x,y) = W_1(x,y) \cup W_2(x,y) \cup W_3(x,y) \cup W_4(x,y) \tag{3.5}$$

Since for a strictly self similar Koch curve, the overall height is same as the initial height of the initiator, the scaling factor, s, is defined as

$$\frac{1}{s} = \frac{1}{2(1+\cos\theta)} \tag{3.6}$$

and the self similarity fractal dimension becomes

$$D = \frac{\log 4}{\log\left[2(1+\cos\theta)\right]} \tag{3.7}$$

For a standard Koch geometry, s=3 and θ=60º, the IFS transformation is

$$W_1\begin{pmatrix} x \\ y \end{pmatrix} = \begin{bmatrix} \frac{1}{3} & 0 \\ 0 & \frac{1}{3} \end{bmatrix} \begin{pmatrix} x \\ y \end{pmatrix} \tag{3.8}$$

$$W_2\begin{pmatrix} x \\ y \end{pmatrix} = \begin{bmatrix} \frac{1}{3}\cos 60^\circ & -\frac{1}{3}\sin 60^\circ \\ \frac{1}{3}\sin 60^\circ & \frac{1}{3}\cos 60^\circ \end{bmatrix}\begin{pmatrix} x \\ y \end{pmatrix} + \begin{pmatrix} \frac{1}{3} \\ 0 \end{pmatrix} \tag{3.9}$$

$$W_3\begin{pmatrix} x \\ y \end{pmatrix} = \begin{bmatrix} \frac{1}{3}\cos 60^\circ & \frac{1}{3}\sin 60^\circ \\ -\frac{1}{3}\sin 60^\circ & \frac{1}{3}\cos 60^\circ \end{bmatrix}\begin{pmatrix} x \\ y \end{pmatrix} + \begin{pmatrix} \frac{1}{2} \\ \frac{1}{3}\sin 60^\circ \end{pmatrix} \tag{3.10}$$

$$W_4\begin{pmatrix} x \\ y \end{pmatrix} = \begin{bmatrix} \frac{1}{3} & 0 \\ 0 & \frac{1}{3} \end{bmatrix}\begin{pmatrix} x \\ y \end{pmatrix} + \begin{pmatrix} \frac{2}{3} \\ 0 \end{pmatrix} \tag{3.11}$$

and self similarity fractal dimension becomes

$$D = \frac{\log 4}{\log 3} = 1.2619 \tag{3.12}$$

3.2 Electrically Small Koch Antennas

3.2.1 Electrically Small Antennas:

The electrically small antennas are investigated in details by H.A.Wheeler [23] for the first time. “A small antenna is one whose size is a small fraction of the wavelength. It is a capacitor or an inductor, and it is tuned to resonance by a reactor of opposite kind. Its bandwidth of impedance matching is subject to a fundamental limitation measured by its “radiation power factor” which is proportional to its “effective volume”.” [23]

Wheeler modeled small antennas as series resistance-inductance (RL) circuit or parallel conductance-capacitance (GC) circuits to express the power factor of the antenna that is related to frequency bandwidth of impedance matching between antenna and the generator. Conductance and resistances represented radiation resistance and L and C represented reactive part of the antenna impedance.

Investigating power factor for small antennas, Wheeler [24] coined term "radiansphere", that is the volume having a radius of one radianlength ($1/2\pi$ wavelength) [25]. It can be interpreted as the boundary between near field and far field of a small antenna. "A small antenna is one somewhat smaller than radiansphere (maximum dimension of a small antenna is less than radianlength), but it has a "sphere of influence" occupying the radiansphere." [24].

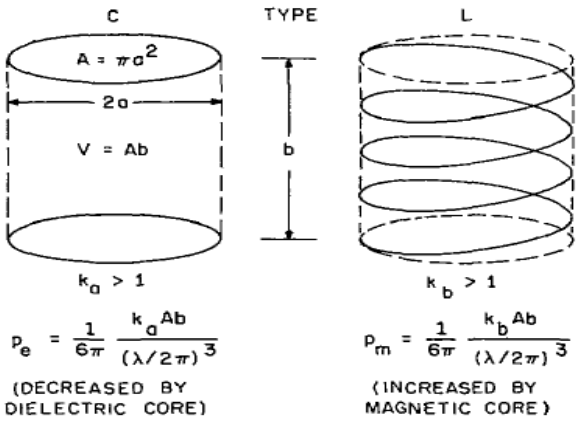

Figure 3.3 Radiation power factor in terms of equivalent volume [23]

In Figure 3.3, the small antennas of both kinds (C and L) occupying equal cylindrical volumes. Those models are used to relate the radiation power factor (PF) and the size.

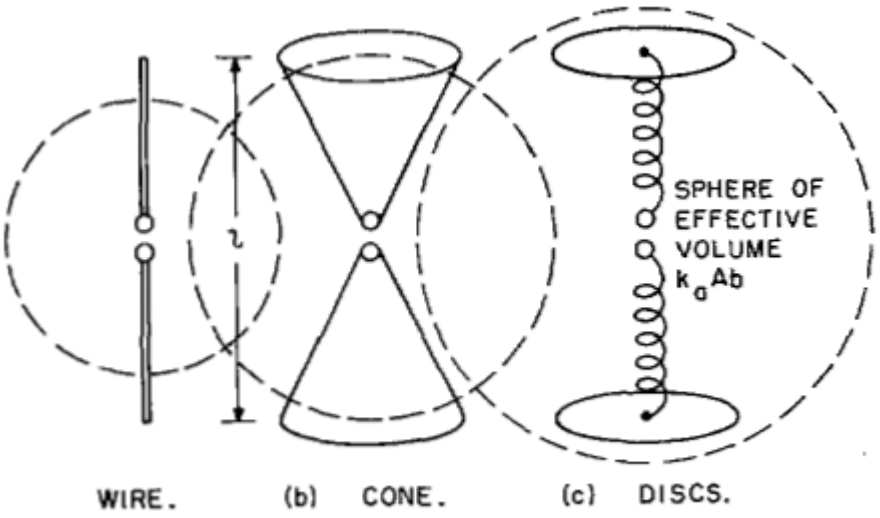

Figure 3.4 Effective volume of axial electrical dipole of same height [23]

The radiation power factor is found to be proportional to volume and also the shape factor. The cylindrical volume (V=Ab) is multiplied by a shape factor (k_a or k_b >1) to give the effective volume (V′= k_aAb or k_bAb).

The formula derived in [23] as

$$rad\ PF = p = \frac{1}{6\pi}\frac{V'}{V_c} \tag{3.13}$$

where,

$$V_c = \frac{4\pi}{3}\left(\frac{\lambda}{2\pi}\right)^3. \tag{3.14}$$

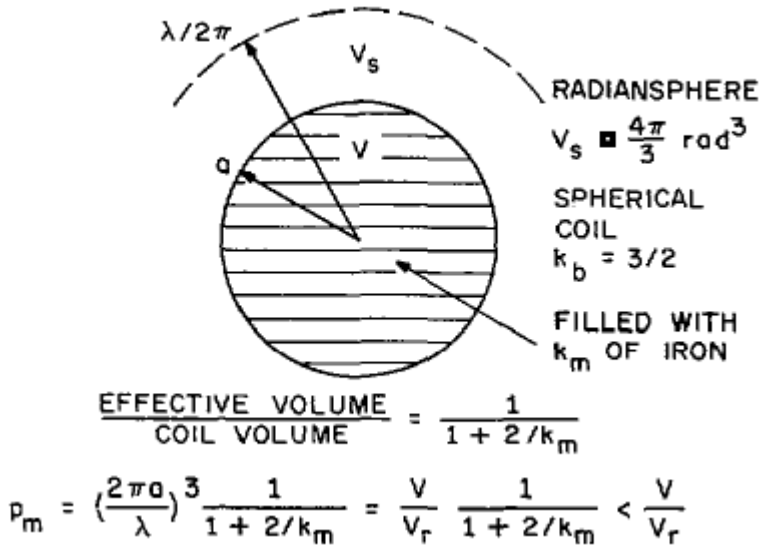

Figure 3.5 Spherical coil with magnetic core and its relation to radiansphere [23]

In Figure 3.5, Wheeler [23] derives one theoretical case of a small coil which has the greatest radiation PF obtainable within a spherical volume. The effective volume of an empty spherical coil has a shape factor 3/2, filling the perfect magnetic core ($k_m=\infty$) multiplies the effective volume by 3:

$$p_m = \frac{2}{9}\frac{(3)(3/2)V}{V_s} = \frac{V}{V_s} = \left(\frac{2\pi a}{\lambda}\right)^3 \tag{3.15}$$

"Wheeler asserts that outside the sphere occupied by the antenna, there is stored energy that conceptually fills the radian sphere, but there is none inside the antenna sphere. In a rigorous description of the electromagnetic field from a small dipole of either kind, the radiation power in the far field is accompanied by the stored energy which is mostly located in the near –field (inside the radiansphere). Since there is no stored energy inside the spherical coil, this removes the "avoidable" stored energy, leaving only the "unavoidable" amount outside the inductor but mostly inside the radian sphere. This unavoidable stored energy is what imposes a fundamental limitation on the obtainable radiation PF" [25].

***3.2.2 Fundamental Limits of Radiation Q of Electrically Small Antennas*:**

Chu [26] derived a theoretical formula that minimum radiation quality factor, Q, of an antenna, which fits inside a sphere of a given radius, is calculated. Later, Harrington extended this approximate theory [27].

According to formulation in [26], [27] the radiation Q is expressed as

$$Q = \begin{cases} \dfrac{2wW_e}{P_{rad}} & W_e > W_m \\ \dfrac{2wW_m}{P_{rad}} & W_m > W_e \end{cases} \tag{3.16}$$

where, W_e is the time-average, non-propagating, stored electric energy,

W_m is the time-average, non-propagating, stored magnetic energy,

ω denotes radian frequency,

and P_{rad} denotes radiated power.

In Chu's theory, [26] the antenna is enclosed by a sphere of radius a, the smallest possible sphere which completely encloses the antenna. The fields of the antenna external to the sphere are represented in terms of a weighted sum of spherical wave functions and the modes exhibit power orthogonality carrying power independently of one another. From the spherical wave-function expansion, the radiation Q is calculated in terms of the time average, non-propagating energy external to the

sphere and the radiated power. For the minimum Q, any stored energy in the sphere must be avoided.

The formula derived in [26] gives minimum obtainable Q;

$$Q = \frac{1}{k^3 a^3} + \frac{1}{ka} \tag{3.17}$$

3.2.3 Electrically Small Koch Antennas:

When the antenna is operated as an electrically small antenna, radiation efficiency of the antenna becomes poor, due to its low radiation resistance and highly stored reactive energy in the neighborhood of the antenna, i.e. high Q. Even that antenna is coupled to the feeding circuit via a matching circuit; the matched bandwidth is very narrow.

As presented in [24], [13], the electrically small antenna is one "whose maximum dimension is less than one radianlength $\lambda/2\pi$". The electrically small antenna limit (ESAL) is $ka = 1$, where a can get minimum value as the radius of the radiansphere which encloses the antenna (radius of the sphere can be considered as the maximum dimension of the antenna, Dmax) and k ($k=2\pi/\lambda$) is the wave number. Keeping a constant, one can get the maximum frequency that the antenna operates as an electrically small antenna. For the frequencies below that frequency the antenna is expected to possess electrically small antenna characteristics. Here arises a question: "Can the self resonance frequency of an antenna be lowered to electrically small antenna frequency limit?"

The self resonance frequency is where minimum antenna Q is achieved without externally loading the antenna. To answer "yes" to this question one should be able to minimize the Q of the antenna even if the antenna behaves as electrically small antenna, i.e. high Q. Apparently, the Q and the radiation power factor (p) are basically inversely proportional. As denoted in equation (3.13) to increase the p, the effective volume of the antenna must be increased. Since, space filling of a

constant volume space, increases the effective volume; the geometry of the antenna must be modified so as to increase the perimeter of the antenna without changing Dmax. When highly iterated Koch and Minkowski curves used as antennas, the "volume space filling" property of the fractals may yield lower resonance frequencies than antennas with simple geometries.

The first use of the Koch curves as antenna was realized by N. Cohen [4]. He reported that the Minkowski loop antenna presented a low resonant frequency, comparing to its electrical length. In spite of their large perimeters, these fractal loops enclose a finite, limited surface. In the same manner, a small dipole of constant end-to end length (height) can be fitted to limited volume, even if the total length of the antenna is increased.

By the revealed improvements in antenna resonance frequency, the "fractal shaped antennas" became a new research topic for antenna engineers in last decades. Researchers investigated many fractal antennas to relate the antenna radiation properties, such as, input impedance, current distribution over the antenna, and radiation pattern to the geometry of the antenna. Since the geometry of the fractal curves are characterized by fractal dimension, D, in following sections, the studies on Koch type antennas in this thesis are related to D as well as comparing the results with previous studies.

Subsequent to N.Cohen; Puente, Romeu and Cardama investigated the behavior of a standard Koch curve ($\theta=60^{o}$) as an electrically small monopole antenna. They mainly studied the fundamental limitations and quality factor (Q) of Koch small antenna, input impedance, current distribution over the antenna and radiation patterns; as a function of iteration number. It was observed that as the iteration number of the antenna increases, the perimeter increases as $(4/3)^{k}$ (k as the iteration number), as a result, the resonance frequency of the antenna decreases. Another observation is the decrease of the Q of the antenna when incrementing the iteration number. By the authors these result are related to D of Koch curve being greater than D of a straight line which is equal to 1. [8]

In [9] the influence of varying D of Koch curve as a function of θ, on primary self resonance frequency, the input impedance at this frequency and the ratio of first two resonant frequencies, was investigated. Based on the results of his numerical simulations and experiments, he asserted that the D of Koch curve was an important mathematical property of fractals when used in antenna engineering.

Since the analysis of the fractals antennas is more complex than simple, antennas with linear geometries (straight lines, circular loops, etc.), there still does not exist well established implicit mathematical expressions to characterize these antennas. Instead of analytical methods, the analyses of the antennas are generally performed by using numerical methods.

CHAPTER 4

PERFORMANCE OF STRICTLY SELF SIMILAR GENERALIZED KOCH ANTENNAS

Many researchers studied Koch curve to determine design parameters of the Koch antennas. ([4],[8],[9]) The findings in those experiments and numerical simulations led many researchers to attribute the significance of the fractal dimension, D as an important antenna design parameter. The fractals have D>1, and always have greater D than of a straight line which has D=1. The results comparing fractal antennas with Euclidean ones, revealed the achievement of lower resonance frequencies in favor of fractal antennas.

In [4] and [8] the standard Koch curves as a function of iteration number, was studied in monopole antenna configuration to investigate the preeminence of these antennas to standard linear monopole antennas of same end-to-end height. The improvements in antenna properties were linked to possessing higher D of Koch curve than the Euclidean ones. In [9], including the standard Koch curve geometry, space-filling property of strictly self-similar generalized Koch curves with various iterations were studied. In [31] the self-similar generalized Koch curves were modified and the properties of these antennas were studied. The common reasoning of improvements for Koch antennas was attached to increase of D, as was done in [8].

However, later, researchers in [32] investigated the influence of the fractal dimension on antenna performance by carrying out simulations and measurements. The studied fractals were Koch monopoles (D=1.26), Sierpinski Gasket (D=1.58),

Hilbert monopoles (D=2) and Peano monopoles (D=2). Upon the results observed, "increasing the fractal dimension did not always improve the antenna radiation and frequency response properties and geometry itself is played main role for these properties of antenna" was reported in [32]. This study was done by comparing different types of fractals, not changing the parameters of one fractal.

In this thesis, the investigation of D on antenna properties was demoted to Koch curves. The standard Koch curves, generalized strictly self-similar Koch curves and modified Koch curves were investigated and the results were compared.

4.1 Fractal Dimension of Strictly Self-Similar Koch Curves

As explained in Chapter 2.2, there are different definitions of D. Since D is a numeric value which gives the idea on the space- filling property of the fractal curve, in this chapter generalized Hausdorf-Besicovich dimension measurement is used to express the fractal self similarity dimension.

Recalling the equation (2.1), the fractal dimension, D of any fractal can be found as;

$$k_1\left(\frac{1}{h_1}\right)^D + k_2\left(\frac{1}{h_2}\right)^D + \ldots\ldots\ldots + k_m\left(\frac{1}{h_m}\right)^D = 1$$

where k_m is the number of copies of the initiator scaled by h_m and m is the number of different scale that fractal contains.

For a generalized strictly self similar Koch curve, m=1, k_m=4 and h_m=s=$\frac{1}{2(1+\cos\theta)}$. Rewriting the equation (2.1), the fractal dimension can be found;

$$k_m\left(\frac{1}{s}\right)^D = 1 \qquad (4.1)$$

$$4\left(\frac{1}{\frac{1}{2(1+\cos\theta)}}\right)^{D}=1 \tag{4.2}$$

$$D=\log^{4}_{2(1+\cos\theta)} \tag{4.3}$$

Table 4.1 Fractal Dimension (D) of a generalized Koch curve as a function of θ

Indention Angle (θ)	Fractal Dimension (D)
10º	1.0055
20º	1.0226
30º	1.0526
40º	1.0986
50º	1.1654
60º	1.2619
70º	1.4041
80º	1.6247
90º	2.0000

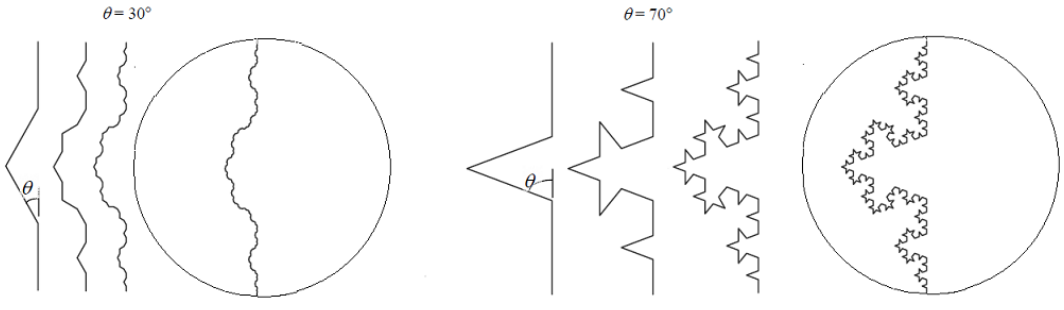

Figure 4.1 Generalized Koch curves of first four iterations with two different indention angles (The fourth iteration is enclosed by a circle with diameter equal to height of initiator) [9]

For a standard Koch curve, θ=60º, and D=1.2619. As function of θ, D gets values from 1 to 2, by incrementing θ from 0 to 90º. It can be seen in Figure 4.1, space-filling increases as the indention angle increases. When θ=90º maximum total length of the antenna is achieved while the end to end height remains constant. The length of the subsections for a given iteration is a function of angle of indention θ [9]. The total length of n^{th} iterated Koch curve can be found as

$$L_{\theta,n} = \left(\frac{2}{1+\cos\theta} \right)^n L_0 \tag{4.4}$$

where L_0 is the length of the initiator.

4.2 Performance Results of Simulated Strictly Self Similar Generalized Koch Antennas

In this part strictly self similar generalized Koch curves are simulated as dipole antennas. The antennas were formerly simulated in FEKO® simulation program, which is a MoM based simulation tool. However, same simulations were done in CST MWS® simulation tool, which uses time domain numeric calculation utilizing FIT (Finite Integration Technique) to accurately mesh the geometries [28]. The simulation results of both simulation tools came out almost same. In the rest of the thesis the CST MWS® simulation results have been presented due to easiness of use to work on simulation output results. The accuracy of the CST MWS® tool is investigated in [29].

4.2.1 Antenna Simulation Models:

The antenna wire radius is chosen to be 0.15 mm, which leads to 0.6mm line width when antenna is to be printed on a dielectric by using the formula [30]. The wire is made from perfect electrical conductor (PEC). The end to end heights of the antennas simulated throughout this chapter are kept as 16 cm. The simulation is performed in 0 to 3GHz. The antennas are fed from the center of the geometry as seen in Figure 4.2.

For simulation, the mesh type is selected as hexahedral; the mesh line per wavelength is set 30, lower mesh and mesh line limits are both chosen as 16. Since the geometry posses more detailed segments as iteration number increases. For 2nd or above iterations the PEC metal edges are refined with factor 5.

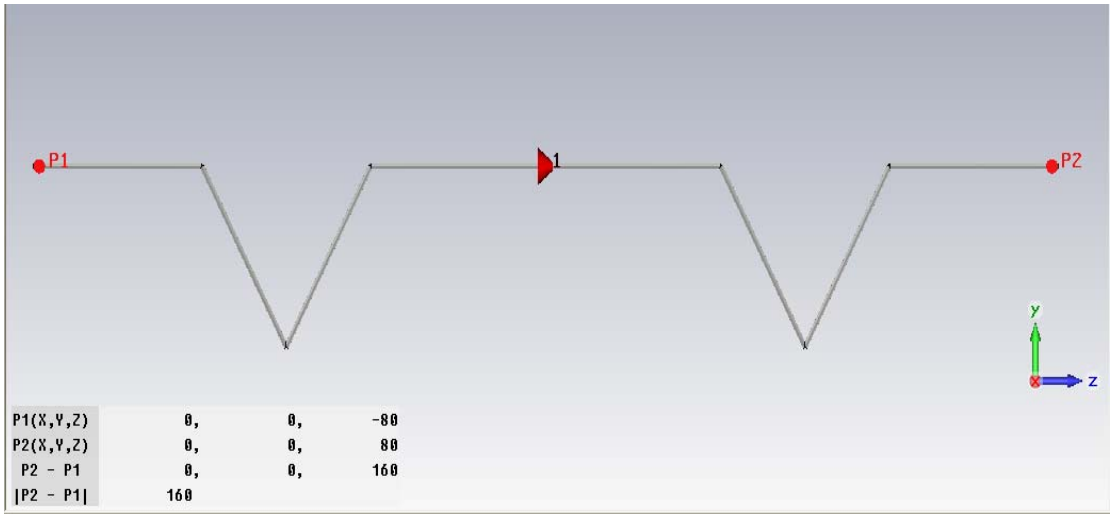

Figure 4.2 Strictly self similar Koch dipole of θ=60º simulation model for 1st iteration

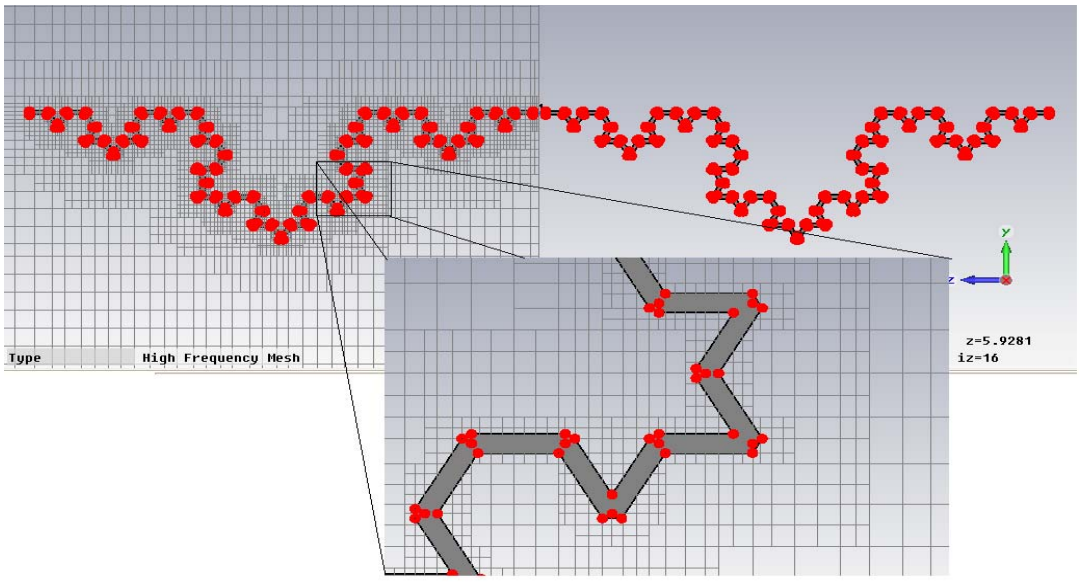

Figure 4.3 Detailed mesh view of strictly self similar Koch dipole of θ=60º simulation model for 3rd iteration.

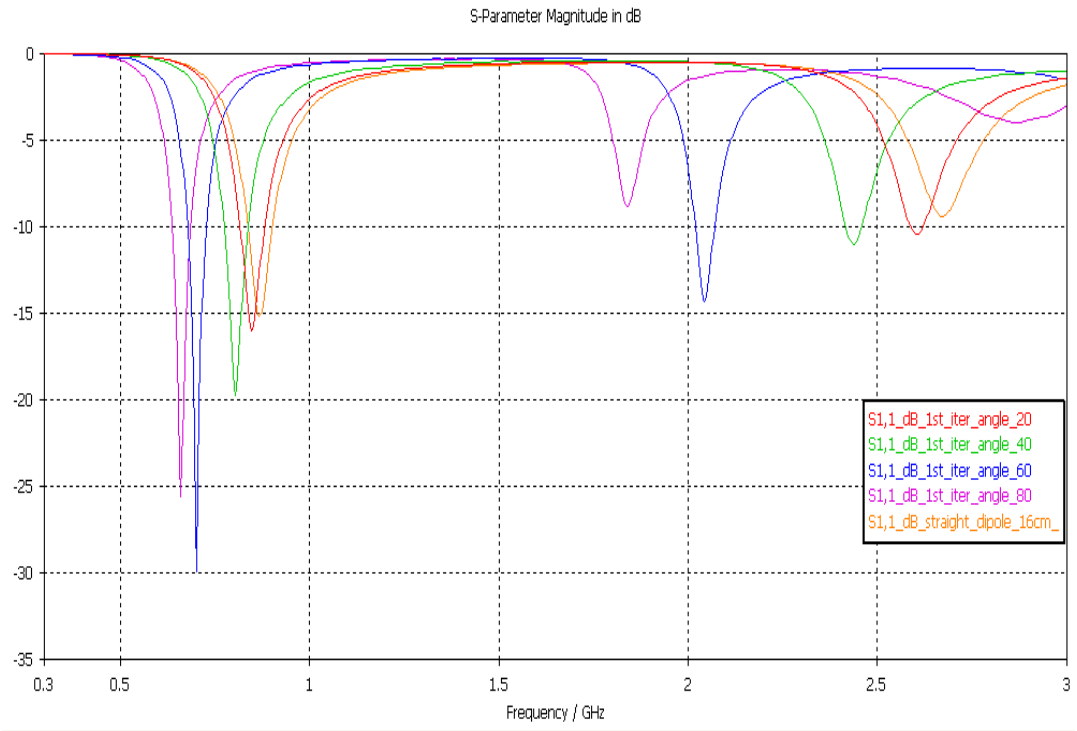

Figure 4.4 Simulation results for the return losses of the Koch dipole antennas of 1st iteration with varying indention angles

4.2.2 Simulation Results for Return Loss (dB):

The distinctive property of Koch curve antennas comparing to simple wire antennas, is enhancement of lowering the resonance frequencies. To illustrate basic relation between Koch geometry (for a strictly self-similar Koch geometry, indention angle, θ is the determinative factor) and resonance frequency, in Figure 4.4, the return loss (in dB scale) for the 1st iteration of the Koch curves are displayed. It is clear that, even for the first iteration, the resonance frequencies of the antenna shift downward with increasing indention angle. For θ=80º, both 1st and 2nd resonance frequencies occur at minimum values comparing the 1st and 2nd resonances frequencies of other antennas in the figure. Moreover, for θ=80º, a 3rd resonance frequency takes place below 3GHz.

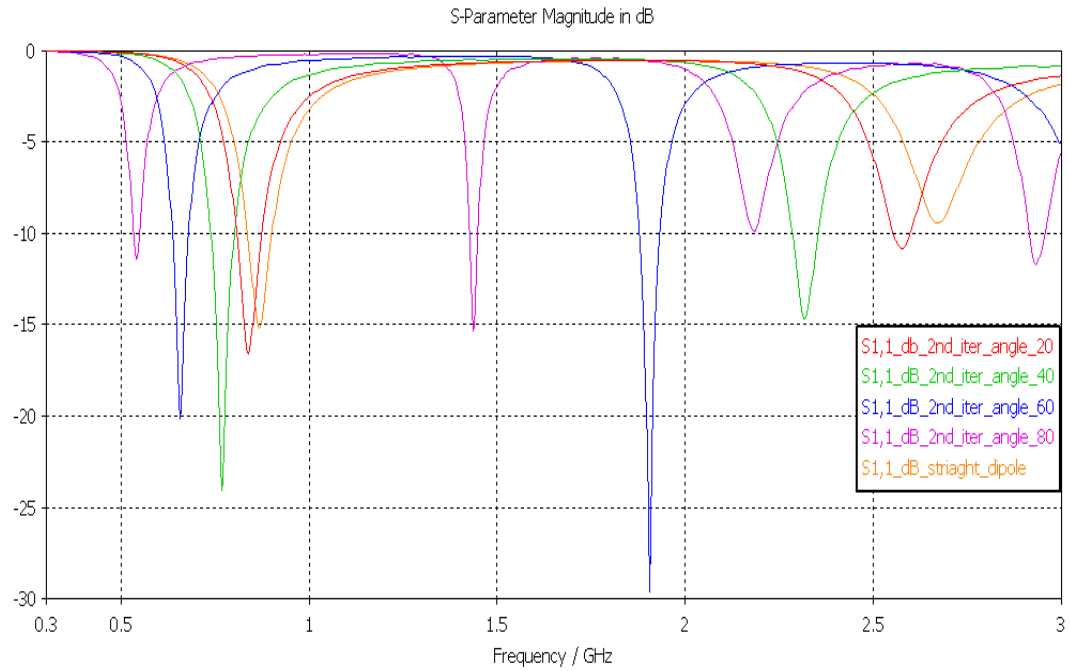

Figure 4.5 Simulation results for the return losses of the Koch dipole antennas of 2nd iteration with varying indention angles

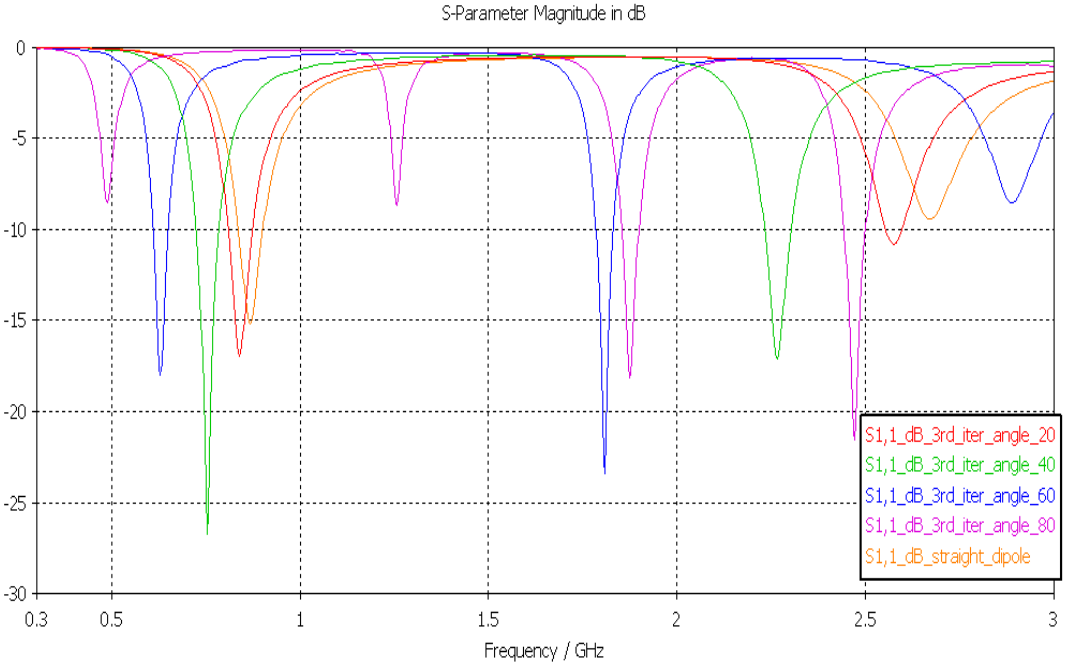

Figure 4.6 Simulation results for the return losses of the Koch dipole antennas of 3rd iteration with varying indention angles

Table 4.2 The resonance frequencies as a function of both indention angle and iteration number.

Indention Angle (θ)	Fractal Iteration Number	1st Resonance Frequency (GHZ)	2nd Resonance Frequency (GHZ)	3rd Resonance Frequency (GHZ)	4th Resonance Frequency (GHZ)
0º (Straight Dipole)	----	0.8674	2.6742	----	----
20º	1	0.8460	2.6112	----	----
	2	0.8378	2.5747	----	----
	3	0.8371	2.5652	----	----
40º	1	0.8046	2.4421	----	----
	2	0.7687	2.3225	----	----
	3	0.75441	2.2699	----	----
60º	1	0.7020	2.0445	----	----
	2	0.6584	1.9058	----	----
	3	0.6309	1.8072	2.8837	----
80º	1	0.6608	1.8394	2.8629	----
	2	0.5405	1.4376	2.1876	2.9354
	3	0.4881	1.2543	1.8709	2.475

It is obvious that there is an inverse relation between the occurrence of resonance frequencies and both indention angle and iteration number. Keeping iteration number constant, the maximum decrease in 1st resonance frequency is obtained for θ=80º. Referring to the Table 4.2, the rate of decrease in resonance frequencies increases as the θ values approaches to 90º.

Moreover, the first and 2nd resonance frequencies of the Koch curve with θ=80º of the 1st iteration is still lower than those of the Koch curve of θ=40º of 3rd iteration. Indeed the total length for the former case is 27.265 cm and 23.2384 cm for the

latter case. One can claim that the low resonance frequencies of higher indention angles are due to the total length the curves possessing higher values than more iterated curves with low indention angle. However, this claim can be refuted by noticing the 1st resonance frequency of Koch curve with θ=60º of 1st iteration and the 1st resonance frequency of Koch curve with θ=460º of 3rd iteration. Despite the larger total length the latter has, the former presents lower resonance frequency.

In [9] it was asserted that D, which is a function of θ, plays an important role in decreasing the resonant frequencies. In the same reference, the primary resonance frequency of a self similar Koch dipole is presented as a function of resonant frequency of a linear dipole of same height, iteration number, and fractal dimension by using curve fitting technique for the results obtained in their studies.

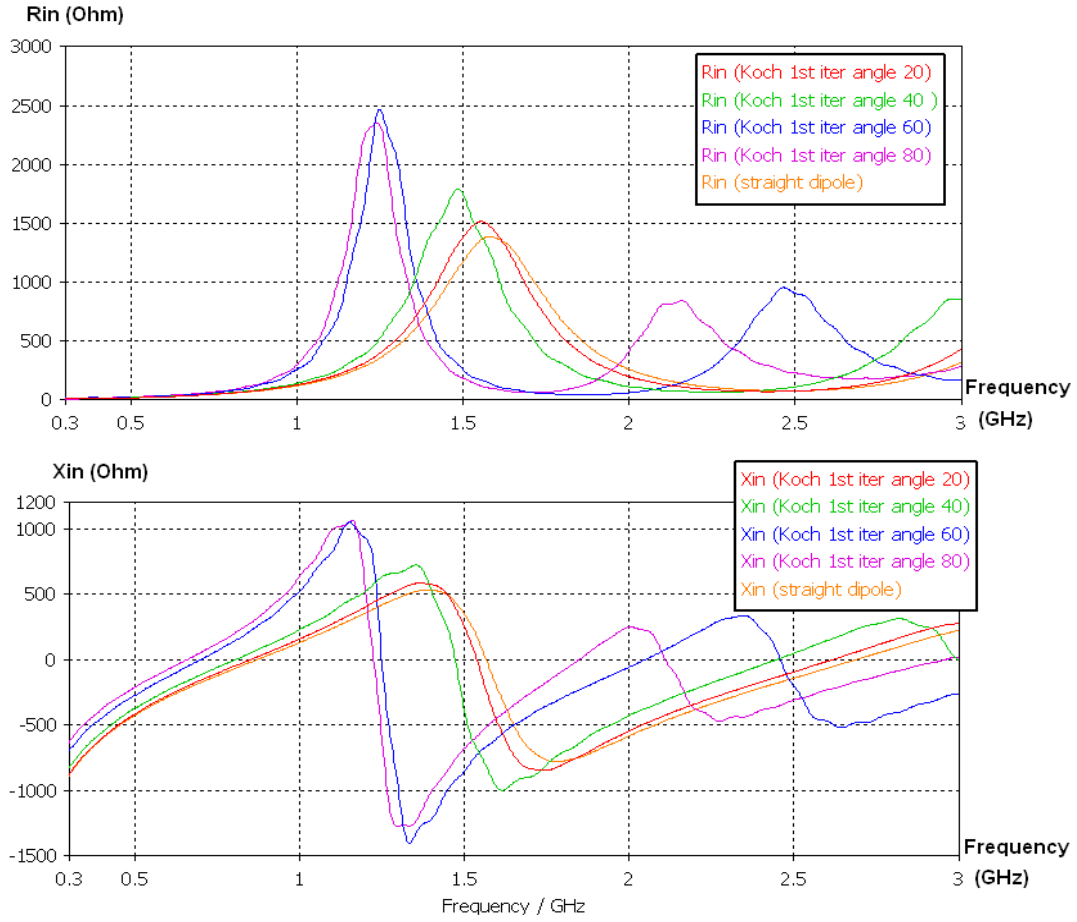

Figure 4.7 Simulation results for real and imaginary part of the input impedances of strictly self similar Koch curve antennas of 1st iteration with different indention angles.

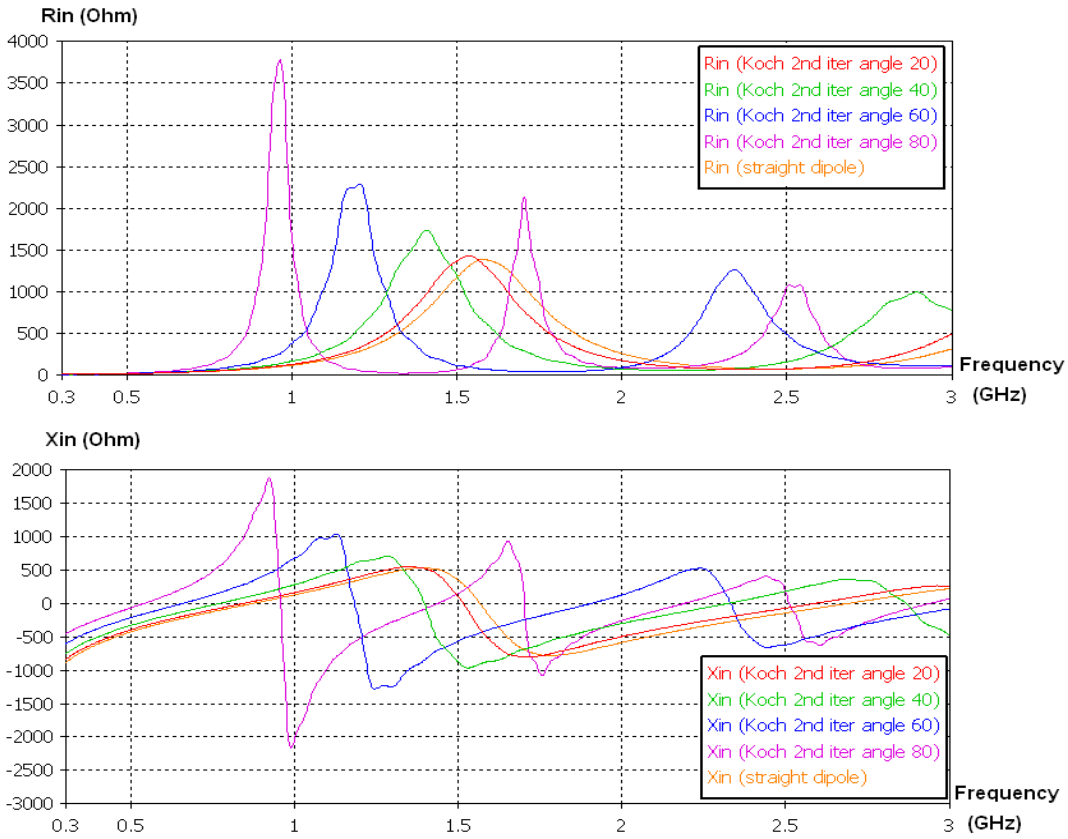

Figure 4.8 Simulation results for real and imaginary part of the input impedances of strictly self similar Koch curve antennas of 2nd iteration with different indention angles.

The input impedance of an antenna can be written as $Z_{in} = R_{in} + jX_{in}$ and the resonance frequencies depend on the input impedance of the antenna. Both real and imaginary parts of the self similar Koch antennas are sketched as function of iteration stage numbers and indention angles in Figures (4.7-4.9).

4.2.3 Simulation Results for Quality Factor (Q):

Noticing on the Figures (4.7-4.9) where imaginary parts of the impedances are plotted, one can see the resonance types; if $X'(w_o) > 0$ where $X(w_o) = 0$, w_o is called as the "*natural resonant frequency*", else if $X'(w_o) < 0$ where $X(w_o) = 0$, w_o is called as the "*natural antiresonant frequency*". Since the antenna is to be coupled to a microwave network with a reference impedance of 50 + j0 ohms via

transmission lines; minimum return loss is achieved when real part of the input impedance of the antenna gets values in the close to 50 Ohm and imaginary part gets values around 0 Ohm. This condition is encountered at natural resonant frequencies; not at the antiresonant frequencies due to high real part of the antenna input impedance at those frequencies even if imaginary part is zero.

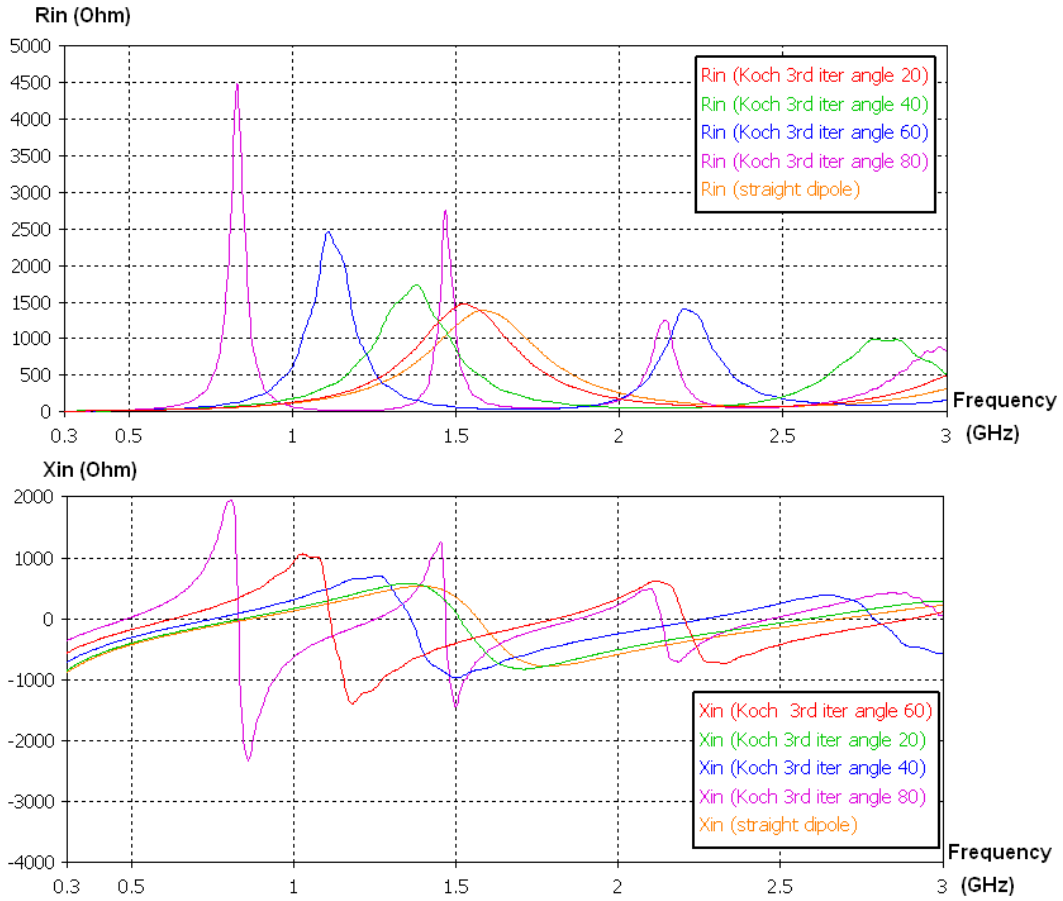

Figure 4.9 The real and imaginary part of the input impedances of a strictly self similar Koch curve of 3rd iteration with different indention angles.

In [33], an approximate measurement of quality factor (Q) is stated as

$$Q_z = w \frac{\left|Z_o^{'}(w)\right|}{2R_o(w)} \tag{4.5}$$

Indeed, in [8] to calculate Q the following formulation is used;

$$Q_{cv} = \frac{w}{2R_{in}}\left(\frac{dX_{in}}{dw} \pm \frac{X_{in}}{w}\right) \tag{4.6}$$

"+" is used when average stored electric energy, W_e is greater than average stored magnetic energy W_m,

"-" is used when average stored magnetic energy, W_m, is greater than average stored electric energy, W_e.

The formulation (4.6) is rewritten in the form [33]

$$Q_{cv}(\omega) = \frac{\omega}{2Rin}\left|X_o'(\omega)\right| \tag{4.7}$$

The derivations of these formulas are obtained in [33]. In [33] $Z_o(w) = Z(w) + X_{added\_resonator}$ refers to input impedance of the antenna after adding a compensating element ($X_{added\_resonator}$) to obtain "zero" reactance at resonance. Q_{cv} is not used because this formula does not provide a reasonable estimate of exact Q for the frequencies about the antiresonance. As a result, in this thesis calculation of Q is done by utilizing Q_z which gives reasonably approximate values of exact Q of the lossy and lossless wire antennas in non-dispersive media.

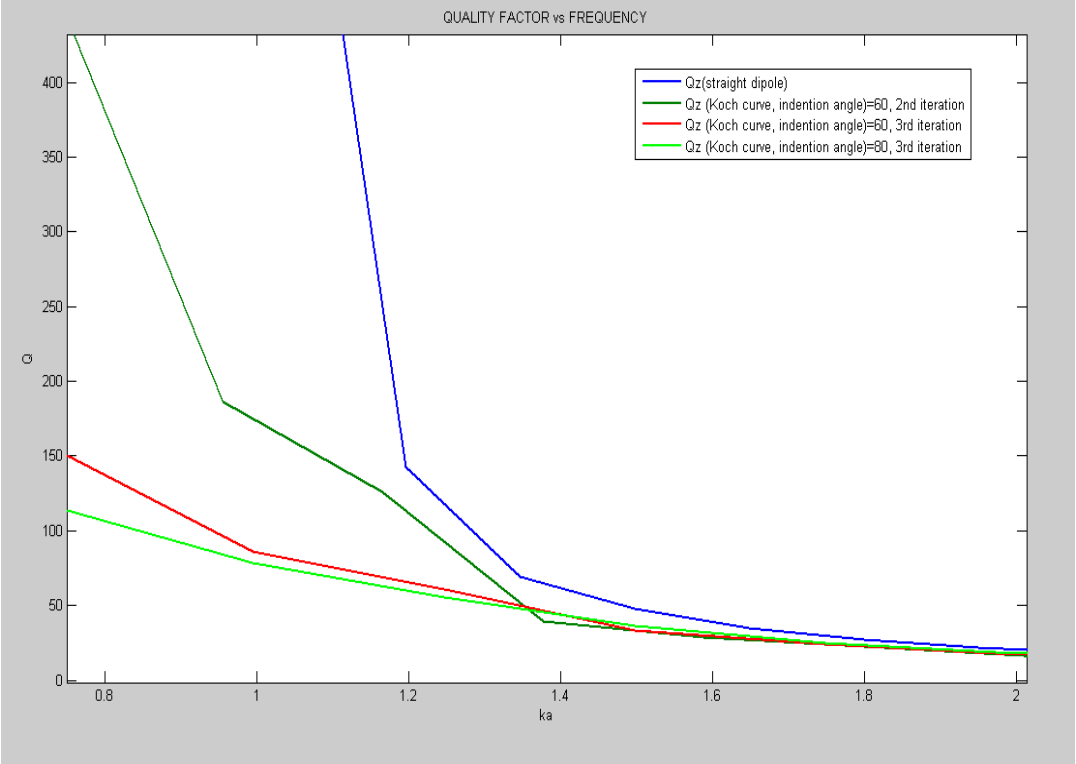

Figure 4.10 Approximate Q of the strictly self similar Koch dipole antennas in the vicinity of ESAL region.

The Figure 4.10 represents the approximate Q of the strictly self similar Koch antennas possessing the first three lowest primary resonance frequencies in Table 4.2. Koch curve with θ=80º of 3rd iteration presents the minimum Q for $f_{ESAL,}$ i.e. *ka*=1, and it is followed by Koch curve with θ=60º of 3rd iteration. The sequencing of minimum Q of the antenna types at f_{ESAL} is same as the order of resonance frequencies listed in Table 4.2 .Keeping frequency constant as reference, real part of input impedance increases and the imaginary part of input impedance decreases in magnitude, as the resonance frequency approaches to that reference frequency. As a result, Q at that frequency is minimized.

Electrically small antenna limit frequency is same for all the antennas simulated in this section since the end to end height is kept constant and can be found as;

$$ka = 1$$

$$\frac{2\pi}{\lambda} a = 1$$

$$\frac{2\pi f}{c} a = 1 \quad \Rightarrow \quad \boxed{f_{ESAL} = 298.416 \quad MHz} \tag{4.8}$$

c=3x10^8 m/s and a=0.16 m

In [8], a standard Koch curve (θ=60º) with end to end height of 6 cm, is used as monopole antenna. In that paper when sketching Q of the antennas with various iteration versus *ka*, "a" was considered as 6 cm and for f < 0.8GHz the antennas were considered as electrically small antennas. According to [24] electrically small (short) monopole can be defined to be one whose overall height, *h*, is less than λ/4π. As a result, for the monopole configuration the definition of radiancircle and ESAL must be redefined as *ka*=0.5 instead of *ka*=1. The minimum Q that can be achieved is a limit and it is impractical to reach that value. If the f_{ESAL} were to be calculated as in [8], it would be surprising to encounter a resonance frequency (f_r=488.1 MHz) even below f_{ESAL}=596.832 MHz. In [13] *ka* is equated to 0.5, since the studies in [13] are done by using monopole antennas.

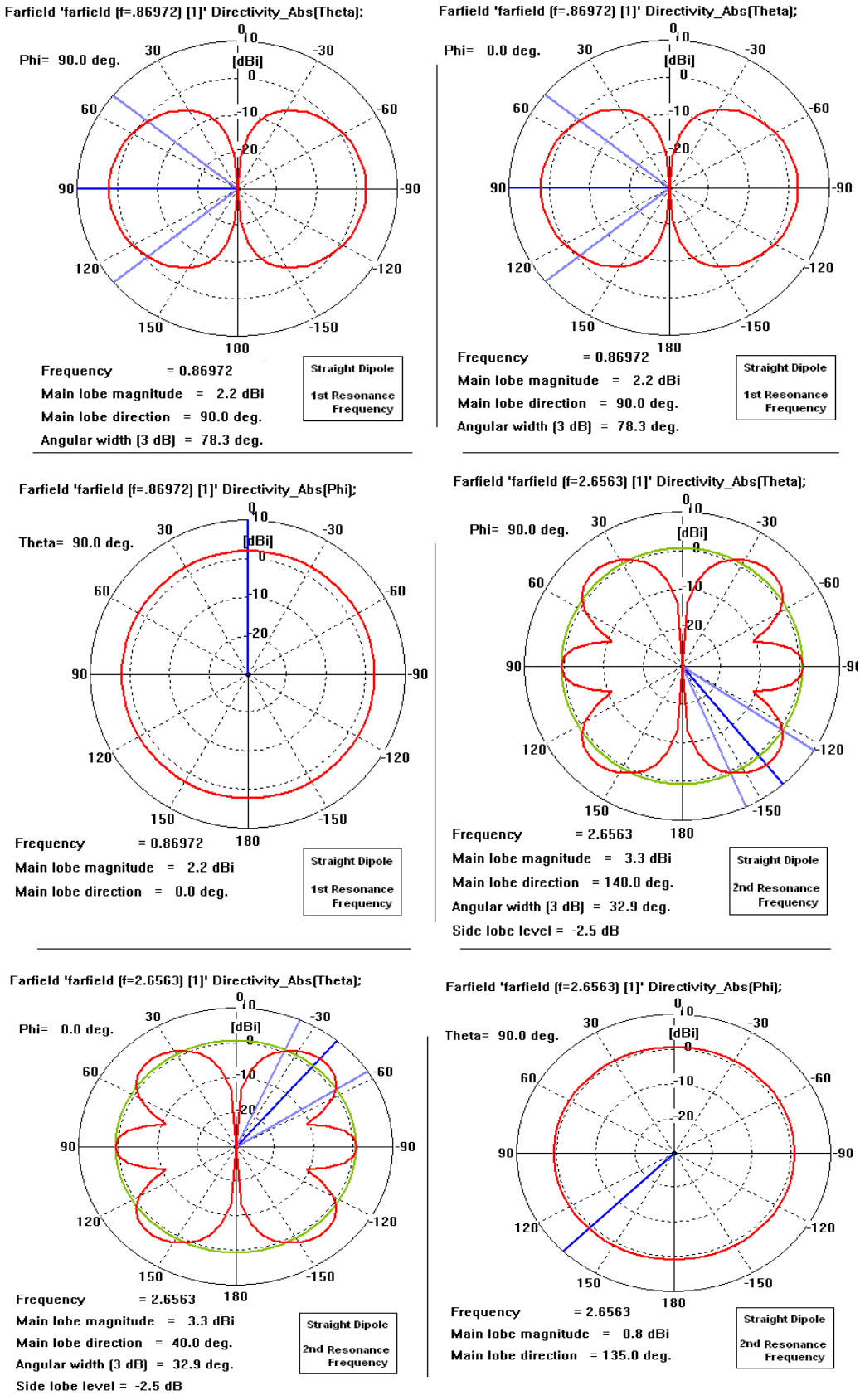

Figure 4.11 Simulation results for radiation patterns of the straight dipole at 1st and 2nd resonance frequencies.

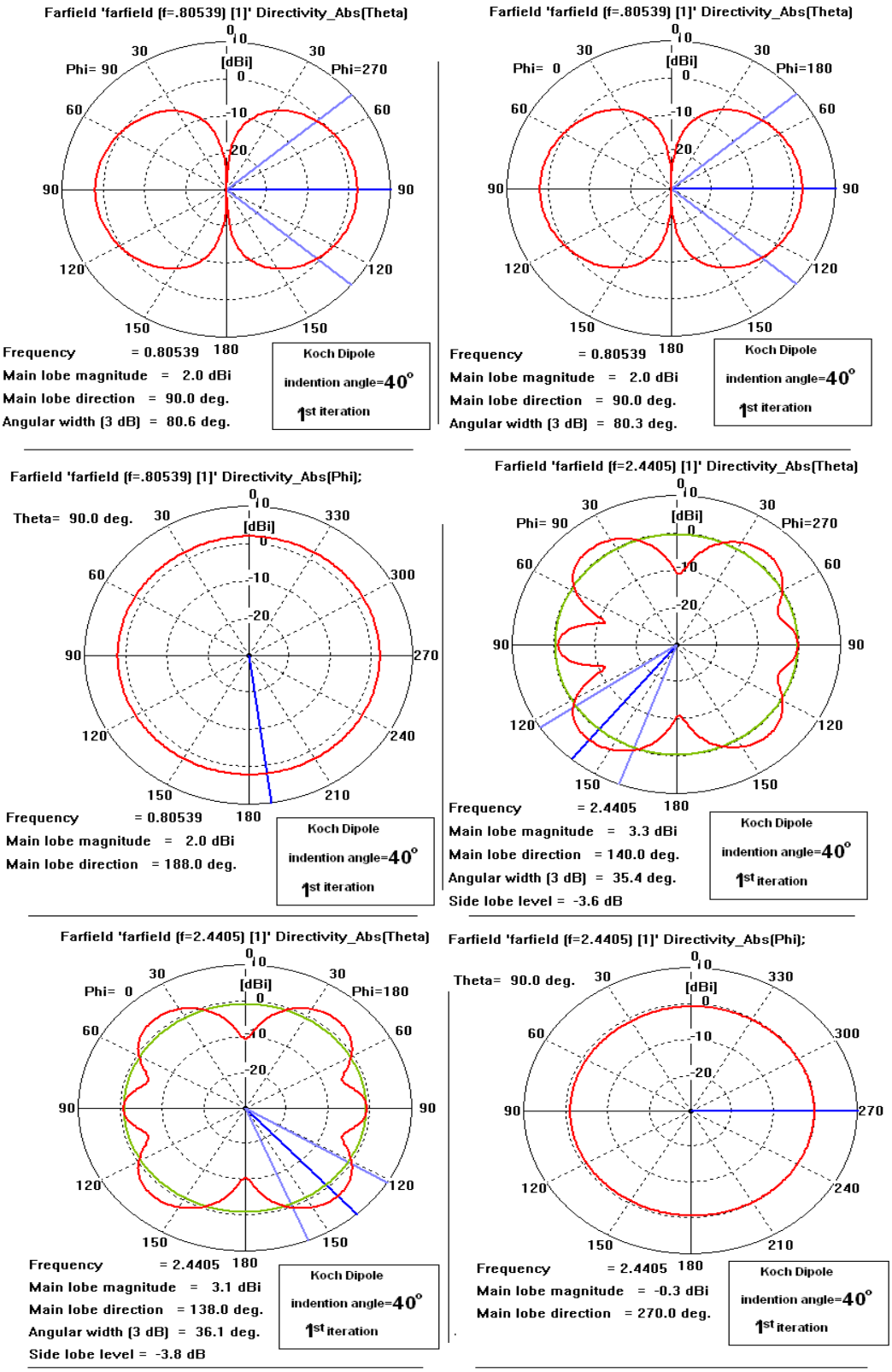

Figure 4.12 Simulation results for radiation patterns of the strictly self similar Koch curve dipole antennas with θ= 40º of 1st iteration at 1st and 2nd resonance frequencies.

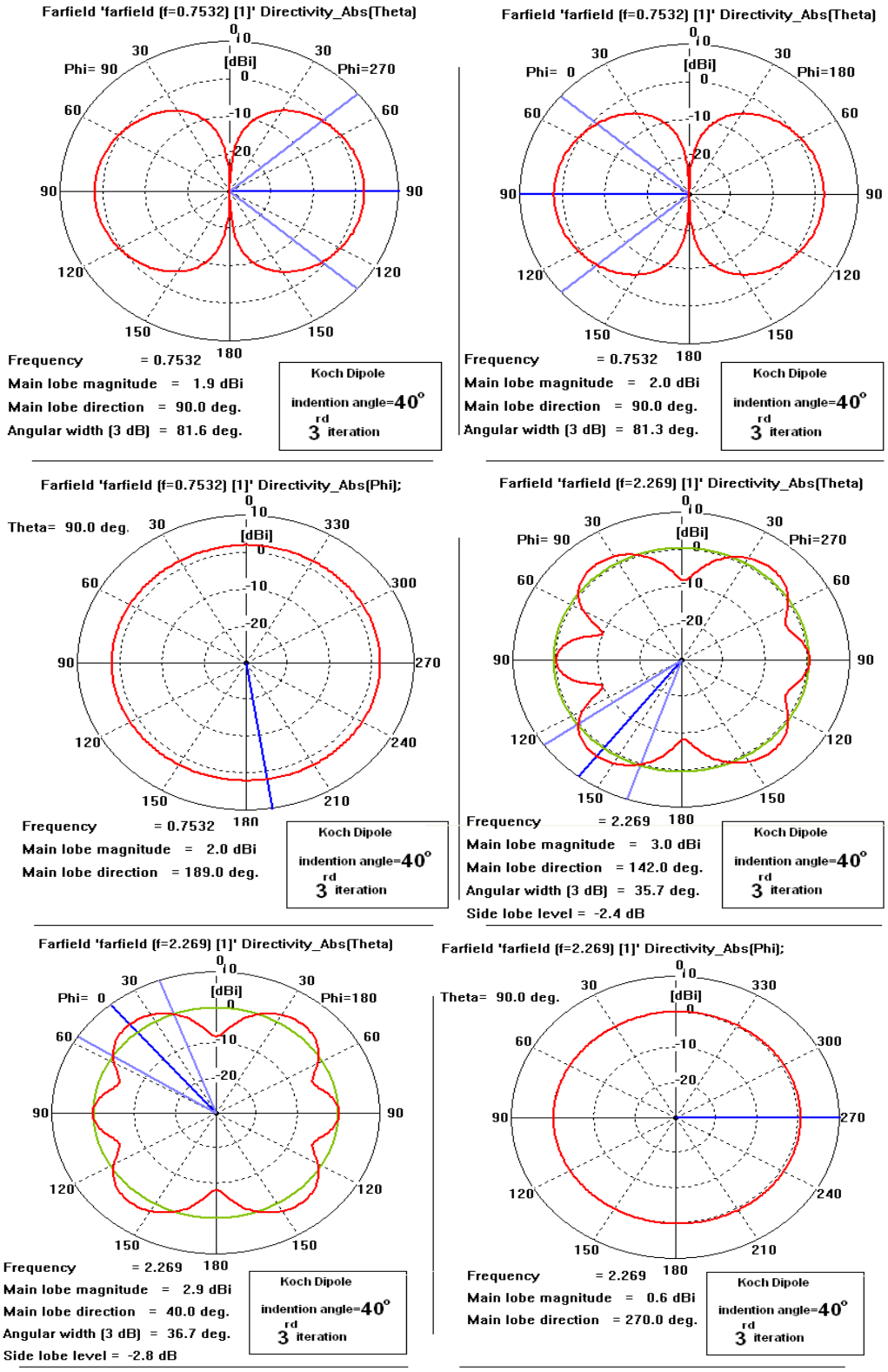

Figure 4.13 Simulation results for radiation patterns of the strictly self similar Koch curve dipole antennas with θ= 40º of 3rd iteration at 1st and 2nd resonance frequencies.

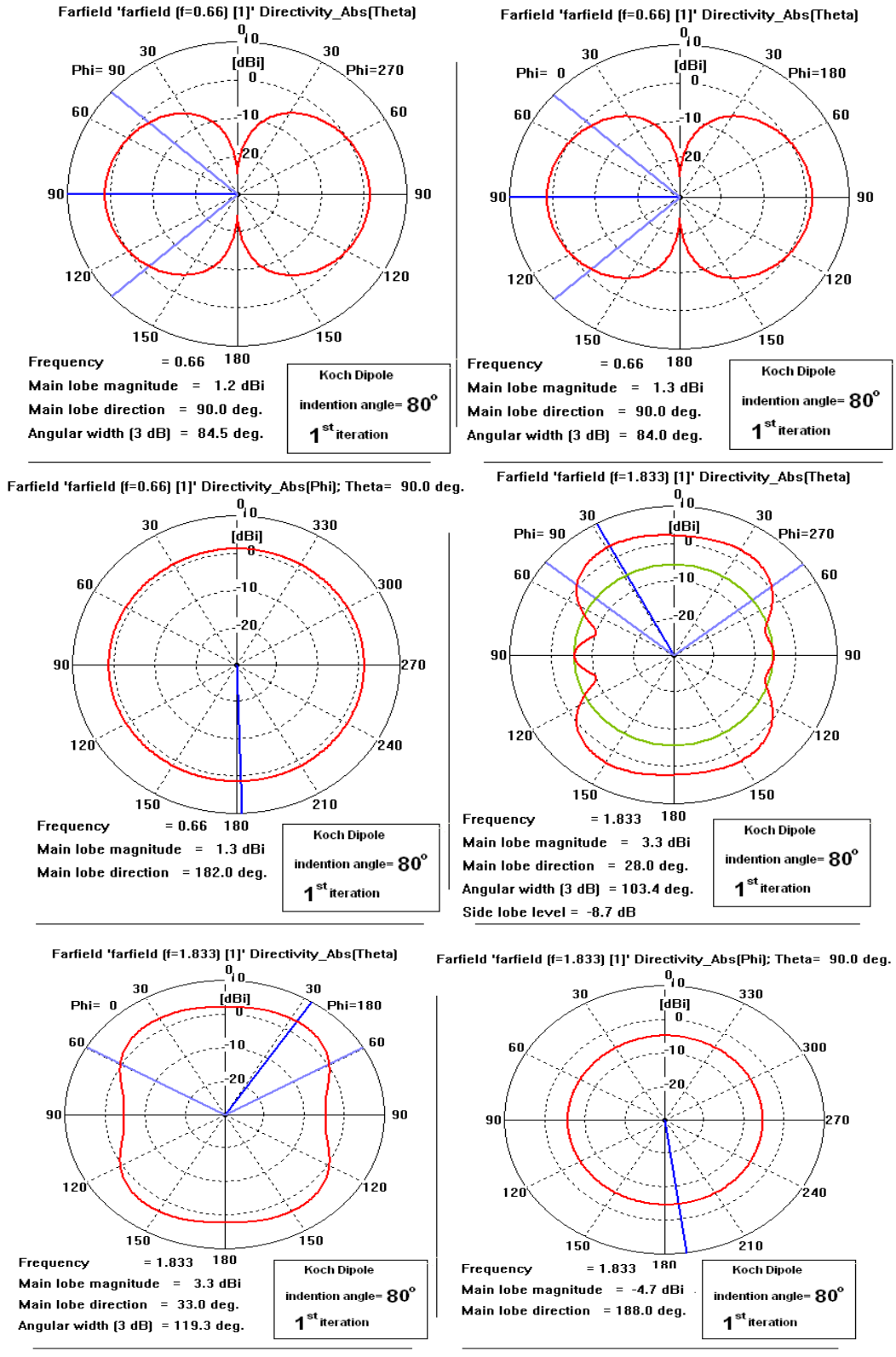

Figure 4.14 Simulation results for radiation patterns of the strictly self similar Koch curve dipole antennas with θ= 80º of 1st iteration at 1st and 2nd resonance frequencies.

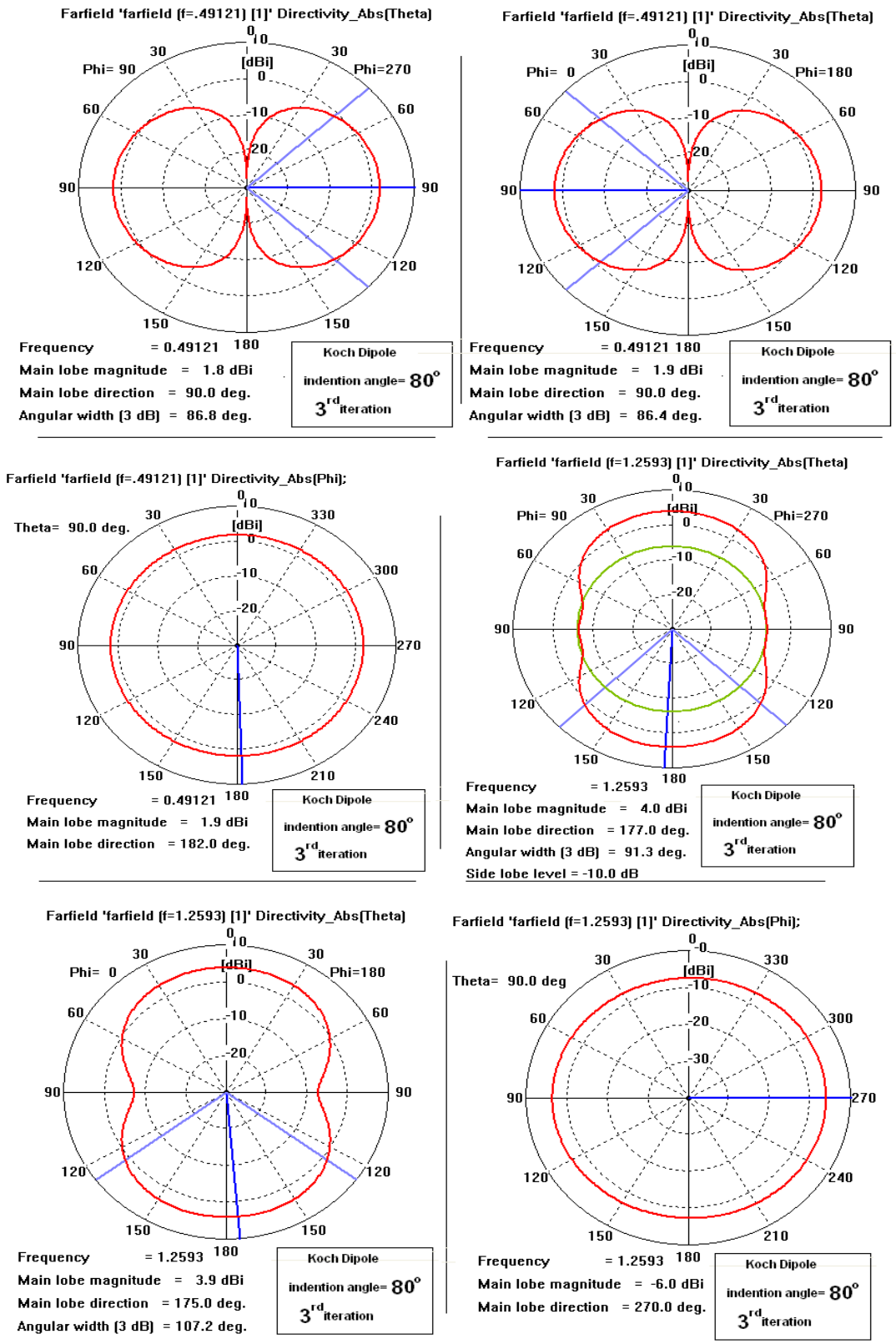

Figure 4.15 Simulation results for radiation patterns of the strictly self similar Koch curve dipole antennas with θ= 80º of 3rd iteration at 1st and 2nd resonance frequencies.

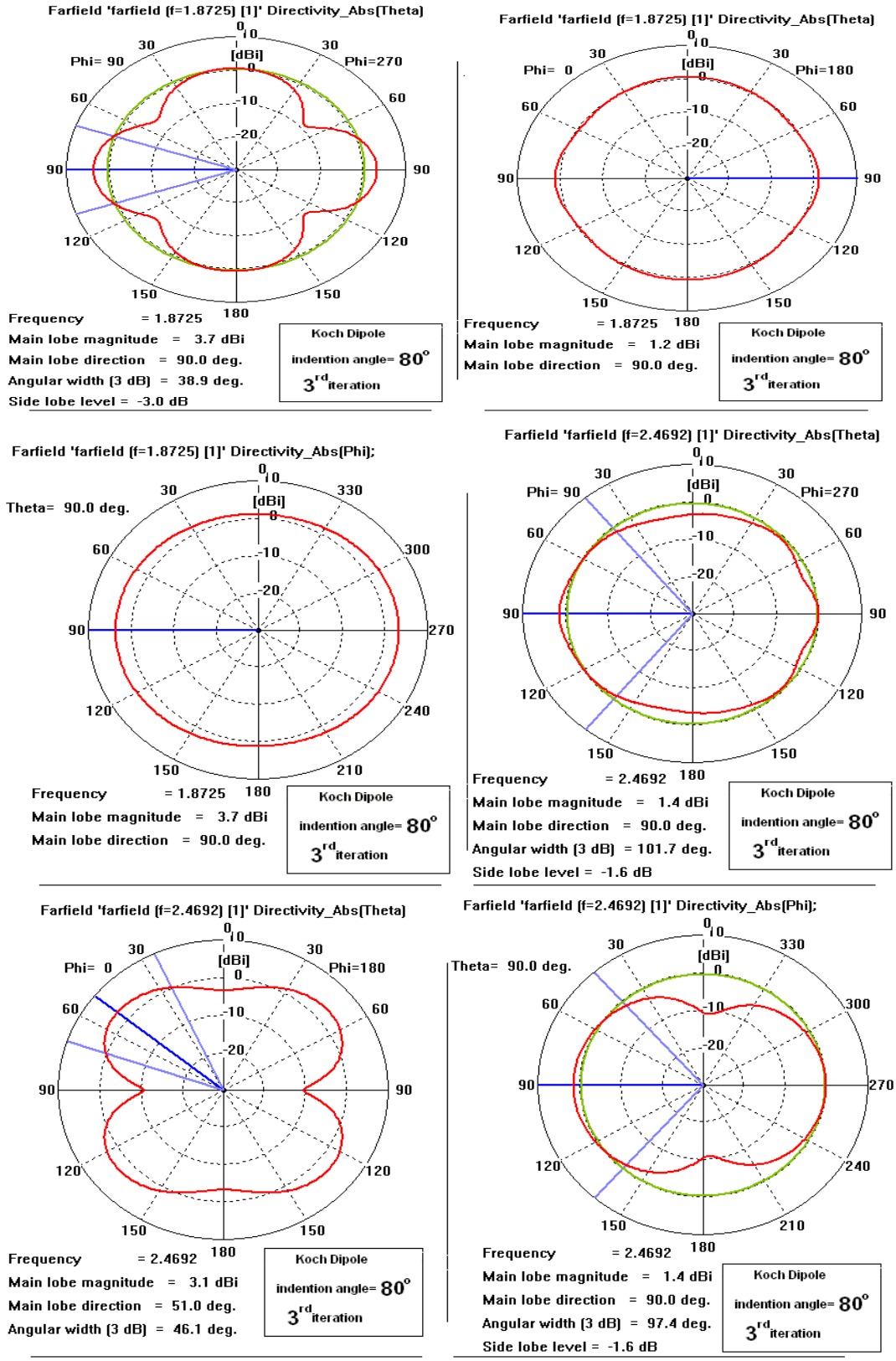

Figure 4.16 Simulation results for radiation patterns of the strictly self similar Koch curve dipole antennas with θ= 80º of 3rd iteration at 3rd and 4th resonance frequencies.

4.2.4 Simulation Results for Radiation Patterns and Current Distribution over the Antennas:

In Figures (4.11-4.16) the far field radiation patterns in polar forms (two elevation cuts, xz and yz planes; azimuth cut, xy plane) are illustrated (Only co-polarization is considered).

In Figure 4.11, the radiation patterns of linear dipole with overall length equal to 16 cm, are displayed at 1^{st} and 2^{nd} resonance frequencies; for 1^{st} resonance, symmetrical omnidirecitonal radiation pattern is observed, on the other hand high level side lobes are observed at 2^{nd} resonance since the antenna possess (electrically) length larger than 1λ at 2^{nd} resonance.

In Figure 4.12, the radiation patterns of strictly self-similar Koch dipole with $\theta = 40^{o}$ of 1^{st} iteration is figured for 1^{st} and 2^{nd} resonance frequencies; for the 1^{st} resonance, omnidirecitonal pattern is observed likewise the linear dipole, while at 2^{nd} resonance, the nulls in the elevation cut planes tend to disappear. For yz plane cut radiation pattern exhibits asymmetry. The asymmetry is due to the geometry of the antenna being asymmetrical in yz plane. In Figure 4.13, 3^{rd} iteration is illustrated. The effect of iteration can be observed noticing the 2^{nd} resonance frequencies. The side lobe levels increase more for 3^{rd} iteration.

In Figures (4.14-4.16), the radiation patterns of strictly self-similar Koch dipole with $\theta = 80^{o}$ of 1^{st} and 3^{rd} iterations are figured respectively. In both iterations, for the 1^{st} resonance frequencies the antennas exhibit omnidirecitonal radiation patterns. However, comparing the radiation patterns at 2^{nd} resonance frequencies for both iterations, the side lobe levels decrease, and at the azimuth cut of patterns, the radiation at xy plane (Theta = 90^{o}) decreases. Main lobe of the radiation pattern orients to end fire directions of the antenna. (Theta=0^{o} and Theta=180^{o})

In Figure 4.16, 3^{rd} and 4^{th} resonances of strictly self-similar Koch dipole with $\theta = 80^{o}$ of 3^{rd} iteration are displayed. At 3^{rd} resonance frequency, side-lobes are

observed. Main lobe exists at Theta=90º, and end fire radiation is observed. For indention angle, θ= 80º, the middle segments of the antenna become folded by 100º, and horizontal polarization stands out for that high indention angled antennas, when their radiation patterns at 2nd or further iterations are surveyed. For 4th resonance, this effect is observed clearly as there exits a null point at Theta=90º for xz cut of the radiation pattern. For yz cut, where the Koch geometry lies, the nulls almost disappear due to the current distribution of the antenna. The current in y direction does not completely cancels out anymore.

To associate the radiation patterns with the surface current distribution of the antenna for the frequencies and geometrical configurations mentioned above, magnitude of tangential component of the current distributions over the antennas are plotted in Figures (4.17-4.22). For the 1st resonance frequencies, the current distribution over the antenna seems to be sinusoidal with maximum at the center (feed), however for further resonance frequencies, the current standing wave patterns undergo 180º phase reversal before reaching end points. As a result, the current in all parts of the antenna does not have same phase.

Moreover, in Figure 4.20, for the 1st resonance frequency of strictly self-similar Koch Dipole of 1st iteration with θ=80º, the current standing wave pattern does not undergo phase reversal and due to high indention angle, the middle segments of the antenna are closely located. Cancellation of the opposite currents in these segments can be seen in the figure.

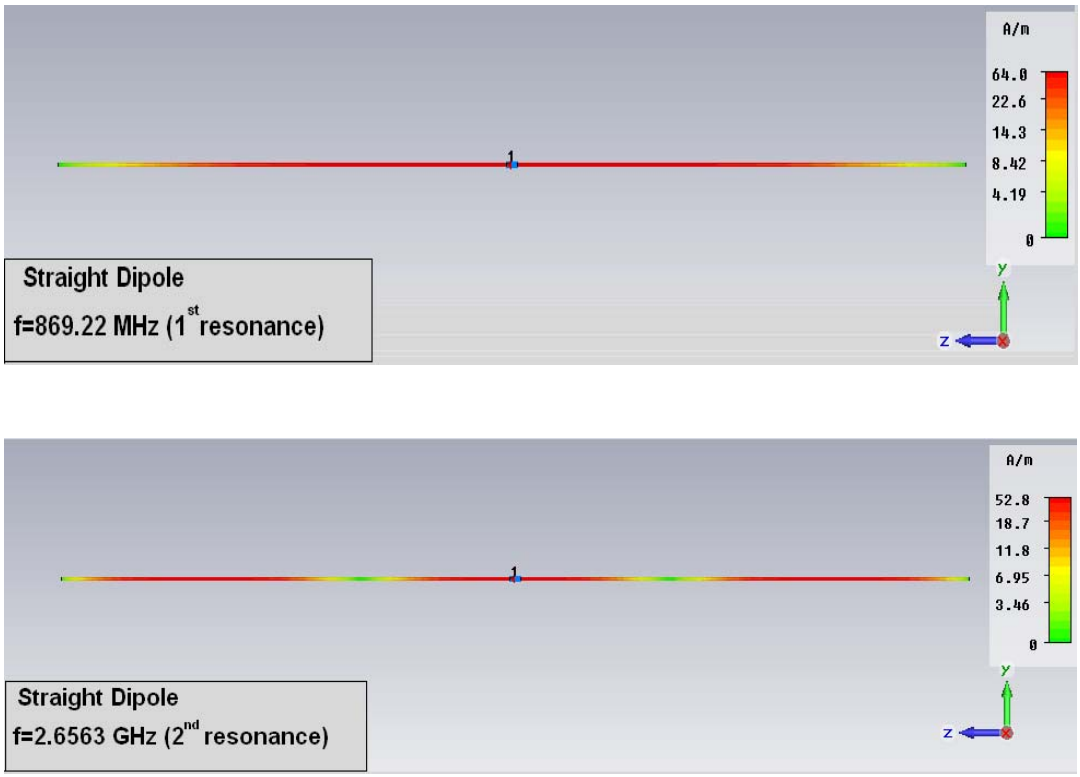

Figure 4.17 Simulation results for current distribution over straight dipole at 1st and 2nd resonances

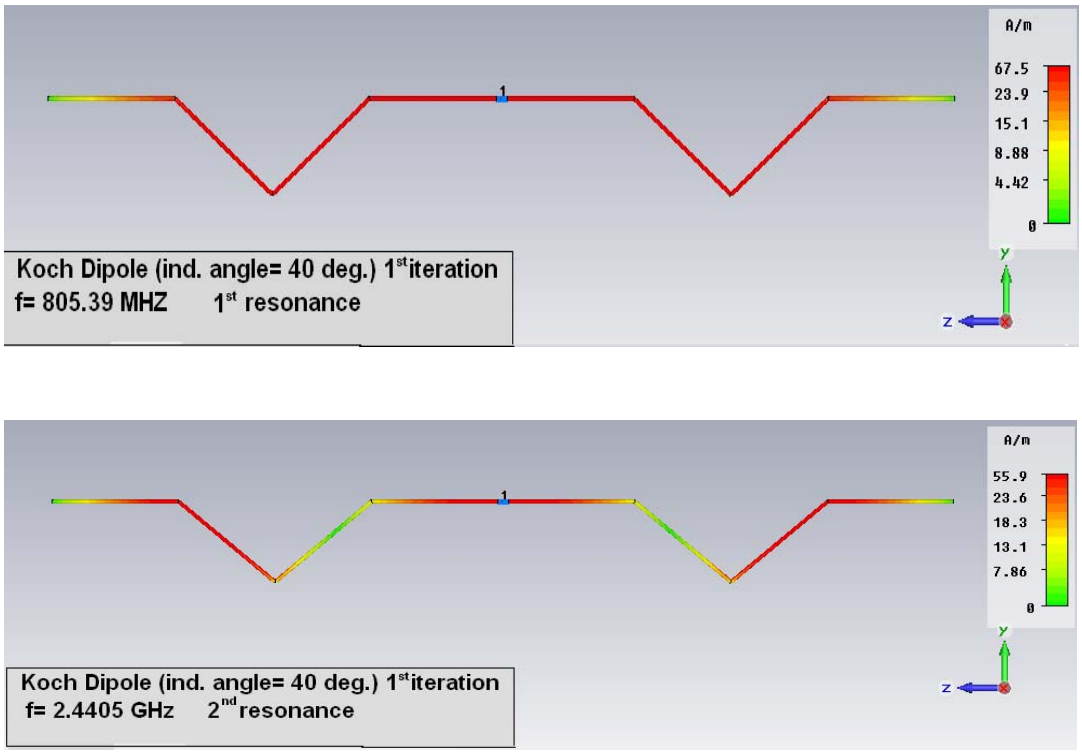

Figure 4.18 Simulation results for current distribution over strictly self-similar Koch Dipole of 1st iteration with θ=40º at 1st and 2nd resonances

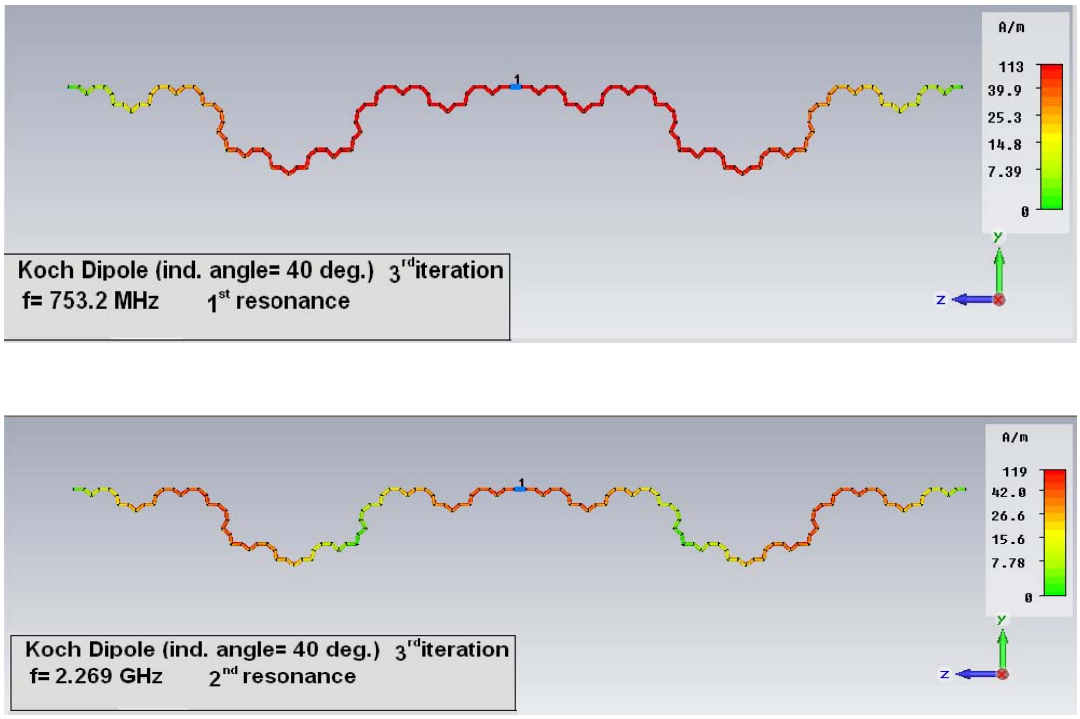

Figure 4.19 Simulation results for current distribution over strictly self-similar Koch Dipole of 3rd iteration with θ=40º at 1st and 2nd resonances

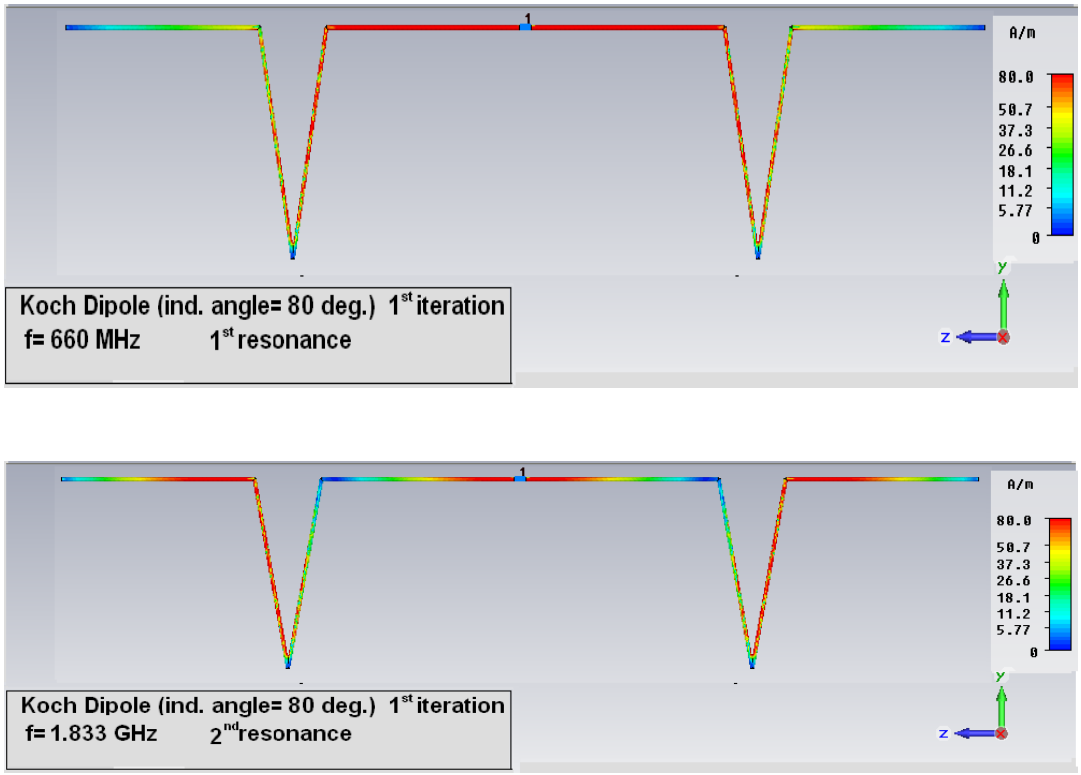

Figure 4.20 Simulation results for current distribution over strictly self-similar Koch Dipole of 1st iteration with θ=80º at 1st and 2nd resonances

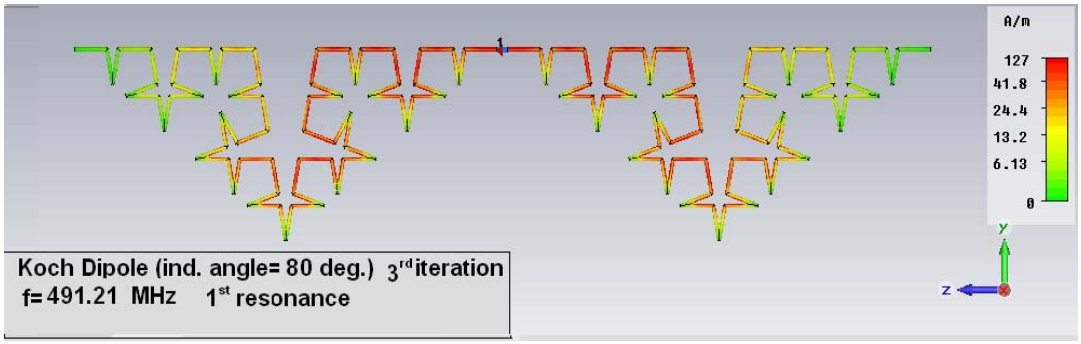

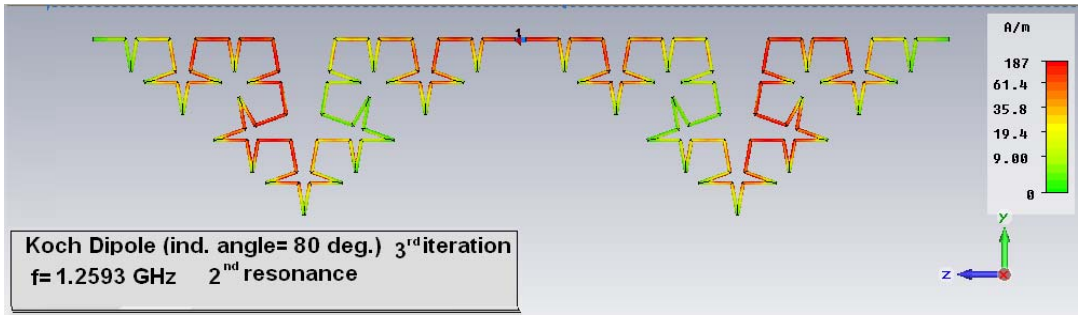

Figure 4.21 Simulation results for current distribution over strictly self-similar Koch Dipole of 3rd iteration with θ=80º at 1st and 2nd resonances

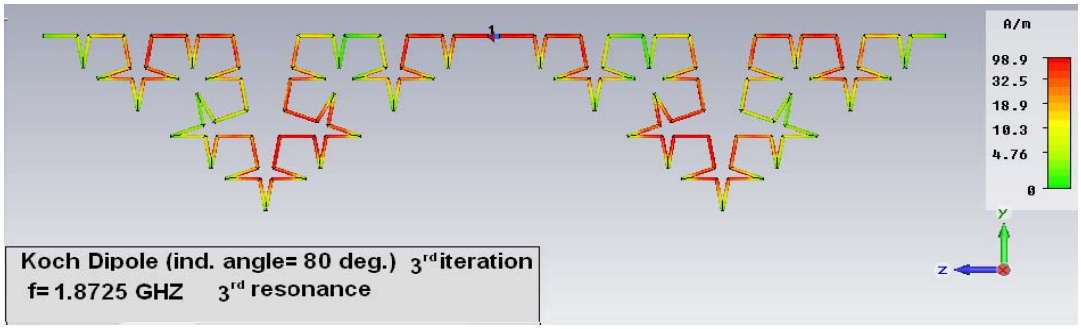

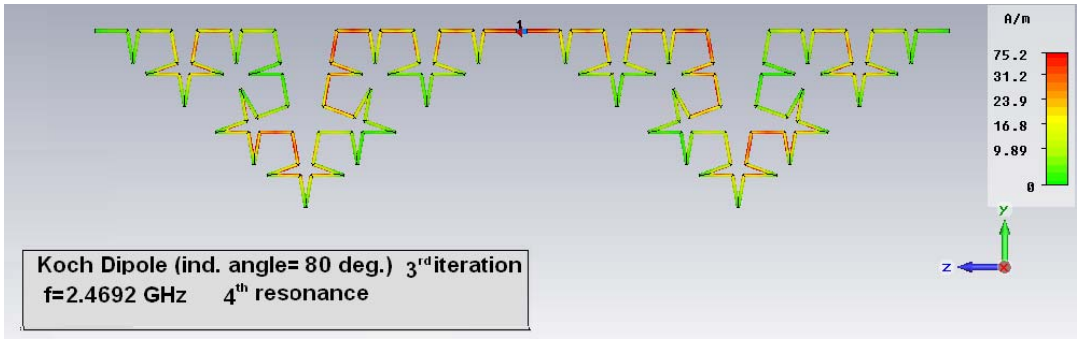

Figure 4.22 Simulation results for current distribution over strictly self-similar Koch Dipole of 3rd iteration with θ=80º at 3rd and 4th resonances

4.2.5 Simulation Results for the Normalized Electrical Length of Antennas:

The relation between current distribution, 1st resonance frequency and fractal iteration was studied in [8] for the standard Koch curve monopole antenna. In [8] two definition were made; "the physical length of the antenna (l_p), as total length of the antenna normalized to its height, $l_p = (4/3)^n$ (n is the iteration number) and the normalized electrical length of the antenna, l_e, as the normalized physical length that a linear monopole antenna should have its 1st resonance at the same frequency of a given Koch monopole, that is defined as $l_e = (4/3)^n \frac{f_r^0}{f_r^n}$, where f_r^n and f_r^0 are resonant frequencies of the K_0 (linear monopole) and K_n (n^{th} iterated standard Koch monopole) antennas, respectively." [8]

In this thesis, this formula is generalized for the generalized strictly self-similar Koch dipole antennas. As a result, in this case l_p is modified as $l_p = \left(2/[1+\cos\theta]\right)^n$

The Figures (4.23-4.26), shows the l_e and l_p relation for the first three iterations of the strictly self similar Koch dipoles whose resonance frequencies are tabulated in Table 4.2. Apparently, the electrical length does not increase at the same rate that the physical length increases. Moreover, the electrical length tends to saturate to a limiting value even if the physical length increases exponentially for each iteration. In [8], this phenomenon was attributed the exponentially growth of number of segments as the fractal iteration increases.

Considering Figure 4.27, where the ratio of normalized electrical length to normalized physical length of generalized Koch dipoles with various indention angles as a function of iteration number is plotted, for θ=20º the ratio deviates the least over the iterations. This can be related to possessing less complex geometry of dipoles with low indention angles compared to those with high indention angles.

In [12] for Meander line and Hilbert curve dipoles the effect of current distribution in lowering the resonant frequency was discussed. "It was demonstrated that highly

compressed meandered space-filling geometries such as self-similar fractals, are less effective at lowering resonant frequency. The space-filling nature of the Hilbert curve fractal geometry was shown to be at an inherent disadvantage in terms of lowering resonant frequency because of the high degree of meandering and wire compression associated with the fractal curve. The primary disadvantage of the space-filling fractal based geometry is the high degree of coupling between parallel wires with opposite current vectors causing a significant reduction in the effective length of the total wire within each arm. Arrangement of wire in a less compressed simpler geometry offers significant advantages in achieving lower resonant frequencies."[12]

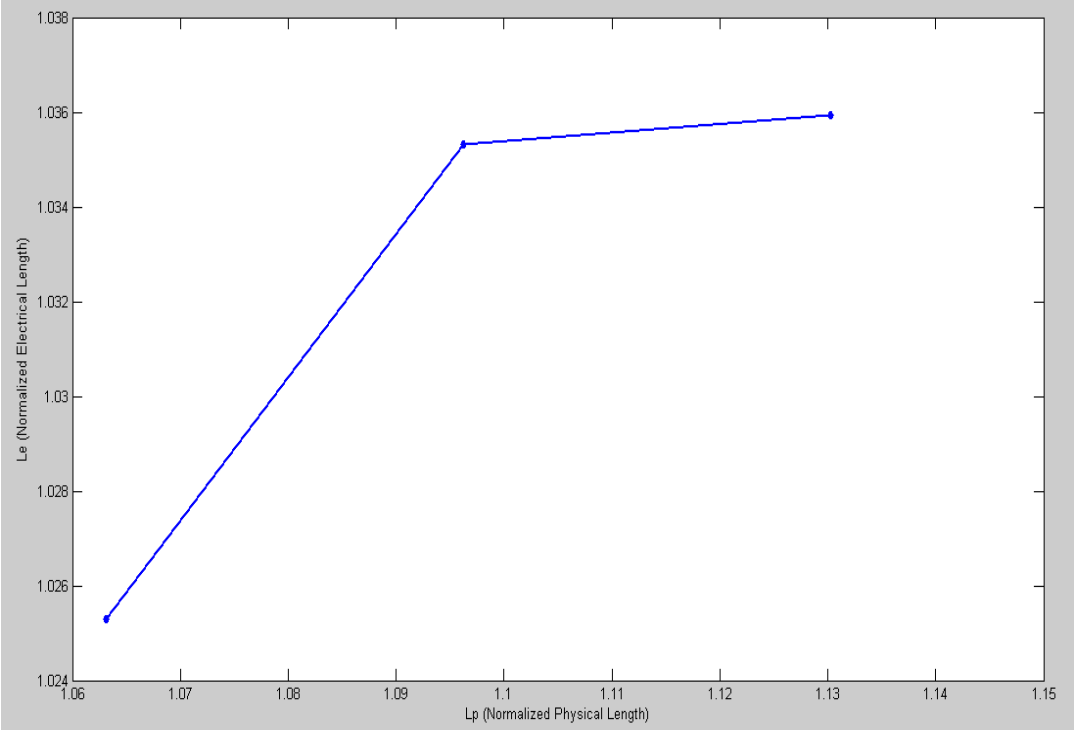

Figure 4.23 l_e vs. l_p relation for first three iteration levels of the generalized Koch dipole with indention angle 20º

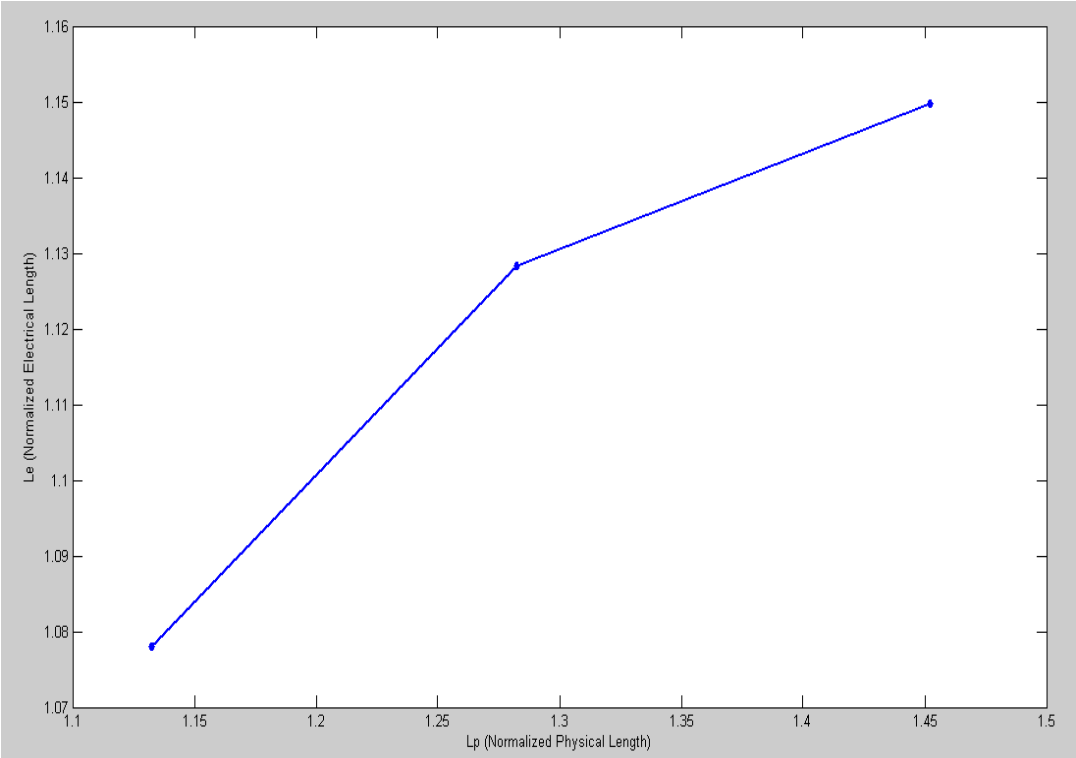

Figure 4.24 l_e vs. l_p relation for first three iteration levels of the generalized Koch dipole with indention angle 40º

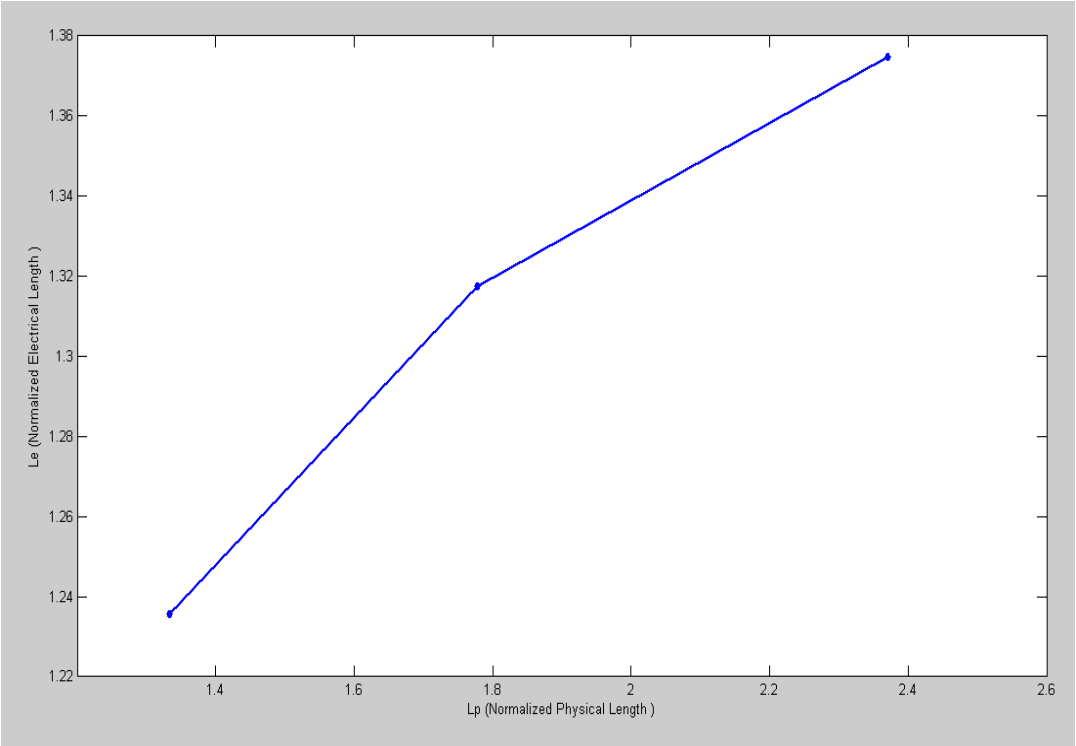

Figure 4.25 l_e vs. l_p relation for first three iteration levels of the generalized Koch dipole with indention angle 60º

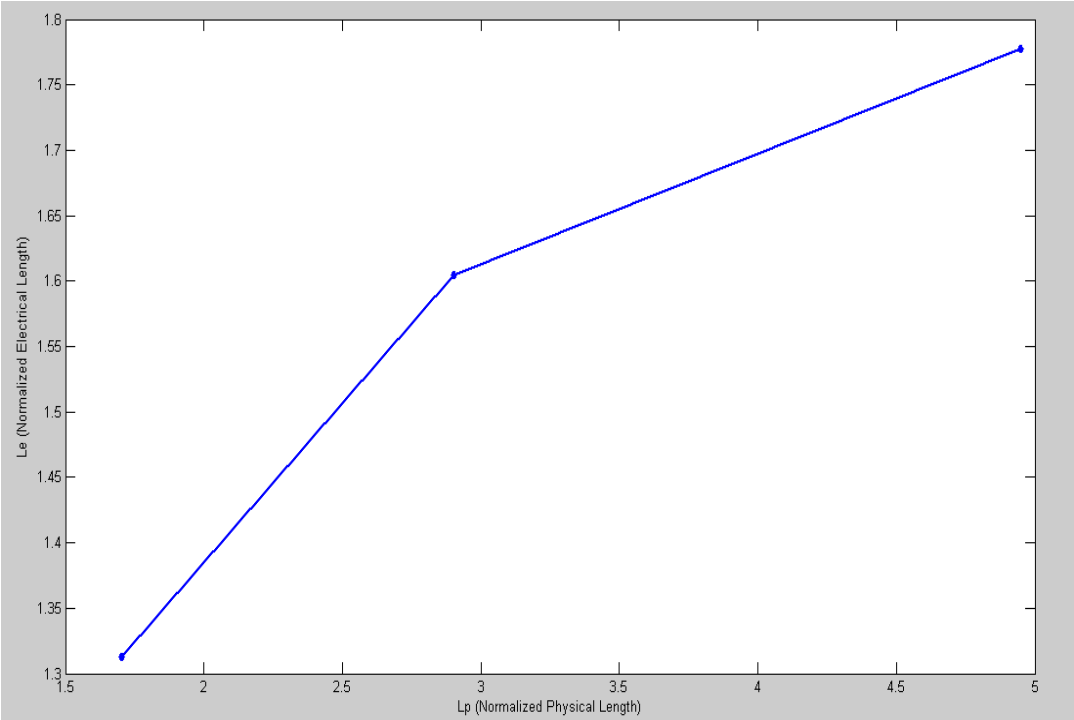

Figure 4.26 l_e vs. l_p relation for first three iteration levels of the generalized Koch dipole with indention angle 80º

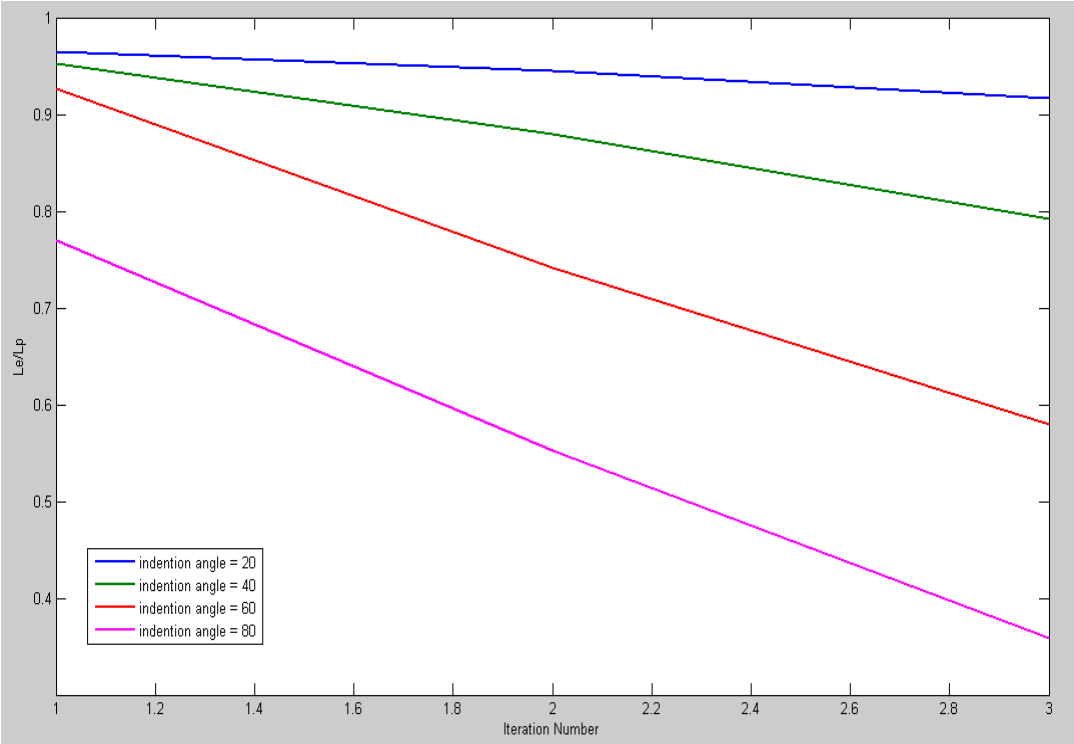

Figure 4.27 l_e/l_p with iteration levels of the generalized Koch dipole with various indention angles. (Only integer numbers in x-axis are to be considered)

A strictly self similar Koch dipole with θ=80º of 3rd iteration with current distribution is illustrated in Figure 4.21. Due to high space filling of the geometry, the segments are closely oriented. Since the segments are not parallel oriented, the coupling between parallel lines is not expected as highly as in the case of Hilbert curve, whose indention angle is, indeed, 90º. However, the performance properties of strictly self similar Koch dipoles with high indention angles are doubtful. Total overall length of the antenna (perimeter) being large, the loss resistance of the antenna becomes large.

CHAPTER 5

PERFORMANCE OF MODIFIED AND NOT STRICTLY SELF SIMILAR KOCH ANTENNAS

Recalling the equation (2.1), the fractal dimension, D of any fractal as a measure of Hausdorf-Besicovich dimension can be found as;

$$k_1\left(\frac{1}{h_1}\right)^D + k_2\left(\frac{1}{h_2}\right)^D + \ldots\ldots\ldots + k_m\left(\frac{1}{h_m}\right)^D = 1$$

The studies on strictly self similar Koch type antennas showed that incrementing indention angle also increases D. According to the results in [9], it was asserted that D is an important design parameter since increase in D yields lower resonance frequencies. Later, in [31] another variant of Koch monopoles with dimensions smaller than the conventional Koch monopoles were studied.

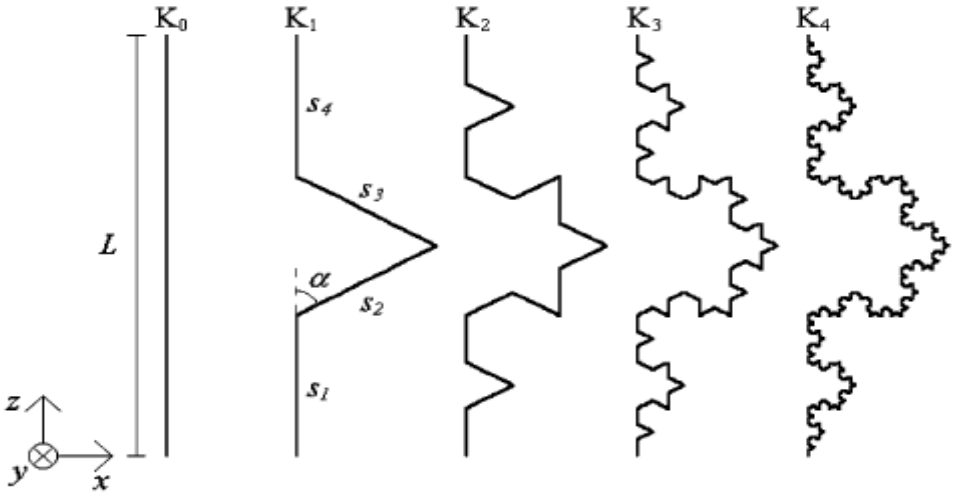

Figure 5.1 The modified Koch generation in [31]

The generation of the modified Koch curve in [31] is illustrated in Figure 5.1. In this configuration $s_1=s_4$, and $s_3=s_2$; for the 1st iteration s_1 and s_4 are kept 1/3 of the

initial length L, as in the case of standard Koch curve generation of 1st iteration. However, indention angle is varied, resulting s_3 and s_2 segments being dependent on α (or θ, as indention angle is represented throughout this thesis). In [31] based on the results, it was observed that when α, consequently D is increased, the resonances appeared in lower frequencies.

5.1 Performance of Simulated Koch Curve Antennas with Not strictly Self-Similar Geometry

In this part of the thesis, the relation of D with lowering the resonance frequency is reexamined for another modified Koch curve antenna generated in this thesis. The definition of D is calculated in the realms of Hausdorf-Besicovich dimension (equation (2.1)) which is used both in [31] and [35].

The modified Koch curve is generated from an initiator of 8 cm length. As in [31] $s_1=s_4$, and $s_3=s_2$, however s_2 is dependent on s_1, via the formulation of $\arctan\theta = \frac{s_1}{4-s_1}$. Four different types of the curve are investigated as antenna configuration by varying s_1 from 0.5 cm to 3.5 cm with 1 cm increment for each type. Only 1st iteration is studied since for further iterations, implementation becomes a serious problem. The curves are illustrated in Figure 5.2. The curves are also labeled as A, B, C and D.

The antennas are configured as dipole antennas with end to end height of 16 cm like other Koch types studied in this thesis. (Geometries in Figure 5.2 are utilized as one arm of the dipole) The antennas are simulated at CST MWS® simulation tool for the frequency range of 0 to 3 GHz. The antenna is modeled with PEC wires with radius of 0.15 mm for each type.

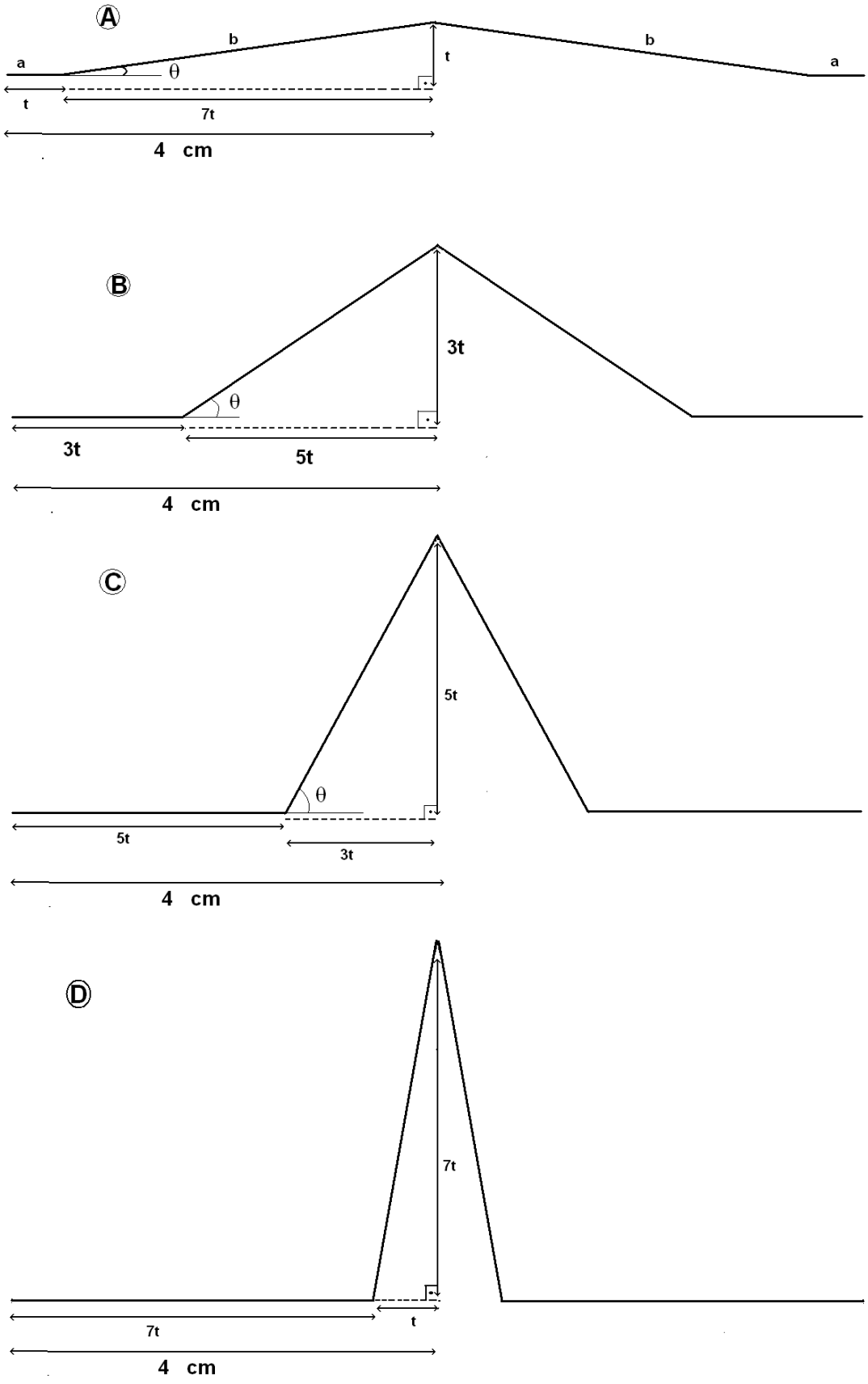

Figure 5.2 Geometry of modified Koch curves

For simulation, the mesh type is selected as hexahedral; the mesh line per wavelength is set 30, lower mesh and mesh line limits are both chosen as 15. The PEC metal edges are refined with factor 5 to increase the accuracy of simulation.

Generation of Modified Koch Geometry Antennas:

$$k_1\left(\frac{1}{h_1}\right)^D + k_2\left(\frac{1}{h_2}\right)^D + \ldots\ldots\ldots + k_m\left(\frac{1}{h_m}\right)^D = 1$$

For these modified Koch curves the formula above can be arranged as;

$$k_1\left(\frac{1}{h_1}\right)^D + k_2\left(\frac{1}{h_2}\right)^D = 1 \qquad (5.1)$$

since $s_1=s_4$, and $s_3=s_2$, $k_1=k_2=2$;

and $h_1 = \frac{s_1}{8}$ and $h_2 = \frac{\sqrt{s_1^2 + (4-s_1)^2}}{8}$

D is calculated in MATLAB® using numerical methods.

Table 5.1 Geometrical properties of modified Koch curve

GEOMETRY LABEL	θ (º)	S_1 (cm)	S_2 (cm)	TOTAL LENGTH (cm)	D
A	8.13	0.5	3.5355	16.142	5.6159
B	30.96	1.5	2.9154	17.6616	2.6840
C	59.04	2.5	2.9154	21.6616	3.6230
D	81.87	3.5	3.5355	28.142	10.8016

Simulation results for the return loss (dB) of Modified Koch Geometry Antennas:

The return losses of the modified antennas in dB scale are given in Figure 5.3, similar to the return loss results in the previous chapter; as the indention angle increases the resonance frequencies are lowered. However, the relation asserted in [9], [31] between D and lowering the resonance frequency does not hold in this case. Because Antenna-A has higher fractal dimension than Antenna-B and antenna-C, however, both resonance frequencies (1st and 2nd) of Antenna-B and Antenna-C are lower than those of Antenna-A.

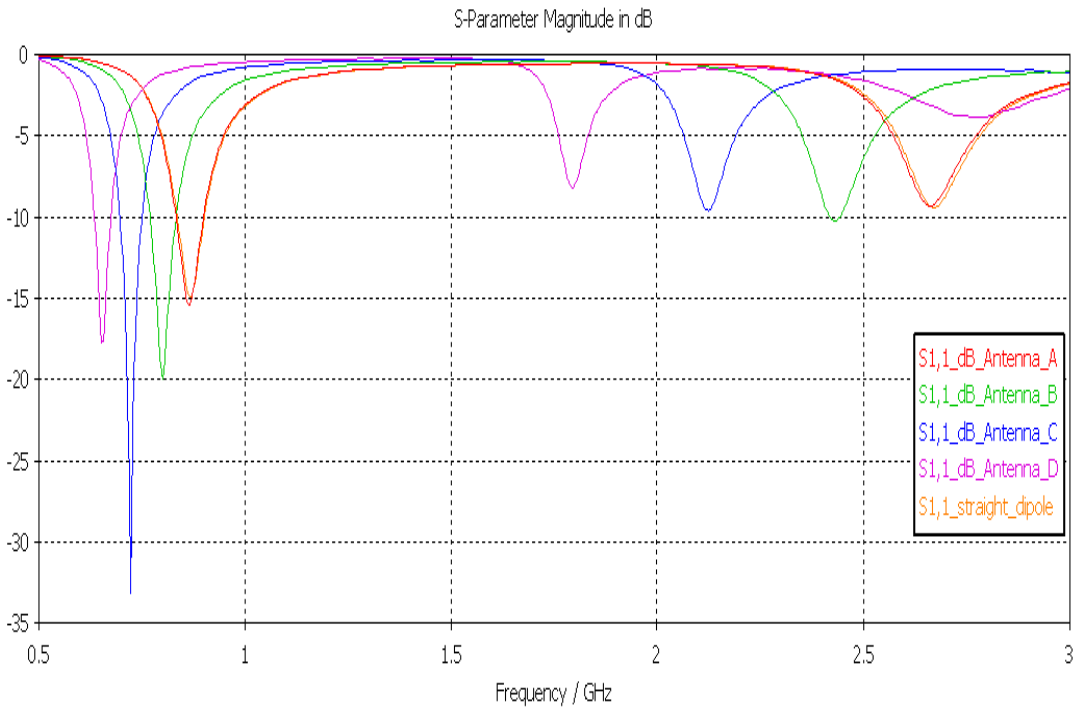

Figure 5.3 The simulation results for the return losses of Modified Koch Antenna for the 1st iteration

Table 5.2 Simulation results for the resonance frequencies of modified Koch antennas

GEOMETRY LABEL	θ (°)	1st Resonance Frequency (GHZ) [f_r^1]	2nd Resonance Frequency (GHZ) [f_r^2]	f_r^2 / f_r^1
Linear Dipole	------	0.8674	2.6742	3.083
A	8.13	0.8584	2.6667	3.106
B	30.96	0.7981	2.42	3.032
C	59.04	0.7228	2.1241	2.9408
D	81.87	0.6605	1.7934	2.7152

Looking at Table 5.2 and Table 4.2 the modified Koch dipoles and 1st iterations of the strictly self similar Koch dipoles exhibit similar radiation properties for very close indention angles and total length. For example, total length of Antenna-D is 28.142 cm and the total length of strictly self similar Koch dipole with indention angle 80º of 1st iteration is 27.26 cm; the 1st and 2nd resonance frequencies of the former are 0.6605 GHz and 1.7934 GHz respectively and for the latter 0.6608 GHz and1.8394 GHz respectively.

In Figures (5.4-5.5), the simulation results for radiation patterns of the antennas listed in Table 5.2 are illustrated for the 2nd resonance frequencies. The patterns exhibit similar characteristics like the antennas of 1st iteration in chapter 4 for close indention angles in Table 5.2 and Table 4.2

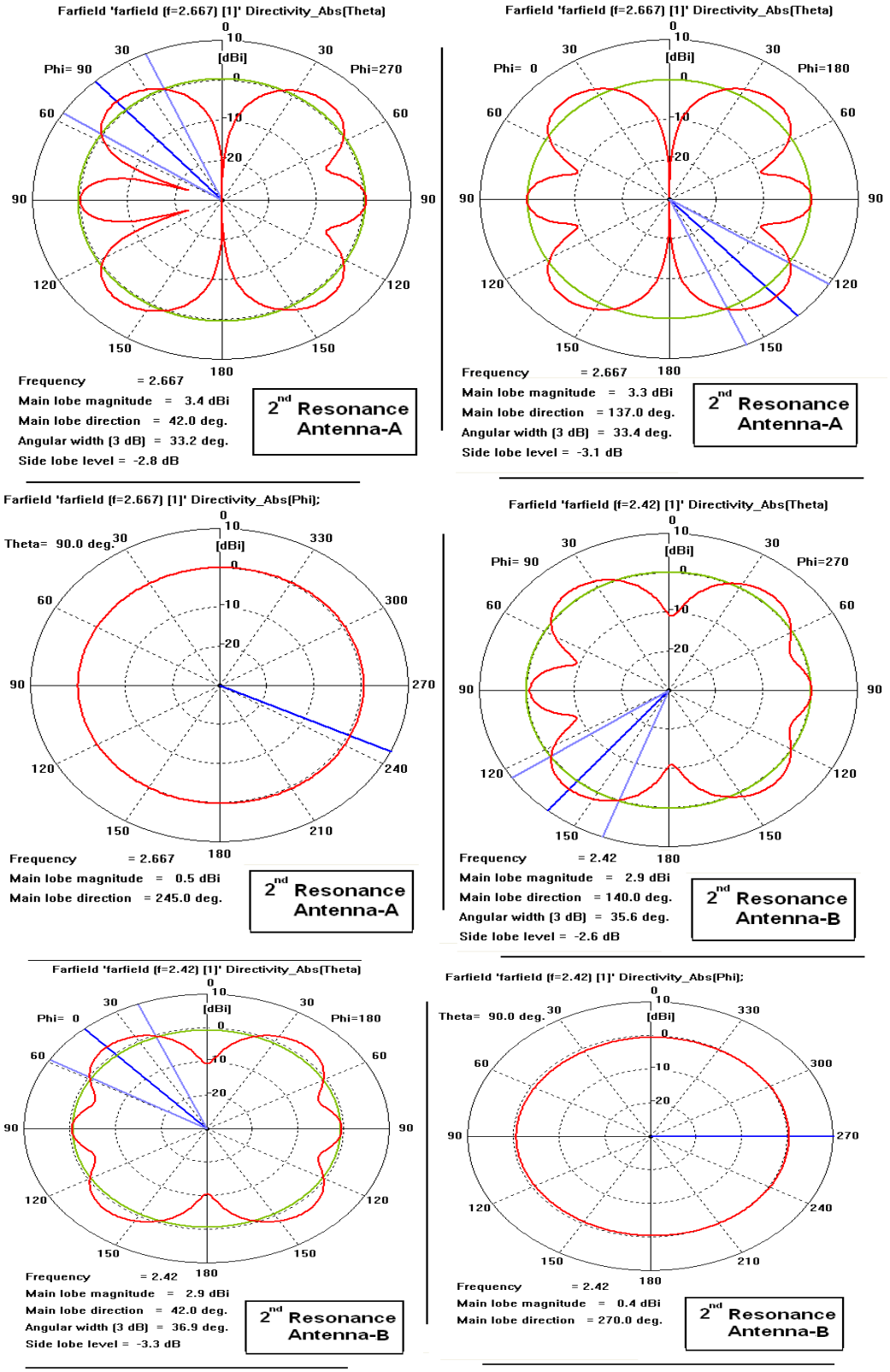

Figure 5.4 The simulation results for radiation pattern of Antenna-A and Antenna-B for both 1st and 2nd resonance frequencies.

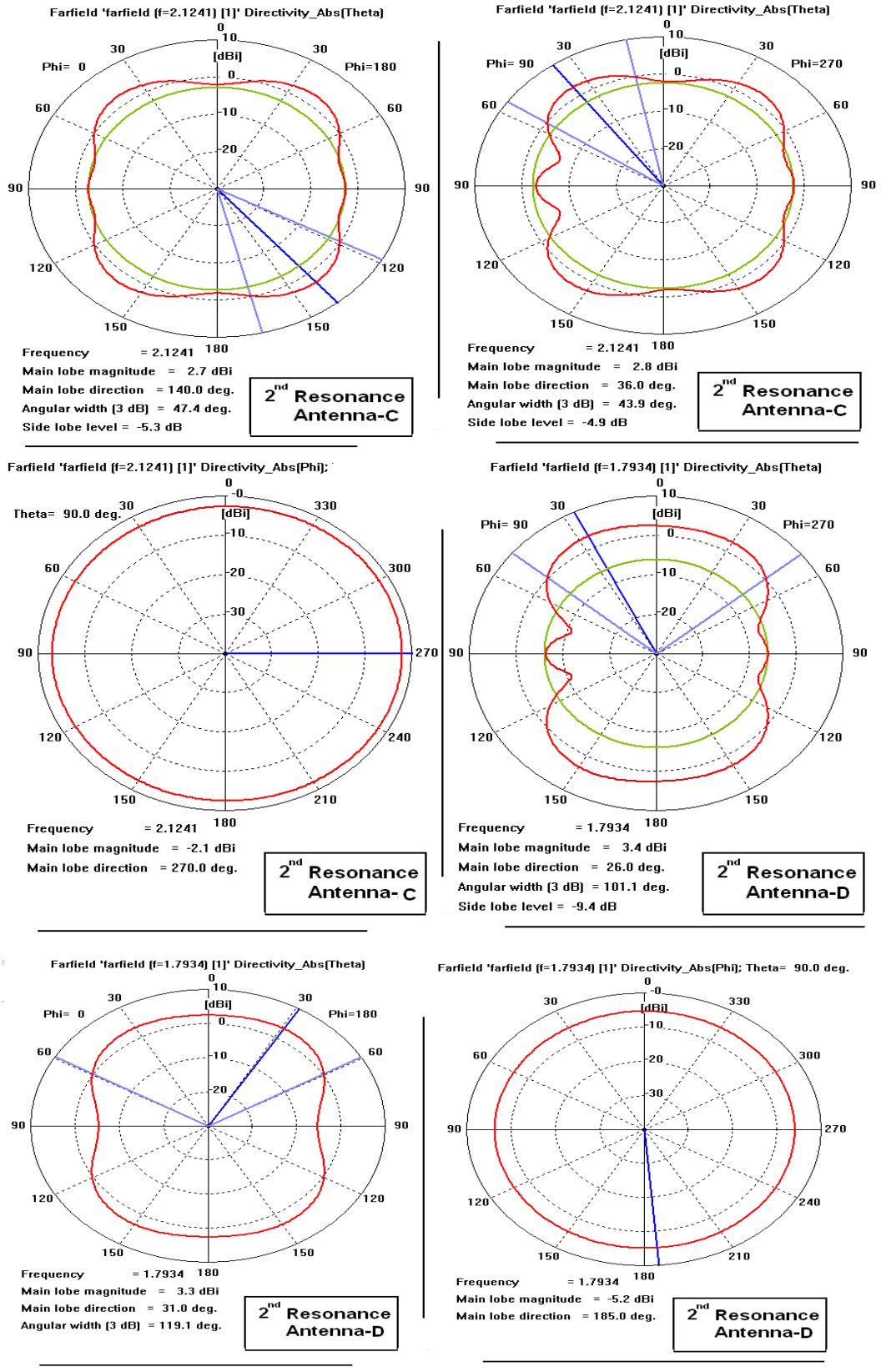

Figure 5.5 The simulation results for radiation pattern of Antenna-C and Antenna-D for both 1st and 2nd resonance frequencies.

5.2 Performance Results of the Koch Curve Antenna Modified by Varying Indention Angle

In previous chapters the effect of iteration and indention angle over antenna radiation properties were discussed. In a standard IFS the scaling factor which is a function of indention angle θ, remains same (see equation (3.6)), passing from one iteration to next iteration.

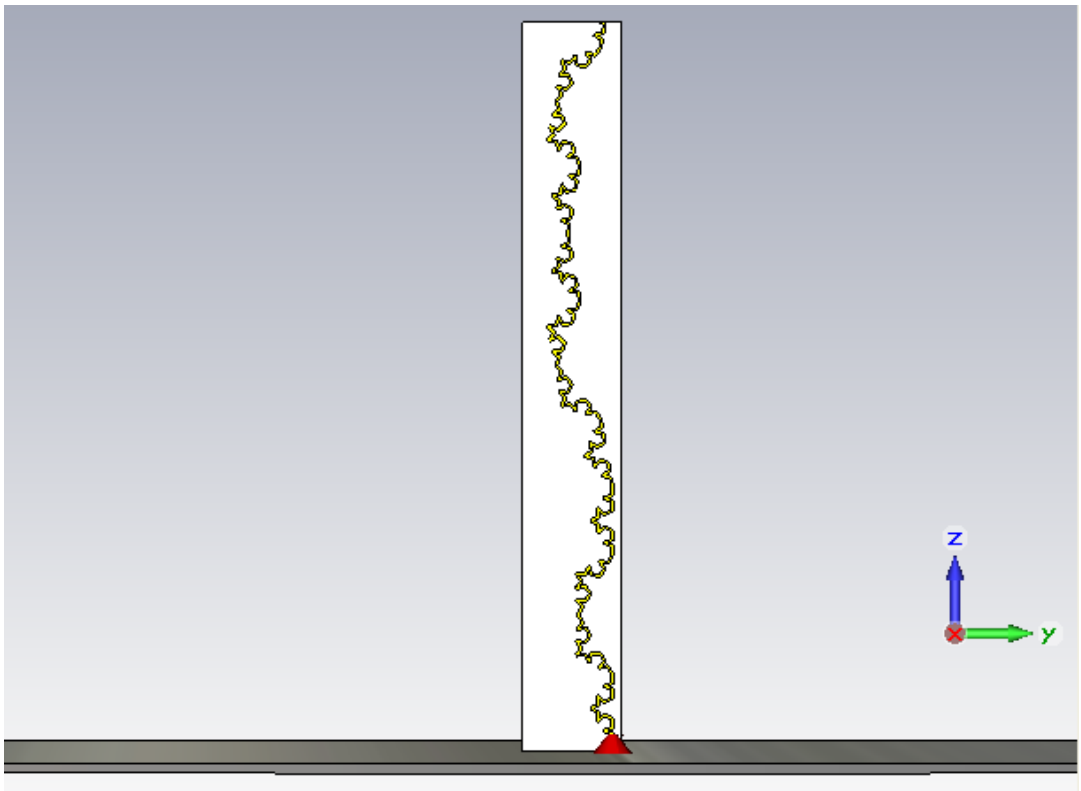

Figure 5.6 The view of simulation model of Koch monopole antenna with varying indention angles

Generation of the curve that is utilized in antenna in Figure 5.6 can be explained starting from the segments yielded in higher iterations (the details of the curve), then noticing how these segments forms the whole curve. Looking through Figure 5.7, may be helpful to visualize the generation of the curve. In Figure 5.7 circled part-A is a standard Koch curve of 2nd iteration. The end to end length (height) of

part A is 7.637 mm. Looking at the circled part-B, one sees that B consists of four copies of part-A, forming a larger Koch curve with indention angle equal to 30º. The last illustration in Figure 5.7, shows how the whole curve is derived form part-B segments. The boundaries of part-Bs are shown by red points P1 and P2, or alternatively P2 and P3. Part-B segments are attached by indention angle 10º.

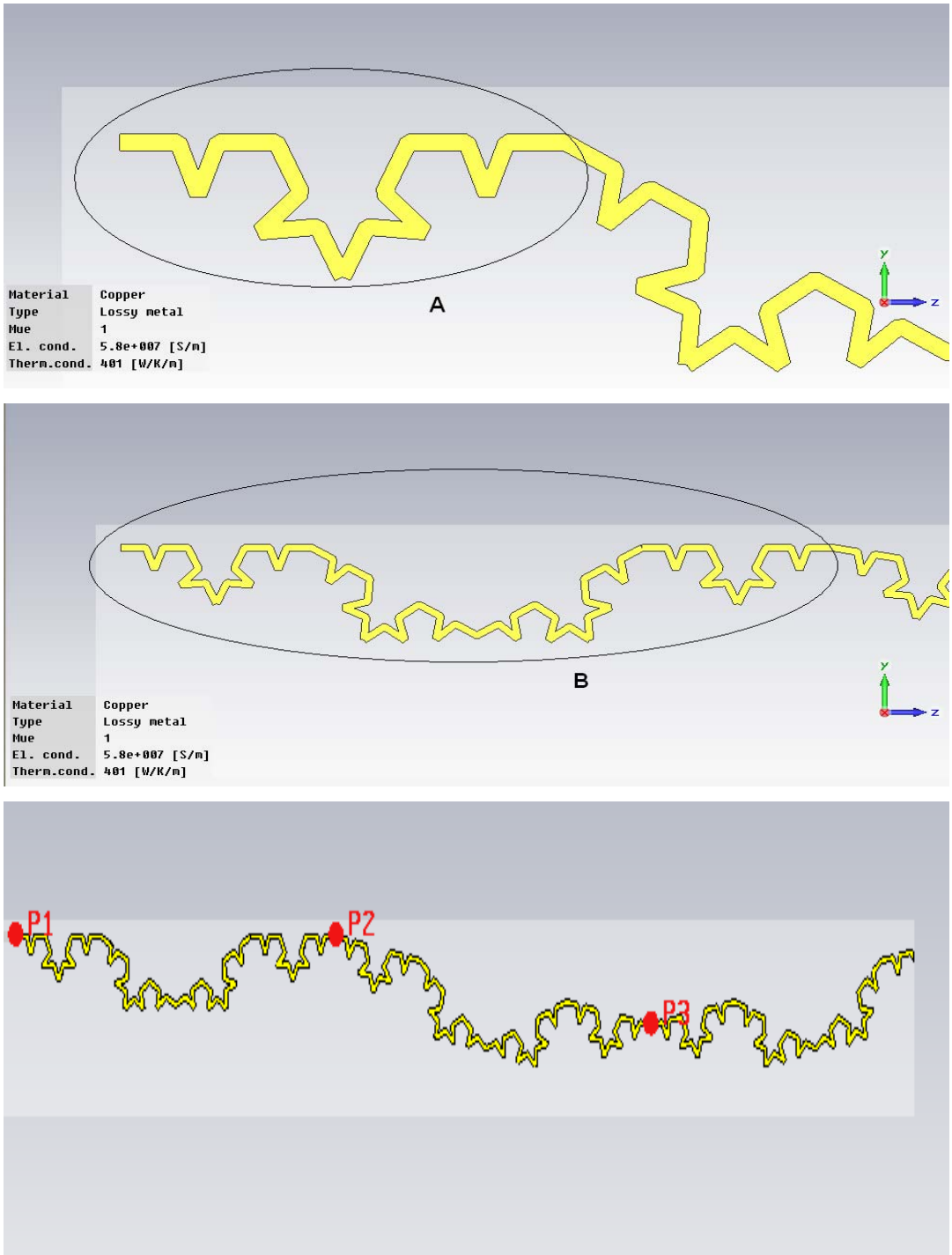

Figure 5.7 Detailed view of Figure 5.6

Notice that, the whole curve does not consist of four equal part-B segments. The curve is truncated where height of the antenna reaches 8 cm. Instead of truncating the antenna; resizing part-A segments of the curve utilized in antenna, would yield smaller segments, and implementation of these segments for practical purpose would be difficult.

The aim of designing such an antenna is to modify the number of resonance frequencies in a given band and closeness of these frequencies one to another.

For both simulation and experimental measurement, the antenna is modeled of lossy copper wire line (electrical conductivity 5.8×10^7 S/m) printed over RO 5880 lossy dielectric material ($\varepsilon_R=2.2$, $\tan\delta=9 \times 10^{-4}$) to yield approximate results obtained in experimental verification. The width of copper line is 0.35 mm and the thickness of the copper line is 0.02 mm. These arrangements are sustained in implementation for experimental verification. For both simulation and practical implementation, the antenna is configured as a monopole antenna, fed by 50 Ohm SMA connector over a circular metallic (Aluminum) ground plane of radius 24 cm. The implemented (printed) antenna is illustrated in Figure 5.9. The simulation is done in CST MWS®, by arranging mesh lines per wavelength as 20, lower mesh limit as 16, and mesh line limit ratio as 14.

The simulation results are compared with the simulation results of a linear monopole of height 8 cm, modeled with same conditions (same wire type, length, thickness, dielectric substrate, etc.) explained in previous paragraph. The performance comparison of the return loss of both antennas in 0-6 GHz can be seen in Figure 5.8. The experimental verification can be seen in Figure 5.10, the return loss of the implemented antenna is measured via Agilent E8358A Network Analyzer in 0.5-6 GHz frequency 1 port calibration.

As seen in Figure 5.8, the linear dipole possess three resonance frequencies in 0-6 GHz range whereas the antenna illustrated in Fig 5.6, posses five resonance frequencies in the same range. It was observed in chapter 4.2 that as the indention

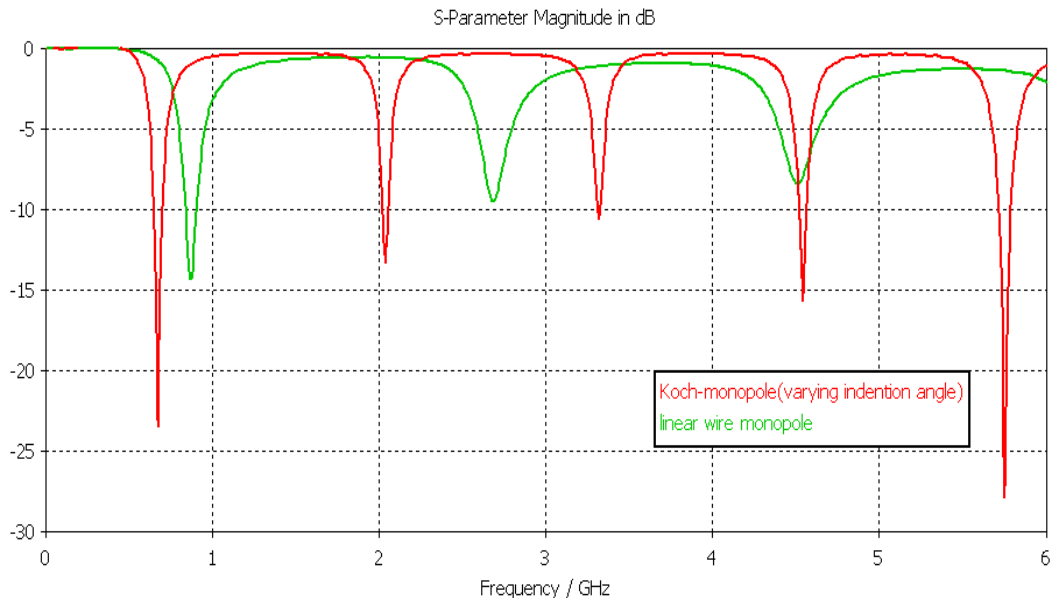

Figure 5.8 The simulation results for the return loss (dB) of linear monopole and Koch monopole antenna shown in Figure 5.6

angle increased for a constant iteration, the rate of decrease in resonance frequency increased.

Koch antenna in Figure 5.6 can be considered as a monopole antenna having fractal geometry generated with an IFS algorithm that indention angle changes for each iteration stage, i.e., indention angle 10º for the 1st iteration, 30º for 2nd iteration and 60º for 3rd iteration. The resonance frequency (primary resonance frequency is 0.7016 GHz) has not lowered as in the case of strictly self similar Koch dipole antenna of 1st iteration with indention angle 80º (primary resonance is 0.6638 GHz) having total length of 27.26 cm. (The overall length of the dipole version of the antenna shown in Figure 5.36 is 35.7 cm). The geometry of the strictly self similar antenna with indention angle 80º of 1st iteration is less complex than that of antenna in Figure 5.36. At Table 4.2, noticing to 1st resonance frequencies of strictly self similar Koch antenna with indention angle 60º of 1st iteration and strictly self similar Koch antenna with indention angle 40º of 3rd iteration, it is seen that the indention angle in 1st iteration determines the rate of decreasing resonance frequency.

The geometry of the antenna in Figure 5.6 has low indention angle for the 1st iteration. Even using further iterations with higher indention angles, performance of lowering the primary resonance frequency of the antenna in Figure 5.6 (note that total length of the antenna exponentially increases as a function of iteration) barely reaches the performance of a less complex self similar Koch antenna with indention angle 60º of 1st iteration monopole antenna, as they possess very close primary resonance frequencies.

The closely distribution of the segments yields high mutual coupling. As a result, the effective electrical length of the antenna decreases.

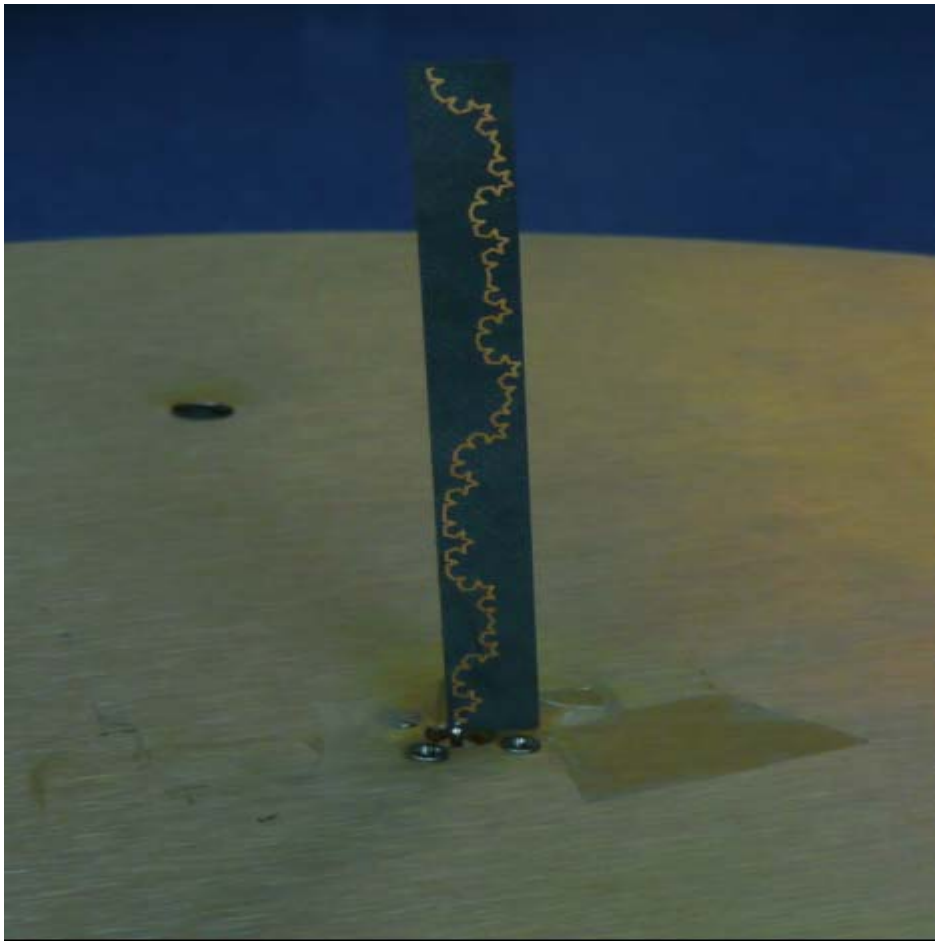

Figure 5.9 Implementation of the Koch monopole antenna in Figure 5.6

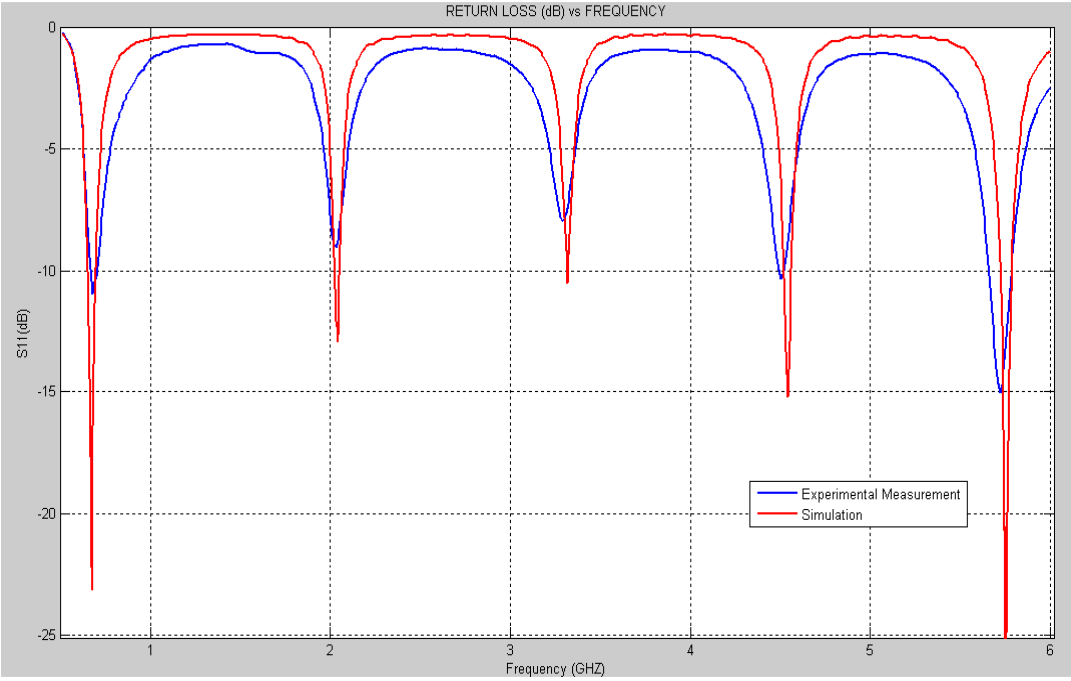

Figure 5.10 Experimental validation of the return loss (dB) Koch dipole antenna shown in Figure 5.6

Table 5.3 The resonance frequency of the antenna illustrated in Figure 5.6

nth Resonance Frequency	Resonance Frequency (GHz)	f_r^{n+1} / f_r^n
n=1	0.7016	2.915
n=2	2.045	1.621
n=3	3.314	1.37
n=4	4.541	1.268
n=5	5.7616	-----

Moreover, as the total length of the wire length increases, the loss resistance increases. As a result, the antenna efficiency decreases.

5.3 Performance Results of Koch Similar Curve Antenna

In Figure 4.27, the ratio of physical length of the antenna to electrical length of the antenna for strictly self similar Koch dipoles with different indention angles are given. The figure implies that as the indention angle increases the ratio decreases when iteration number is increased. Low ratio implies low antenna radiation efficiency, since total loss resistance of the antenna increases as the physical length increases (the width of the lines are kept constant). However, the reduction rate of 1st resonance frequency does not increase as a function of iteration stage.

In this chapter, a Koch similar curve is generated and utilized to acquire high l_e/l_p ratio as well as achieving decrease the resonance frequency. The generation of the model is illustrated in Figure 5.11. The generation of the curve is as follows; a segment A, which is a 1st iterated strictly self similar Koch curve with θ=80º having end to end height 2.347 mm, is created. Segment B is also a 1st iterated strictly self similar Koch curve, with θ=60º. However, one sub-segment of B is replaced with segment A.

Same procedure for segment B is applied to generate segment C and segment D, with the indention angles 40º and 20º respectively. However, one sub-segment of D is truncated where end to end length of the geometry reaches 8 cm.

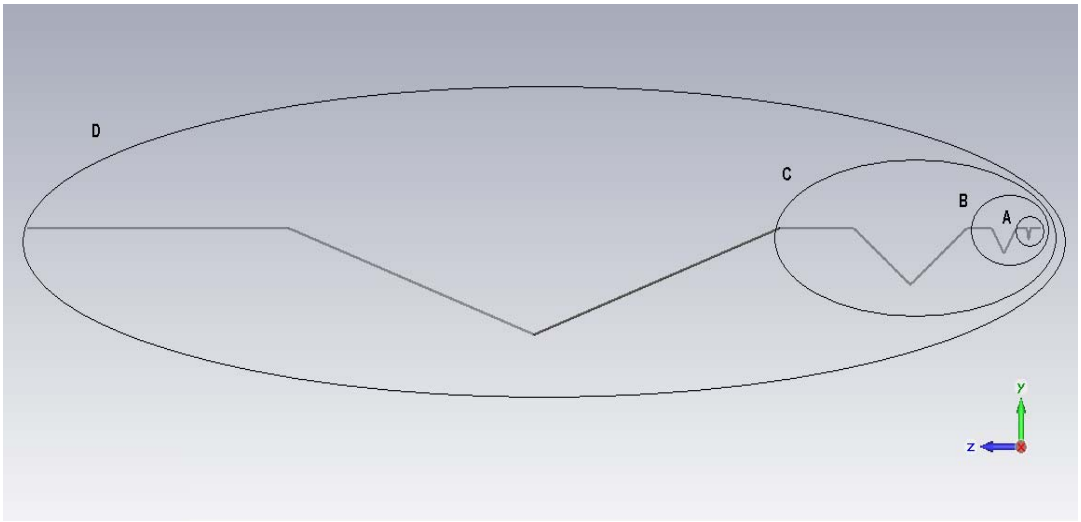

Figure 5.11 Generation steps for Koch similar curve

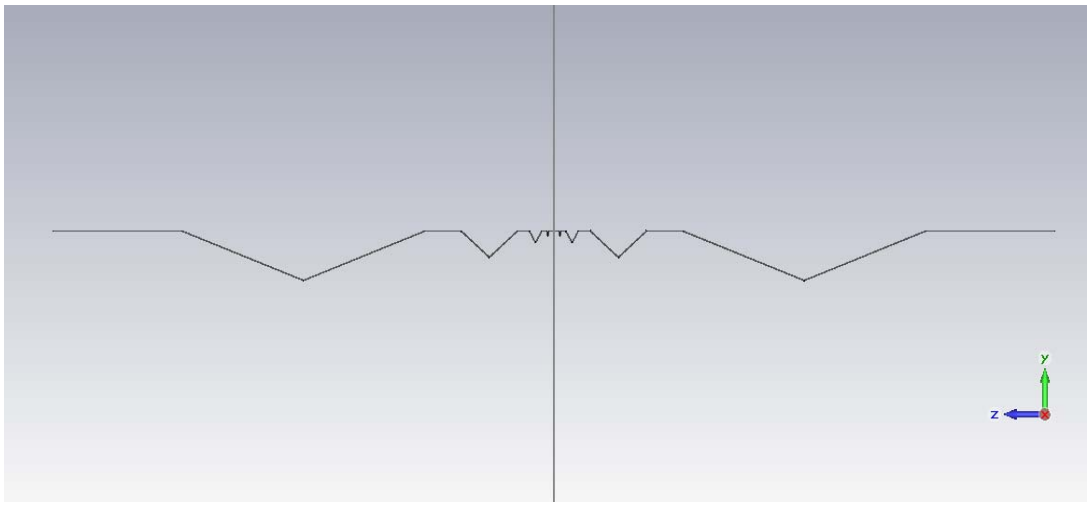

Figure 5.12 Wire model for simulation of Koch similar dipole

In Figure 5.12, the wire model for simulation of Koch similar dipole is illustrated. The end to end length is kept as 16 cm to compare the results with those in previous chapters. The overall length of the geometry is 21.3 cm. The simulation is done in CST MWS® in 0.5 to 6 GHz frequency range.

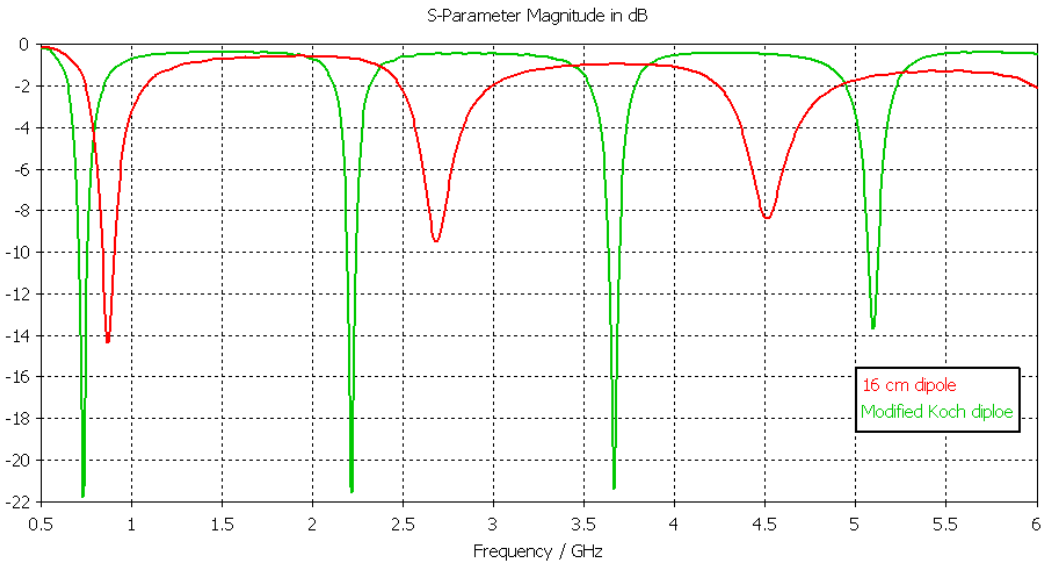

Figure 5.13 The simulation results for return losses of the Koch similar dipole and 16 cm dipole

The simulation result of return losses of the antenna that is shown in Figure 5.12 and a dipole with height of 16 cm, is plotted in Figure 5.13. The 1st resonance frequencies of 16 cm dipole and Koch similar dipole are 0.867 GHz, 0.727 GHz. The dipole antenna having its 1st resonance at 0.727 GHz has overall length of 20.3 cm assuming the dipole has its 1st resonance when the length of the antenna is λ/2. This is the electrical length of the antenna illustrated in Figure 5.12, according to the definition of normalized electrical length explained in chapter 4.2.5. l_e/l_p is found as 0.953. The electrical length of the antenna is close to physical length of the antenna.

1st resonance frequency of 3rd iterated strictly self similar Koch dipole with indention angle of 40º, is 0.75441 GHZ as indicated in Table 4.2. The total length of the antenna is 23.238 cm. In Figure 4.27 the l_e/l_p ratio is less than 0.9.

For the experimental measurement, the antenna is made of lossy copper wire line (electrical conductivity 5.8×10^7 S/m) printed over RO 5880 lossy dielectric material (ε_R=2.2, tanδ=9×10^{-4}) The width of copper line is 0.35 mm and the thickness of the copper line is 0.02 mm. These arrangements are sustained for simulation of the printed antenna in CST MWS®. For both simulation and practical implementation, the antenna is configured as a monopole antenna, fed by 50 Ohm SMA connector over a circular metallic (Aluminum) ground plane of radius 24 cm. The implemented (printed) antenna is illustrated in Figure 5.14. The comparison of the simulation and experimental results for the return loss of the antenna is given in Figure 5.15. The return loss of the implemented antenna is measured via Agilent E8358A Network Analyzer in 0.5-6 GHz frequency 1 port calibration.

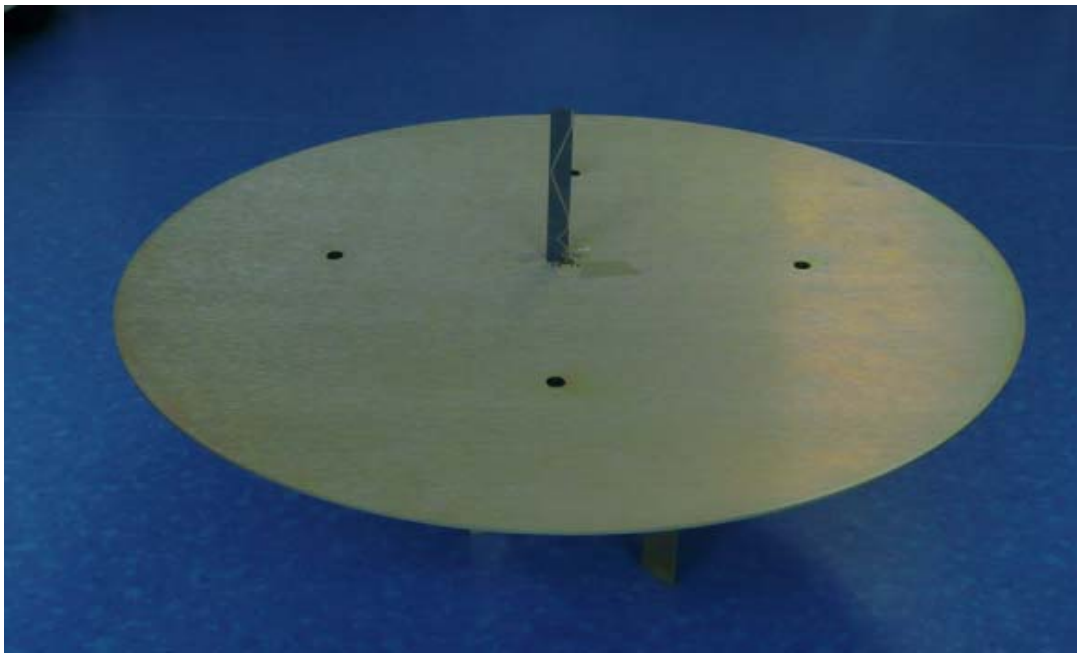

Figure 5.14 Physical implementation of Koch similar monopole antenna

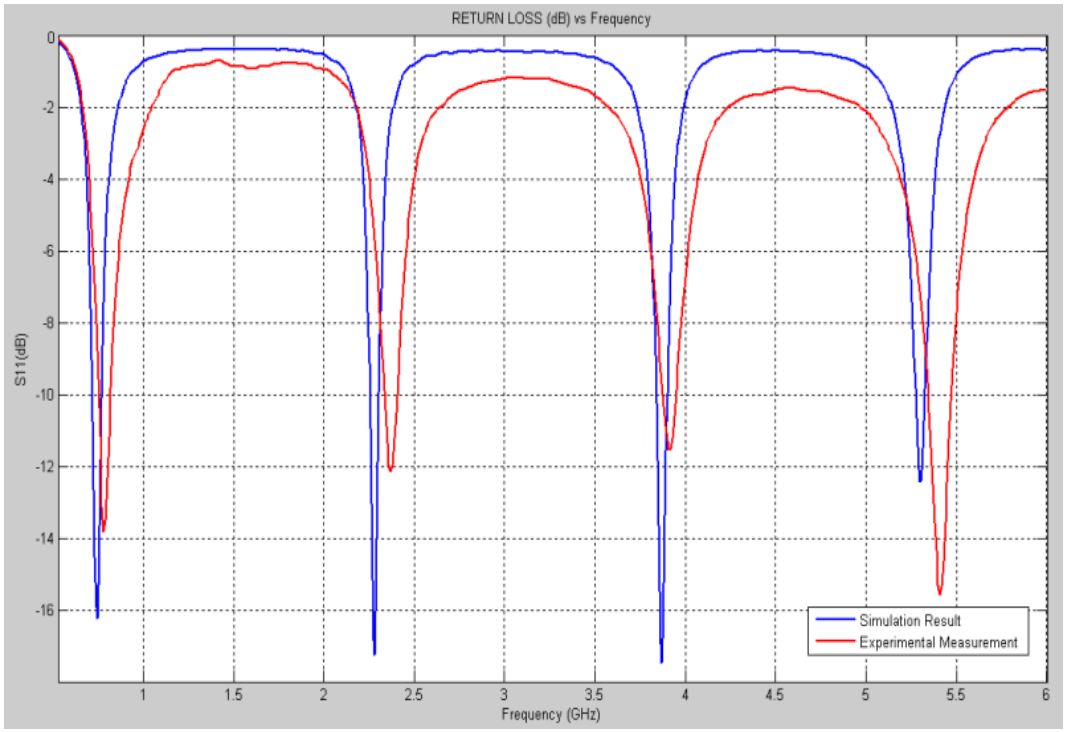

Figure 5.15 Comparison of the simulation and experimental results for the return loss of Koch similar antenna

CHAPTER 6

KOCH CURVE SUPERIMPOSED SIERPINSKI TRIANGLE GASKET MONOPOLE ANTENNA

In previous chapters the Koch curves were utilized as antenna geometries to find out the relation between the geometry of the antenna and the resonance frequencies of the antenna, and it was shown that the space-filling property of the Koch geometries enhances lowering the resonance frequency.

In [18] and [34], the multiband properties of the standard Sierpinski Triangular antenna were investigated. In [16], the multiband properties of generalized Sierpinski Gasket antenna were studied. In these studies, the multiband behavior of the antenna was attributed to self similar current distribution over the antenna at resonance frequencies.

In this chapter a generalized Sierpinski Triangle Gasket (mod-3) monopole is simulated to observe the effect of geometry to the antenna radiation properties. Based on this geometry, a geometry which is a combination of Koch Curve and Sierpinski Triangle was created. The created geometry is simulated using CST MWS® electromagnetic simulation tool and also the antenna was implemented practically.

6.1 Sierpinski Triangle Gasket Monopole Antennas

To generate 1st iteration of a standard Sierpinski Triangle gasket, first, main equilateral triangle is divided into four equal pieces, which are indeed ½ scaled

versions of the main triangle. Afterwards, the central triangle is subtracted from the whole geometry. The generation of the standard Sierpinski Triangle gasket is illustrated in Figure 6.1. Same procedure is applied to all remaining triangles iteratively to generate further iterations. If the iteration is applied infinitely, the ideal Sierpinski Triangle gasket is obtained.

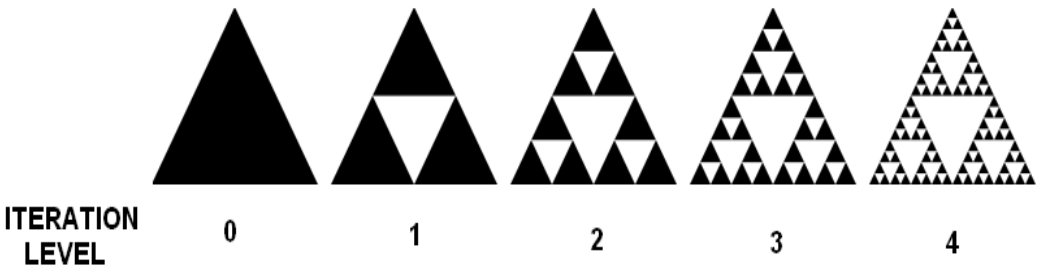

Figure 6.1 Generation of Standard Sierpinski Triangle geometry

A new type of Sierpinski Triangle gasket was derived in [37], by using well known Pascal's Triangle. These types of Sierpinski Triangles are called as *mod-p* Sierpinski Gasket. The generation of mod-p geometries is explained as follows, "Consider an equilateral triangular grid whose rows shall be labeled by n= 1, 2, 3…. Each row contains n nodes and to each node a number is attached. This number is the coefficient of binomial expansion of $(x+y)^{n-1}$. Now delete from this grid those nodes that are attached to numbers that are exactly divisible by *p*, where *p* is a prime number. The illustration of derivation of Sierpinski Gaskets from Pascal's triangle is found in Figure 6.2." [16]

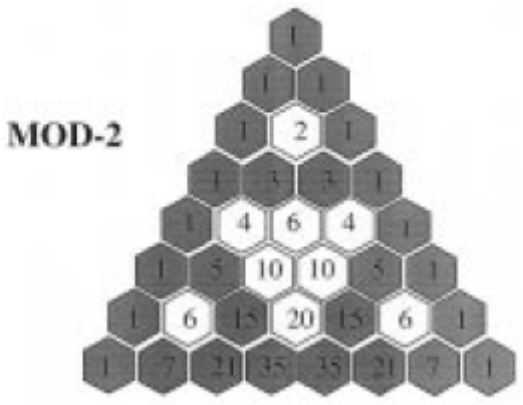

Figure 6.2 Derivation of the Sierpinski Gaskets from Pascal's Triangle [16]

The standard Sierpinski Triangular Gasket can be regarded as mod-2 Sierpinski gasket. Mod-3 and mod-5 Sierpinski Gaskets of 3rd iteration in monopole antenna configuration is seen in Figure 6.3.

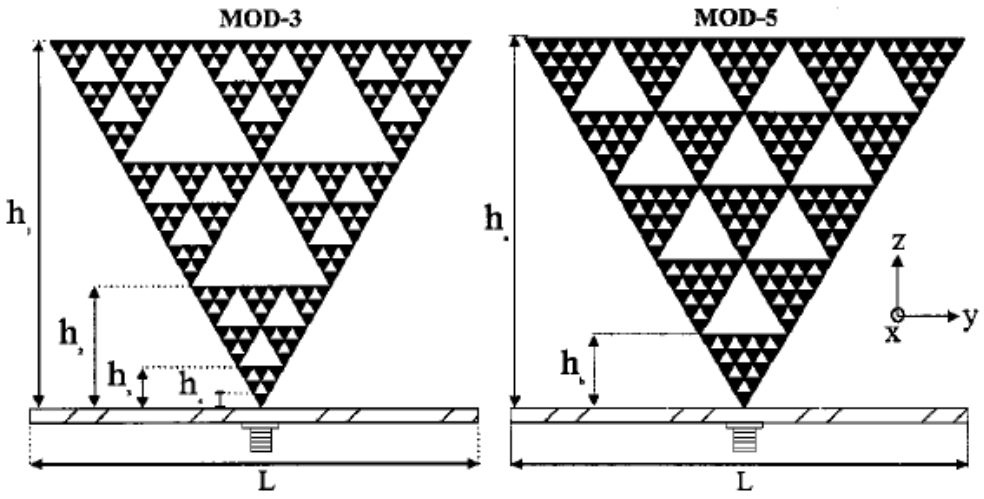

Figure 6.3 Two Sierpinski Gaskets a) mod-3 Sierpinski gasket for 3rd iteration b) mod-5 Sierpinski gasket for 3rd iteration [16]

To observe the effect of self- similar geometry of Sierpinski Triangle Gasket to antenna radiation properties and frequency response, a mod-3 Sierpinski Gasket monopole of 2nd iteration is created in CST MWS®. The geometry of the antenna is illustrated in Figure 6.4.

For the CST MWS® simulation, the antenna height is chosen as 6.2 cm and the antenna material is lossy copper. The antenna is printed on RO 5880 dielectric substrate with ε_R=2.2. The thicknesses of the metal and dielectric substrate are chosen as 0.02 mm and 1mm, respectively. The antenna is modeled as monopole over a round metal plate (Aluminum) with radius 24 cm as ground plane. The antenna is fed from the tip of the antenna as seen in Figure 6.4.

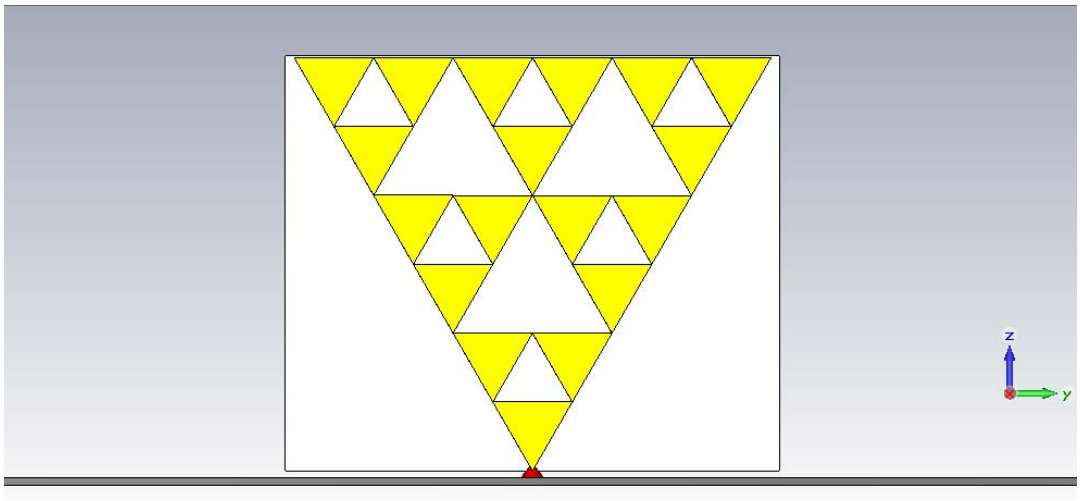

Figure 6.4 Simulation model of mod-3 Sierpinski Gasket of 2nd iteration monopole antenna in CST MWS®

The antenna is simulated from 0 to 12 GHz. The meshing parameters are as follows; lines per wavelength is 16, lower mesh limit is 14, mesh line limit ratio is 100 and subgridding is activated.

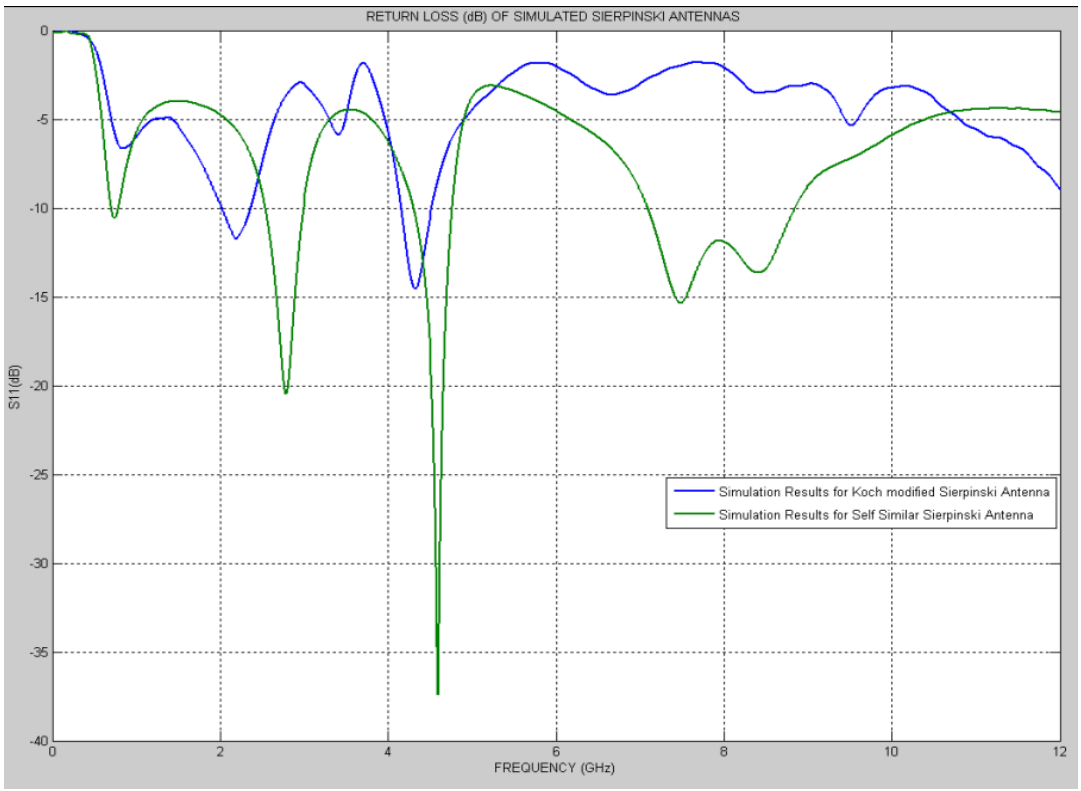

Figure 6.5 The return loss of simulated modeled antennas for a) self-similar mod-3 Sierpinski antenna in Figure 6.4 b) Koch modified Sierpinski antenna in Figure 6.8

As seen in Figure 6.5, according to the simulation results for the self similar mod-3 Sierpinski antenna (green curve), the antenna possesses four main resonance frequencies in simulation frequency range. For the 2nd and further resonance frequencies, the resonance frequencies are to be log periodic spaced with a factor of approximately 1.63, as seen from the Table 6.1. This ratio is almost same for the mod-3 Sierpinski Gasket monopole antenna with 3rd iteration (but different antenna height) studied in [16].

Table 6.1 Simulation results for the resonance frequencies of the antenna in Figure 6.4

n^{th} resonance	Resonance Frequency (GHZ)	f_{n+1}/f_n
1	0.7629	-----
2	2.7486	3.6
3	4.5775	1.66
4	7.4526	1.63

The simulation results for the radiation patterns of the antenna modeled in Figure 6.4 are shown in Figures 6.6-6.7. For the 1st resonance antenna exhibits omnidirecitonal pattern as expected. For the 2nd and further resonance frequencies the antenna pattern in elevation for φ=90º-270º cut, the pattern keeps omnidirecitonal characteristics to some extend, however ,the antenna pattern in elevation for φ=0º-180º cut, main beam radiates at different elevation angles. According to the simulation results the antenna pattern loses its periodicity of similar radiation pattern at resonance frequencies.

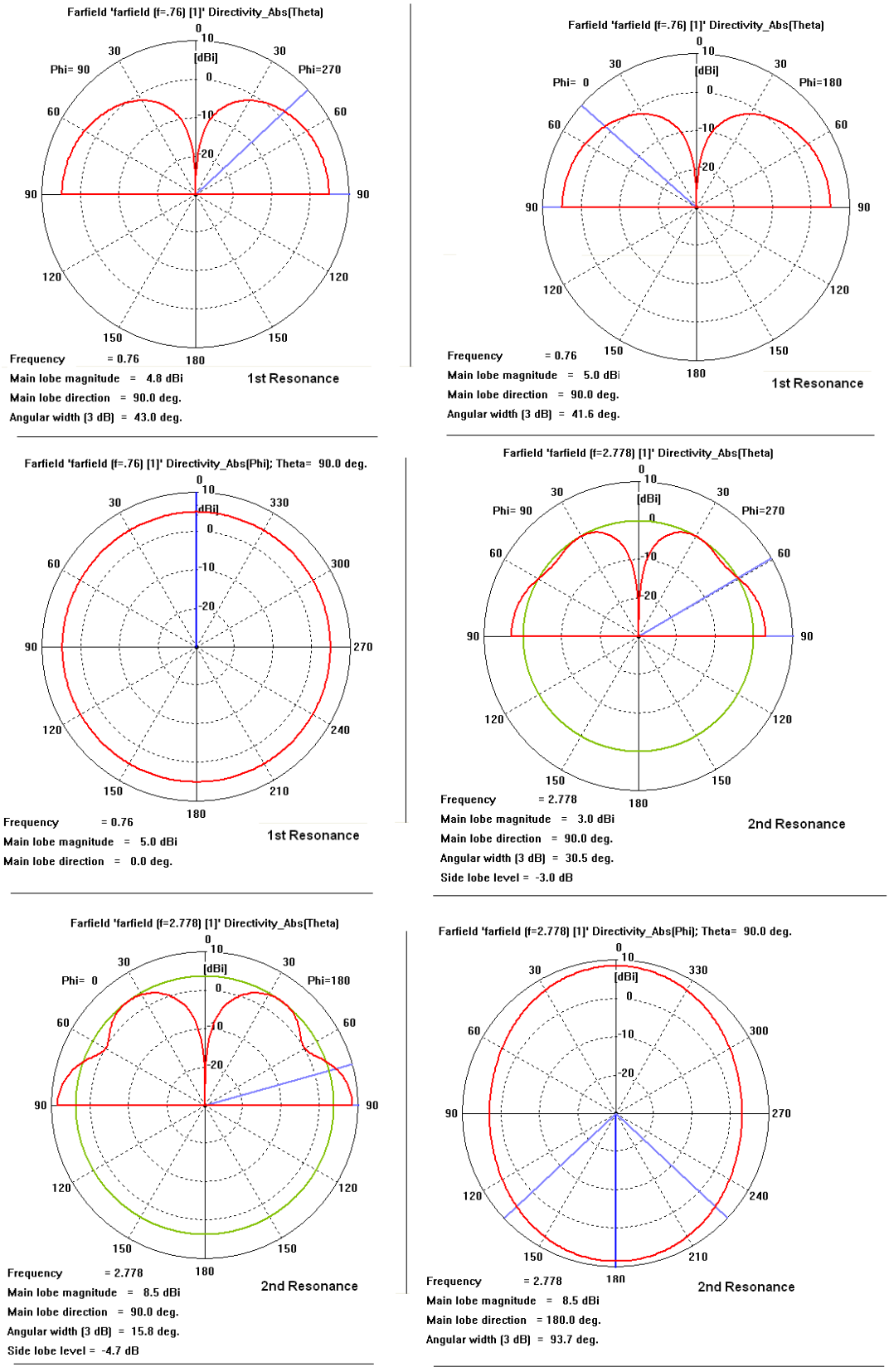

Figure 6.6 The simulation results for radiation patterns of the antenna in Figure 6.4 at 1st and 2nd resonance frequencies

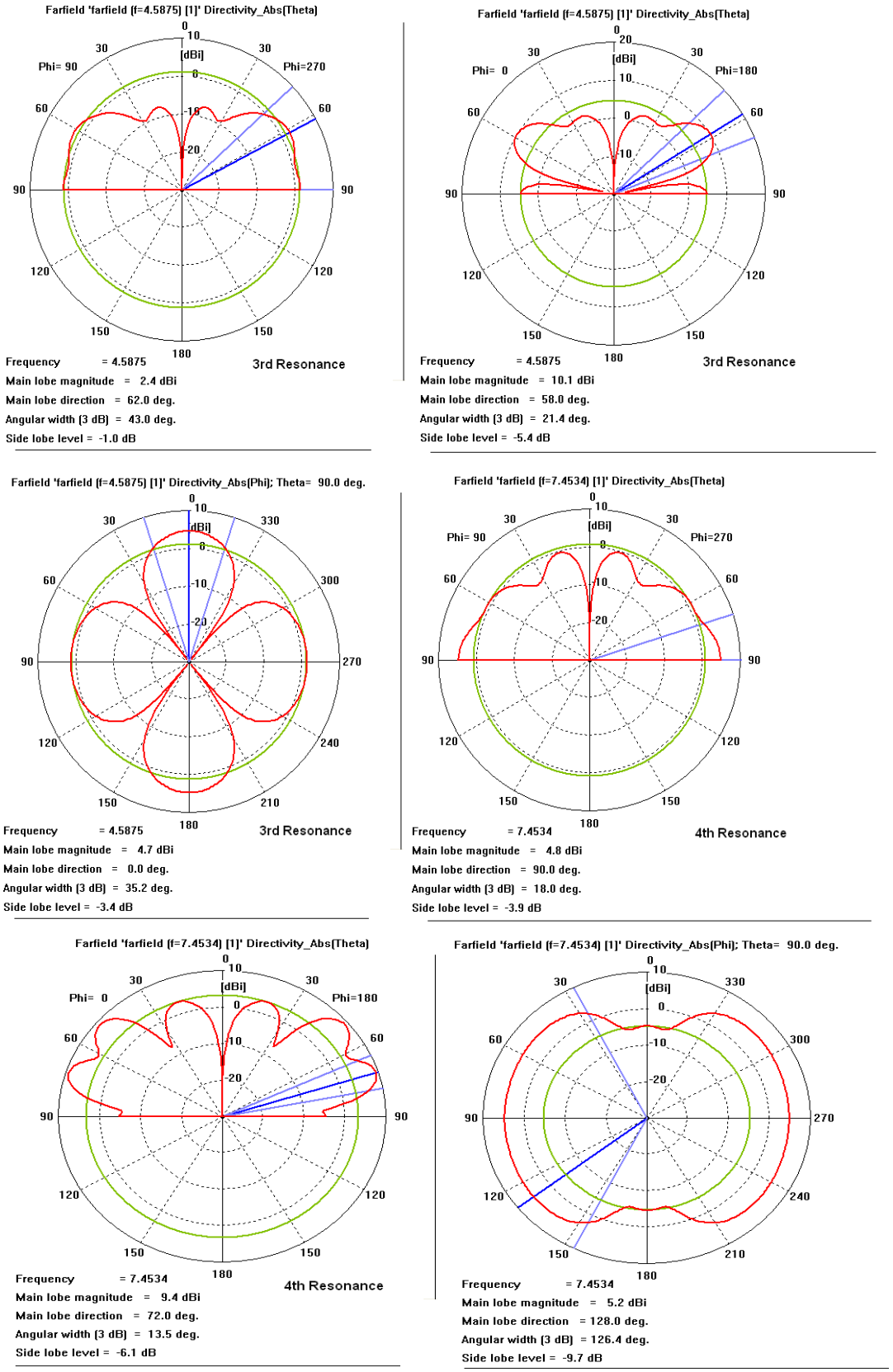

Figure 6.7 The simulation results for radiation patterns of the antenna in Figure 6.4 at 1st and 2nd resonance frequencies

6.2 Koch Superimposed Sierpinski Monopole Antenna

To explore the effect of Koch geometry to antenna radiation characteristics and frequency response of the Sierpinski Gasket antennas, which are presented as multiband antennas in [16] and [18]; a modified geometry that is a combination of Koch geometry and mod-3 Sierpinski antenna is derived. For simulation the geometry is created in CST MWS® and illustrated in Figure 6.8.

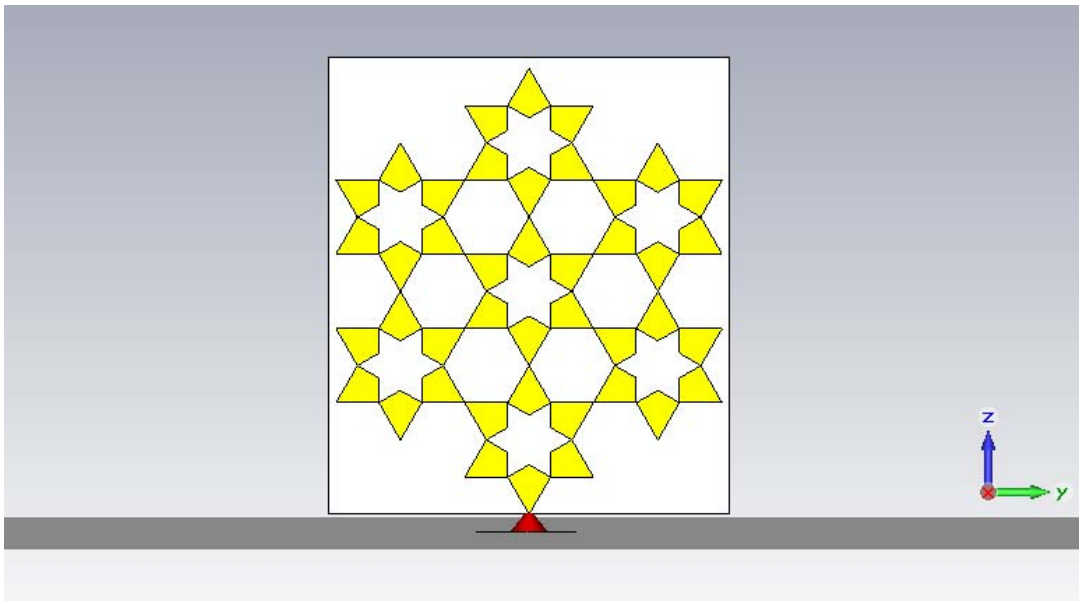

Figure 6.8 The simulation model of Koch Modified Sierpinski monopole antenna

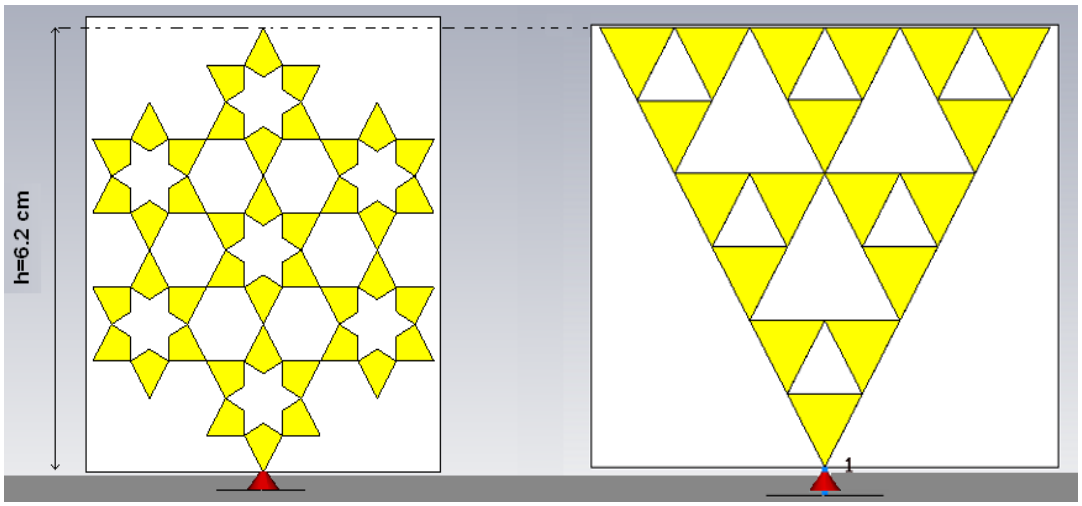

Figure 6.9 The view of simulation models Sierpinski monopole antennas

The antenna in Figure 6.8 has height of 6.2 cm, and the geometries are compared in Figure 6.9. The Koch superimposed Sierpinski monopole antenna is not directly derived from a mod-3 Sierpinski Triangular gasket. The antenna in Figure 6.8 consists of 7, six-arm star shaped segments. From the center of the segments a $1/\sqrt{3}$ scaled and 30º rotated versions of these segments are removed.

For both simulation and experimental measurement of the printed antenna, the antenna is made from lossy copper the antenna material is lossy copper. The antenna is printed on RO 5880 dielectric substrate with ε_R=2.2. The thicknesses of the metal and dielectric substrate are chosen as 0.02 mm and 1mm, respectively. The antenna is modeled as monopole over a round metal plate (Aluminum) with radius 24 cm as ground plane. The antenna is fed from the tip of the antenna as seen in Figure 6.8.

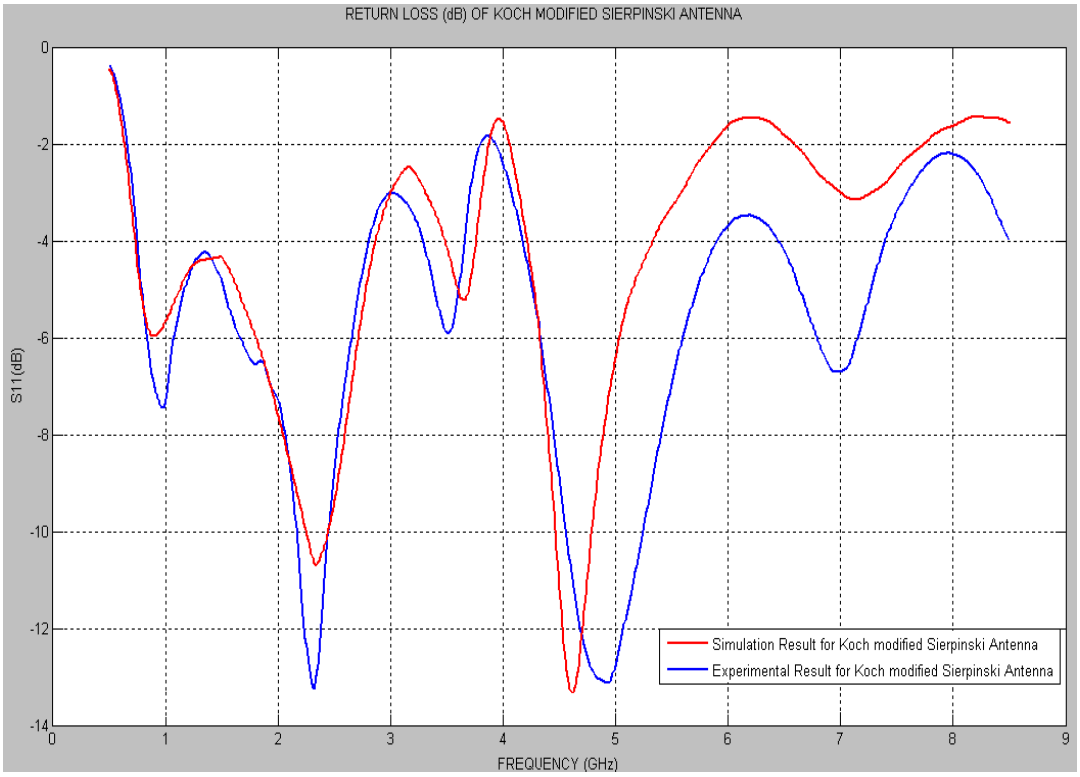

Figure 6.10 Comparison of the return loss (dB) results for simulation and experimental measurement model of Koch Modified Sierpinski Monopole Antenna

The simulation results for the return loss of the antenna are plotted in Figure 6.5. In the plot, the frequency response of the Koch superimposed Sierpinski triangle and the mod-3 Sierpinski monopole antennas that are illustrated in Figure 6.9, can be compared. The log periodic behavior of the resonance frequencies of the mod-3 Sierpinski monopole does not exist for the Koch superimposed one. The main resonance frequencies (the resonances where return loss is less than -10 dB) of the Koch Superimposed one appear at lower frequencies than those of self- similar mod-3 Sierpinski Triangle monopole. Moreover, for the Koch superimposed Sierpinski Triangle monopole, there exist resonances where return loss can not reach -7 dB or lower values.

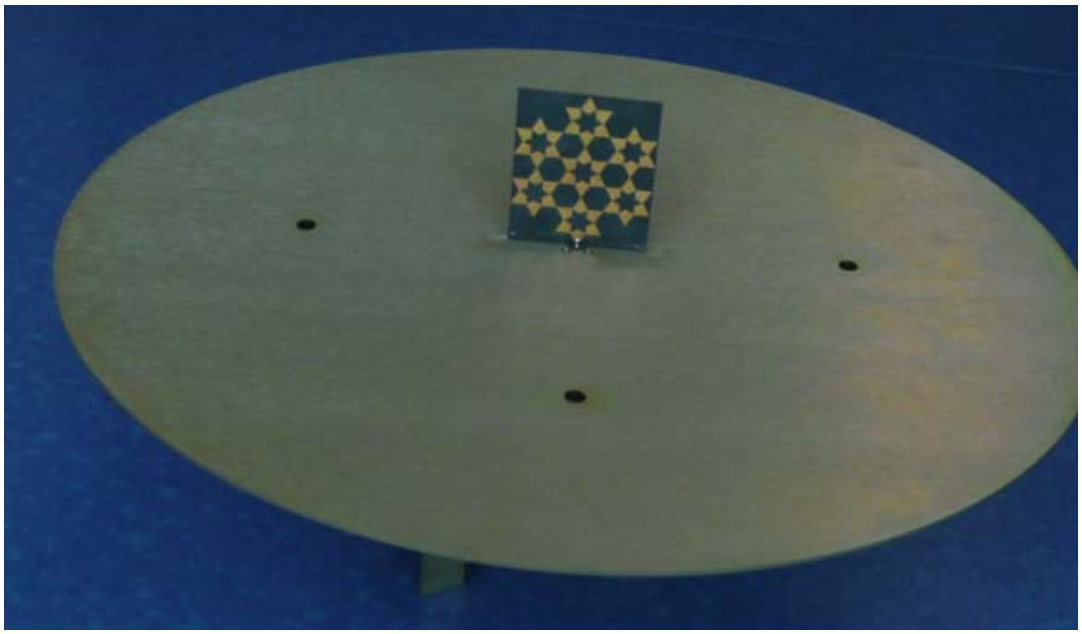

Figure 6.11 The physical implementation of the antenna in Figure 6.8

The comparison for the return loss of the simulation and experimental results are shown in Figure 6.10. The 1st main resonance frequency of the antenna occurs at the same frequency for the simulation and experimental measurement. However, 2nd resonance frequency shifts towards 5 GHz. The shift can be attributed to physical affect of the soldering of the sharp tip of the antenna to the feed connector.

The radiation pattern of the antenna is simulated in CST MWS® and the results are plotted in Figure 6.13 and Figure 6.14. Two elevation plane cuts (at xz (φ=0º) and yz (φ=90º)) and one azimuth plane (xy (θ=90º)) are plotted for each of the main resonance frequencies and the frequencies where return loss of the antenna is about -4 dB.

The radiation pattern of the physically implemented antenna is measured in Aselsean Inc. Anechoic Chamber Test Facilities. The measurement is done in 2-8 GHz range and the measurement frequency points are determined as the main resonance frequencies and the frequencies where return loss of the antenna is about -5 dB. For frequencies below 2GHz omnidirecitonal radiation patterns are expected. The radiation patterns exhibited similar radiation patterns for main resonance frequencies and the frequencies where the return loss is less than – 5 dB.

During measurements, the antenna (AUT) is in receiver mode and the source antenna is transmitter mode. Source antenna is linearly polarized 2-8 GHz horn. So co-polarized pattern of the AUT is measured when the source antenna is vertically placed in the test region. The results of the measurements are given in Figure 6.15 and Figure 6.16 for the co-polarized pattern. Since the implementation is done as monopole antenna, the θ range for the radiation pattern plots are considered from 0º to 90º. The set up of the anechoic chamber can be seen in App. A.

The superimpose of Koch geometry to Sierpinski Gasket monopole antenna did not improve the frequency response of the antenna. Rather than achieving closely spaced resonance frequencies, resonances where return loss is about -5dB at those frequencies appeared. This can be attributed to disruption of self similarity of mod-3 Sierpinski gasket. However, the current distribution on the antenna has not changed in the resonances; as a result the pattern similarity of the antenna is preserved.

Figure 6.12 The Koch superimposed Sierpinski Triangle monopole antenna under test in tapered anechoic chamber in Aselsan Inc. facilities

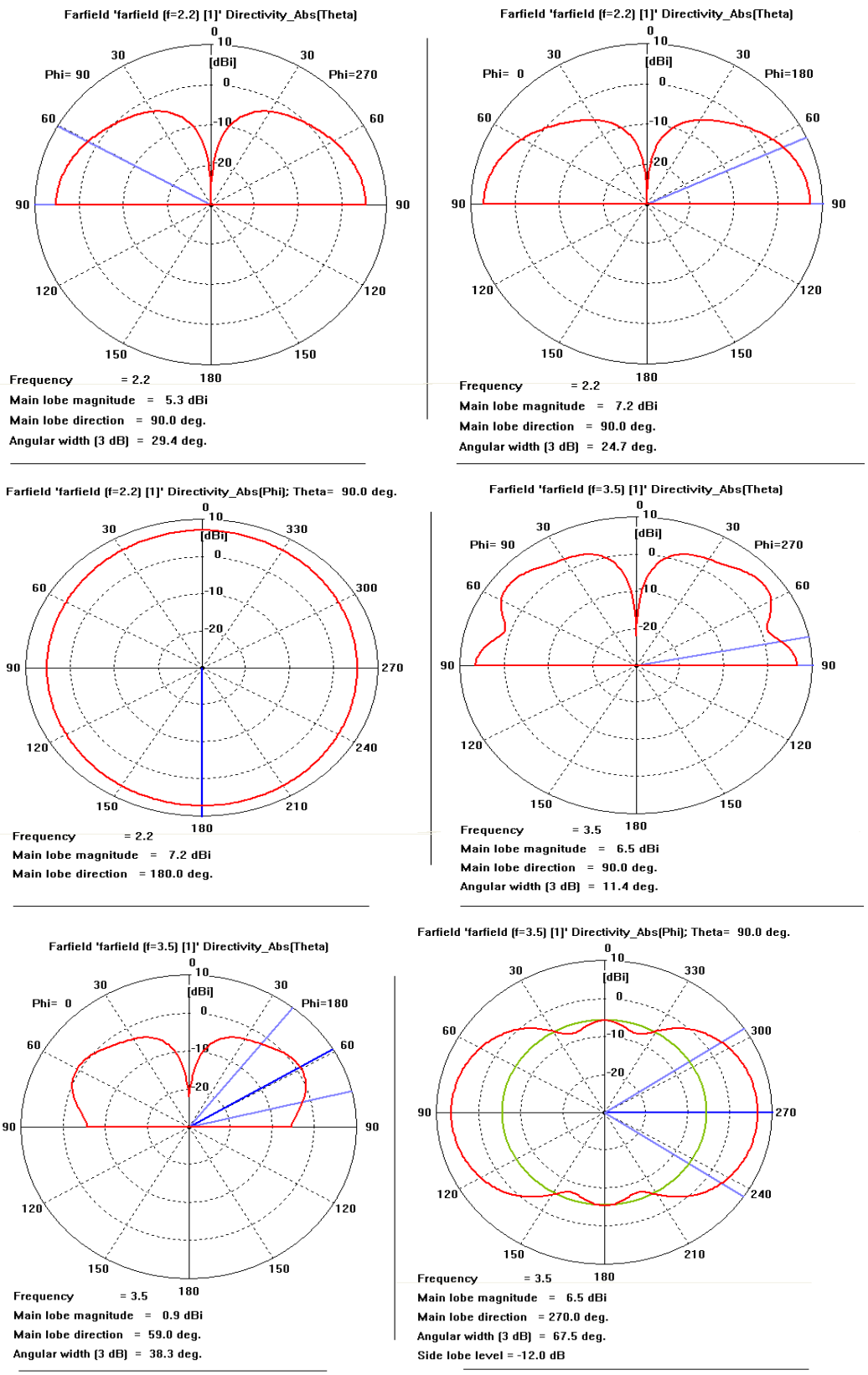

Figure 6.13 The simulation results for the radiation patterns of the antenna in Figure 6.8 for f=2.2 GHz and f=3.5 GHZ

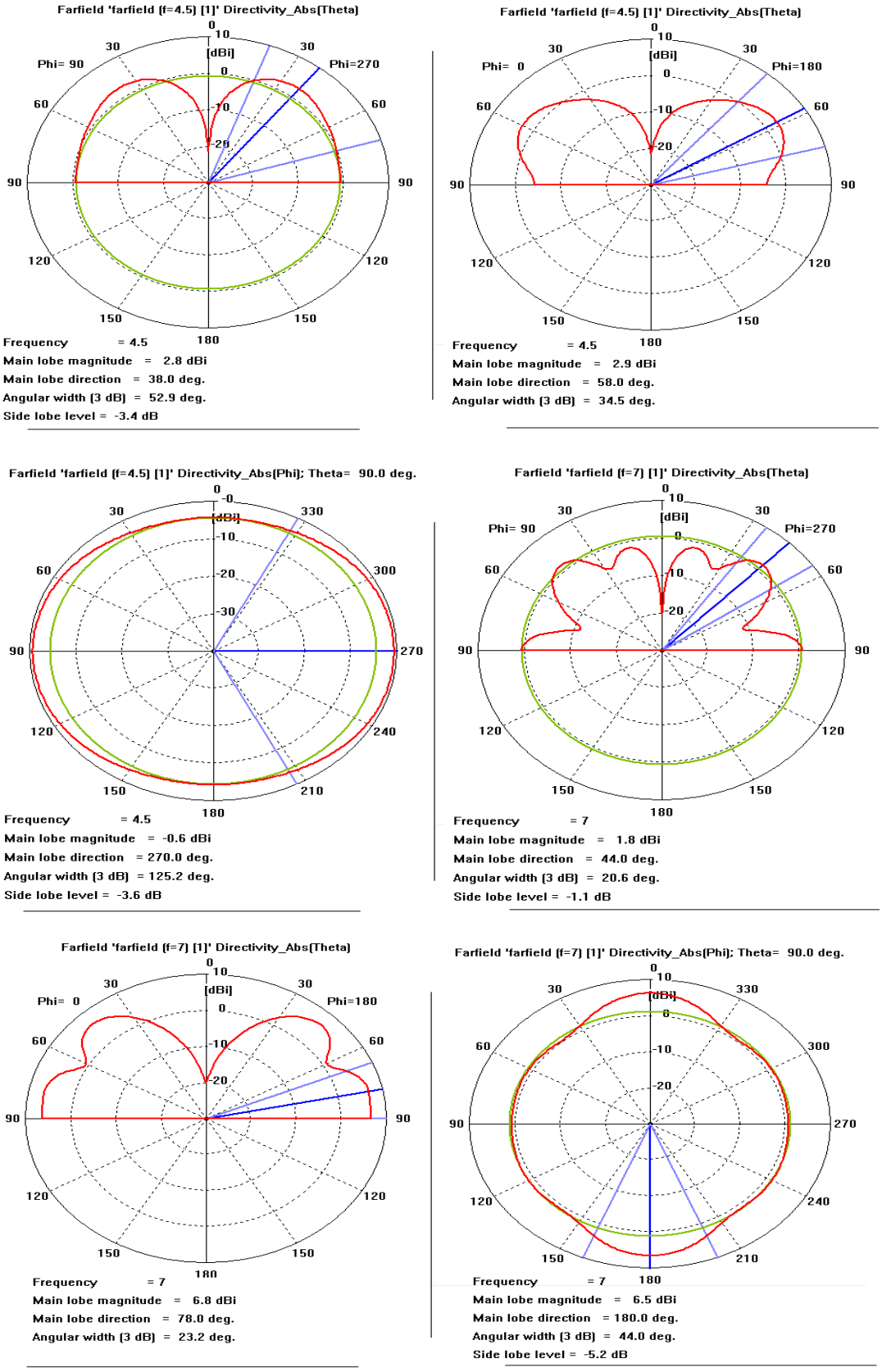

Figure 6.14 The simulation results for the radiation patterns of the antenna in Figure 6.8 for f=4.5 GHz and f=7 GHZ

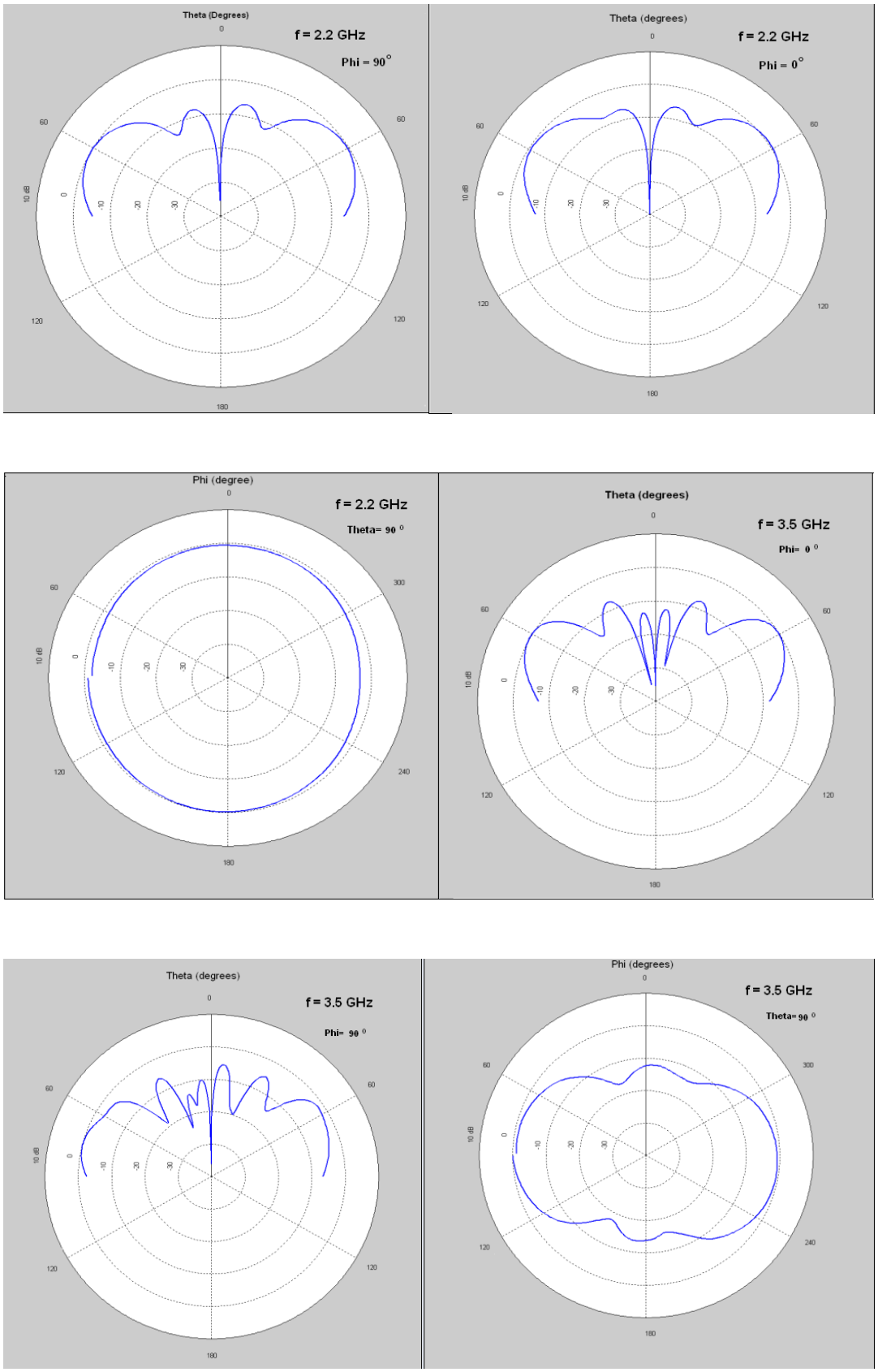

Figure 6.15 The experimental measurement results for the radiation patterns of the antenna in Figure 6.11 for f=2.2 GHz and f=3.5 GHZ

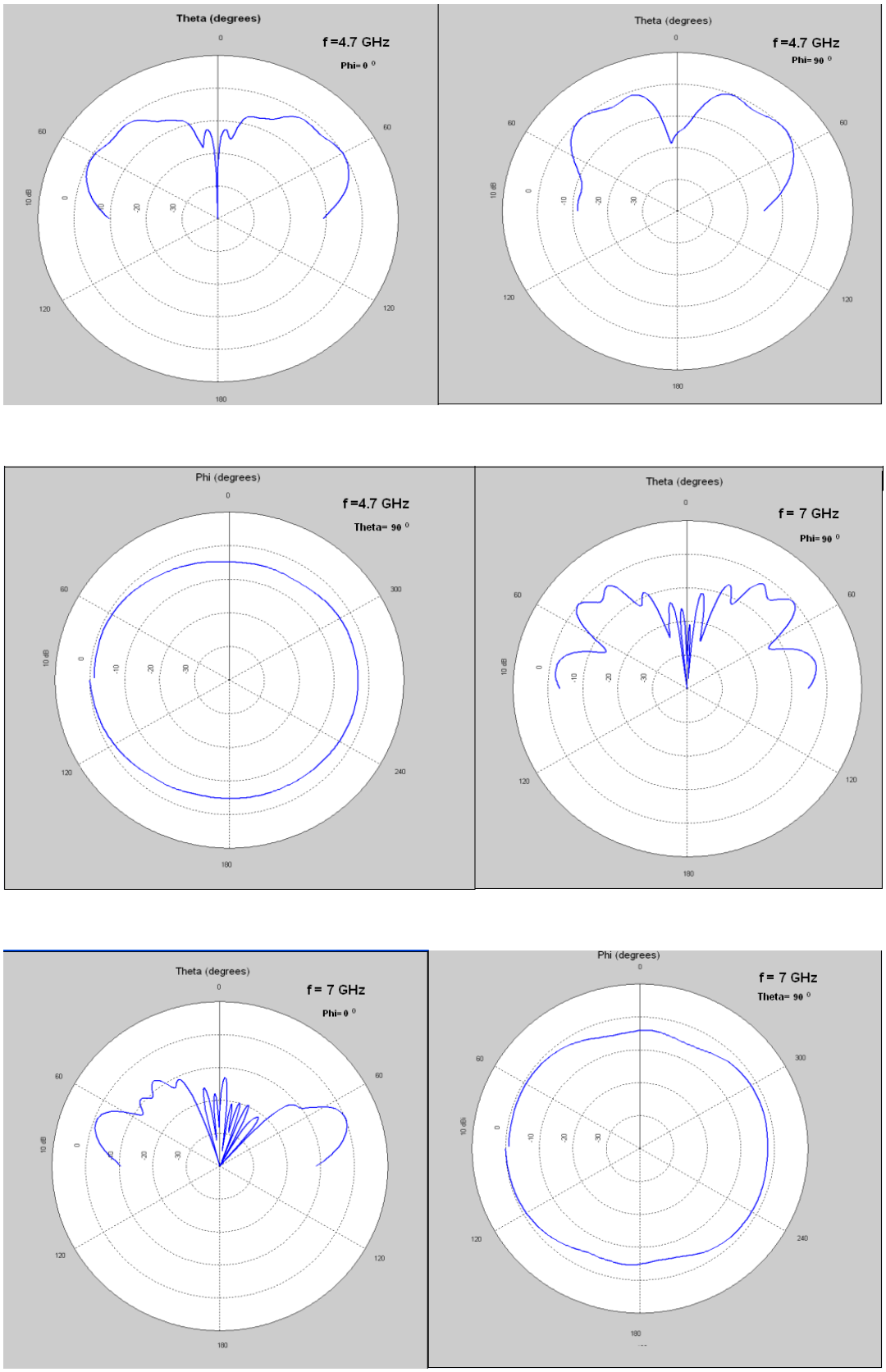

Figure 6.16 The experimental measurement results for the radiation patterns of the antenna in Figure 6.11 for f=4.7 GHz and f=7 GHZ

CHAPTER 7

CONCLUSION

Even if the use of the fractal geometries in science and engineering is new to literature, the fractals are frequently encountered in many applications. The fractal geometries have become popular in antenna engineering since N. Cohen introduced several fractal geometries enhancing antenna radiation and input impedance properties when utilized an antennas. However, there is no guarantee for improving antenna radiation and input impedance properties when utilizing any kind of fractal geometry. Only few of the fractals improved radiation performance when used as antenna

Based on the studies in literature, a number of antennas utilizing self similar fractal geometries were found to exhibit multiband frequency characteristics and decreased resonance frequencies. The antennas utilizing Koch Curve, Minkowski Loop, Hilbert Curve and Koch Loop geometries are shown to succeed in decreasing the resonance frequencies and improving radiation efficiency of electrically small antennas due to space filling property of these fractal geometries. Moreover, the multiband property of Sierpinski Carpet and Sierpinski Triangle Gasket Antennas were studied.

In this thesis, the effects of properties and parameters of Koch geometry to antenna radiation and frequency response are studied. The performances of the Koch antennas are investigated via varying the indention angle of the generalized self similar Koch curves. The Koch antennas possessing higher indention angle exhibited lower resonance frequencies than those possessing lower indention angles. Even 1^{st} iteration of Koch antennas having higher indention angles

exhibited lower resonance frequencies than 3rd iteration of Koch antennas having lower indention angles. The indention angle at 1st iteration dominated the rate of decreasing the resonance frequency. To verify this phenomena a modified Koch curve is defined in chapter 5.2, whose indention angle at 1st iteration is low. Low indention angle resulted low rate of decreasing resonance frequency. To compensate the low rate of decrease of the resonance frequency, the geometry of the antenna is further iterated with higher indention angles. Even if the iteration angle increased and the length of the antenna increased due to further iterating the geometry, the resulting antenna could not reach the performance of an antenna with less complex geometry (a strictly self similar Koch curve with high indention angle of 1st iteration)

However, for the Koch antennas with low indention angles, the electrical length of the antenna is close to physical length of the antenna. Even if Koch antennas with high indention angles achieved maximum rate of decrease in primary resonance frequency, the ratio of electrical length of those antennas to their physical length is small. In chapter 5.3 a Koch similar curve is generated and implemented as antenna, to obtain antenna having high ratio of electrical length to physical length as well as decreasing the primary resonance frequency of the antenna better than Koch antennas with low indention angles.

In chapter 5.1 it is shown that the fractal dimension, D can not be a design parameter for modified Koch antennas. It is shown that antennas with geometries having lower D can have lower primary resonance frequency than antennas having higher D.

In chapter 6, Koch geometry is combined with Sierpinski (Triangle) Gasket. The Sierpinski gasket monopole possesses log periodic behavior in resonance frequencies. It was expected to make the resonance frequencies appear closer. However, superimposing Koch curve to Sierpinski could not achieve bringing the resonance frequencies closer and log-periodic behavior of the antenna is lost.

The Koch geometry is known as a space filling curve, that when utilized as antenna it is expected to possess primary resonance frequency lower than its Euclidean counterpart of same end-to-end height. However, the decreasing of the resonance frequency is dependent to parameters of the geometry. The geometry must be modified (optimized) to achieve efficient antenna as well as having low resonance frequency. The optimization parameters can be basically indention angle and iteration level. Moreover, by using genetic algorithm certain loads can be added to geometry to obtain versatility of changing resonance frequencies.

In future studies, for improving increasing radiation efficiency, the printed Koch fractal antennas can be implemented as slot antennas. The strip dipole and slot are complementary antennas. The solution from the slot can be found from the solution of an equivalent dipole by using duality and Babinet's principles. The resulting antenna may yield higher radiation resistance and lower loss resistance.

REFERENCES

1. B.B. Madelbrot, *The Fractal Geometry of Nature*, New York: W.H. Freeman, 1982.

2. Kiyun Han, *Sierpinski Fractal Antennas*, *PhD thesis,* Southern Illinois University Carbondale, Oct. 2003, pp [7]

3. H. Lauwerier, *Fractals; Endlessly Repeated Geometrical Figures*, Princeton, New Jersey: Princeton University Press, 1991

4. N. Cohen, "Fractal antenna applications in wireless telecommunications*," in Professional Program Proc. of Electronics Industries Forum of New England*, 1997, IEEE, pp. 43-49, 1997.

5. Wikipedia, free encyclopedia, http://en.wikipedia.org/wiki/Fractal, available on June 12,2009

6. Mathworld, http://mathworld.wolfram.com/Fractal.html, available on June 12,2009

7. C. Puente-Baliarda, J. Romeu, R. Pous, J. Ramis, and A. Hijazo, "Small but long Koch fractal monopole," *Electron. Lett*., vol. 34, pp. 9-10, 1998.

8. C.P. Baliarda, J. Romeu, and A. Cardama, "The Koch monopole: A small fractal antenna," *IEEE Trans. Ant. Propagat.*, vol. 48 pp. 1773-1781, 2000.

9. K.J. Vinoy, K.A. Jose, and V.K. Varadan, "Multiband characteristics and fractal dimension of dipole antennas with Koch curve geometry," *IEEE 2002 AP-S Inter. Symp*., 2002.

10. George S. A. Shaker and Safieddin Safavi-Naeini, "Highly Miniaturized Fractal Antennas", *University of Waterloo, Waterloo, Ontario,*

11. Raj Kumar, P. Malathi and J. P. Shinde, "Design of Miniaturized Fractal Antenna", *Proceedings of the 37th European Microwave Conference*

12. Steven R. Best and Jarrett D. Morrow, "The Effectiveness of Space-Filling Fractal Geometry in Lowering Resonant Frequency", *IEEE Antennas and Wireless Porooagation Letters,* Vol. 1, 2002

13. Steven R. Best, "On the Performance Properties of the Koch Fractal and Other Bent Wire Monopoles", *IEEE Trans. Ant. Propagat.*, vol. 51 No. 6 pp. 1296-1300, 2003

14. C. Puente, J. Claret, F. Sagues, J. Romeu, M.Q. Lopez-Salvans and R Pous, "Multiband properties of a fractal tree antenna generated by electrochemical deposition," *Electron. Lett.*, vol. 32, pp. 2298-2299, 1996.

15. M. Sindou, G. Ablart and C. Sourdois, "Multiband and wideband properties of printed fractal branched antennas," *Electron. Lett.*, vol. 35, pp. 181-182, 1999.

16. Jordi Romeu, Jordi Soler, **"**Generalized Sierpinski Fractal Multiband Antenna" *IEEE Trans. Ant. Propagat.*, vol. 49 No. 8 pp. 1237-1239, 2001

17. M. K. A. Rahim, M. Z. A. Abdul Aziz, and N. Abdullah,"Wideband Sierpinski Carpet Monopole Antenna", *Asia Pasific Conference on Applied Electromagnetics Proceeedings, Malaysia,* 2005

18. M. Navarro, J.M. Gonzalez, C. Puente, J. Romeu, and A. Aguasca, "Self-similar surface current distribution on fractal Sierpinski antenna verified with infra-red thermograms," *IEEE-APS International Conf. IEEE* pp. 1566-1569, 1999.

19. C. Puente, J. Romeu, R. Bartoleme, and R. Pous, "Perturbation of the Sierpinski antenna to allocate operating bands," *Electron. Lett.*, vol. 32, pp. 2186- 2187, 1996.

20. C.T.P. Song, P.S. Hall, H. Ghafouri-Shiraz and D. Wake, "Fractal stacked monopole with very wide bandwidth," *Electron. Lett.*, vol. 35, pp. 945-946, 1999.

21. D.H. Werner, P.L. Werner, D.L. Jaggard, A.D. Jaggard, C.Puente, and R.L. Haupt, "The theory and design of fractal antenna arrays," *Frontiers in Electromagnetics*, D.H. Werner and R. Mittra (Eds.), pp. 94-203, 1999.

22. D.H. Werner and P.L. Werner, "On the synthesis of fractal radiation patterns," *Radio Science*, vol. 30, pp. 29-45, 1995.

23. H.A. Wheeler, "Small Antennas," *IEEE Trans. Ant. Propagat*, vol. AP-23, pp. 462-469, 1975.

24. H. A. Wheeler, "Fundamental limitations of small antennas," *Proce.IRE*, vol. 35, pp. 1479–1488, Dec. 1947.

25. H. A. Wheeler, "The radiansphere around a small antenna," *Proce.IRE*, pp.vol47 1325–1331, Dec. 1959.

26. L. J. Chu, "Physical limitations on omni-directional antennas," *J. Appl. Phys.,* vol. 19, pp. 1163-1175, Dec. 1948.

27. R. F. Harrington, "Effect of antenna size on gain, bandwidth and efficiency," *J. Res. Nut. Bur. Stund.,* vol. 64-D, pp, 1-12, Jan./Feb. 1960.

28. Computer Simulation Technologies, http:// www.cst.com, available on May 12, 2009

29. G. Afacan, *The Electrical Characteristics of Antennas in their operational Environment,Ms Thesis,* pp 6-41, METU, 2007

30. C. A. Balanis, *Antenna Theory, Analysis and Design*. New York: Wiley, 1982.

31. K.Q. da Costa and V. Dmitriev, **"**Theoretical analysis of a modified Koch monopole with reduced dimensions", IEE Proc.-Microw. Antennas Propag., Vol. 153, No. 5, October 2006

32. J. M. González-Arbesú, S. Blanch, andJ. Romeu, "Are space-filling curves efficient small antennas?," *IEEE Antennas Wireless Propagat. Lett.*, vol. 2, no. 10, pp. 147–150, 2003.

33. A. D. Yaghjian, S. R. Best, "Impedance,Bandwidth and Q of Antennas", *IEEE Trans. Ant. Propagat.*, vol. 53 No. 4 pp. 1298-1324, 2005

34. Puente, J. Romeu, R. Pous, and A. Cardama, "On the behavior of theSierpinski multiband antenna," *IEEE Trans. Antennas Propagat.*, vol.46, pp. 517–524, Apr. 1998.

35. Gianvittorio, J.P., and Rahmat-Samii, Y.: 'Fractal antennas: a novel antenna miniaturization technique, and applications', *IEEE Antennas Propag. Mag.,* 2002, 5, (1), pp. 20–35

36. B.H. Kaye, A *Random walk through Fractal Dimensions*, New York: VCH, 1994.

37. N. S. Holter, A. Lakhtakia, V. K. Varadan, V. V. Varadan, and R. Messier,"On a new class of fractals: The Pascal-Sierpinski gaskets," *J. Phys. A:Math. Gen.*, vol. 19, pp. 1753–1759, 1986.

38 N. Gökalp, "*Beam Steerable Meanderline Antenna Using Varactor Diodes and Reconfigurable Antennas Designs by MEMS Switches",* M.S Thesis, METU, August , 2008, pp 106-108

APPENDIX

A. ASELSAN Tapered Anechoic Chamber Measurement System [38]

The measurements and evaluation of the sinuous antennas are performed in an anechoic chamber (see Figure A.1). Anechoic chamber is a reflection free (i.e. the reflectivity levels of the absorbers covering the whole room are very low, about–20 dB) room inside of which is covered by absorbers.The tapered anechoic chamber is designed in the shape of pyramidal horn that tapers from the small source end to a large rectangular test region, and with high quality absorbing material covering the side walls, floor and ceiling. The tapered anechoic chamber in the R&D department of Aselsan Inc. is used with an azimuth over elevation positioner holding up the antenna under test, a polarization positioner holding up the standard transmitter antenna, an Agilent PNA model vector network analyzer, and HP PII series computers using programs written in HP VEE program at Aselsan and which communicate with the above listed equipment through the aid of HP-IB's .Antenna measurement set up in anechoic chamber is shown in Figure A.2.

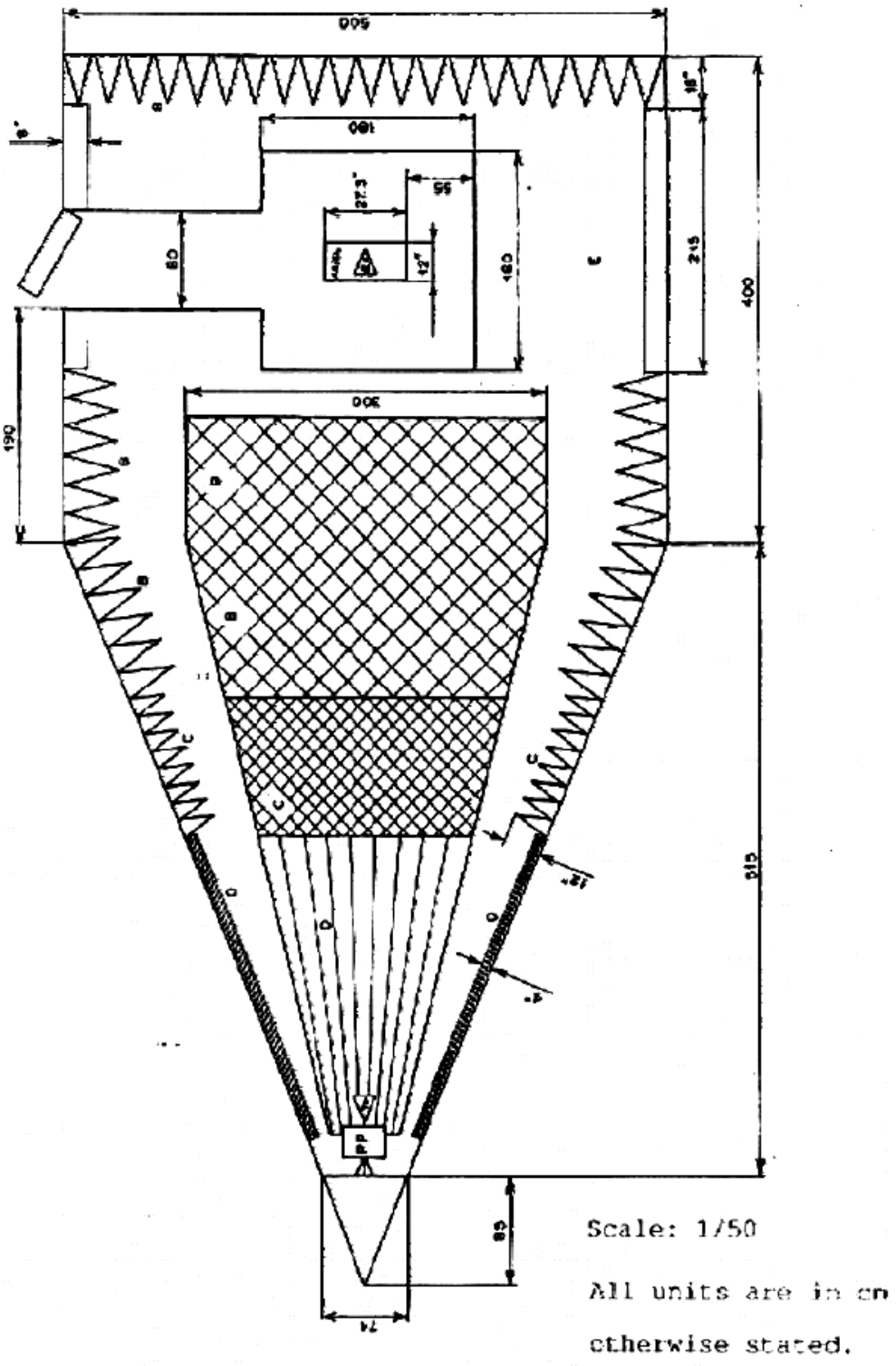

Figure A.1 Top view of the Tapered Anechoic Chamber in Aselsan Inc

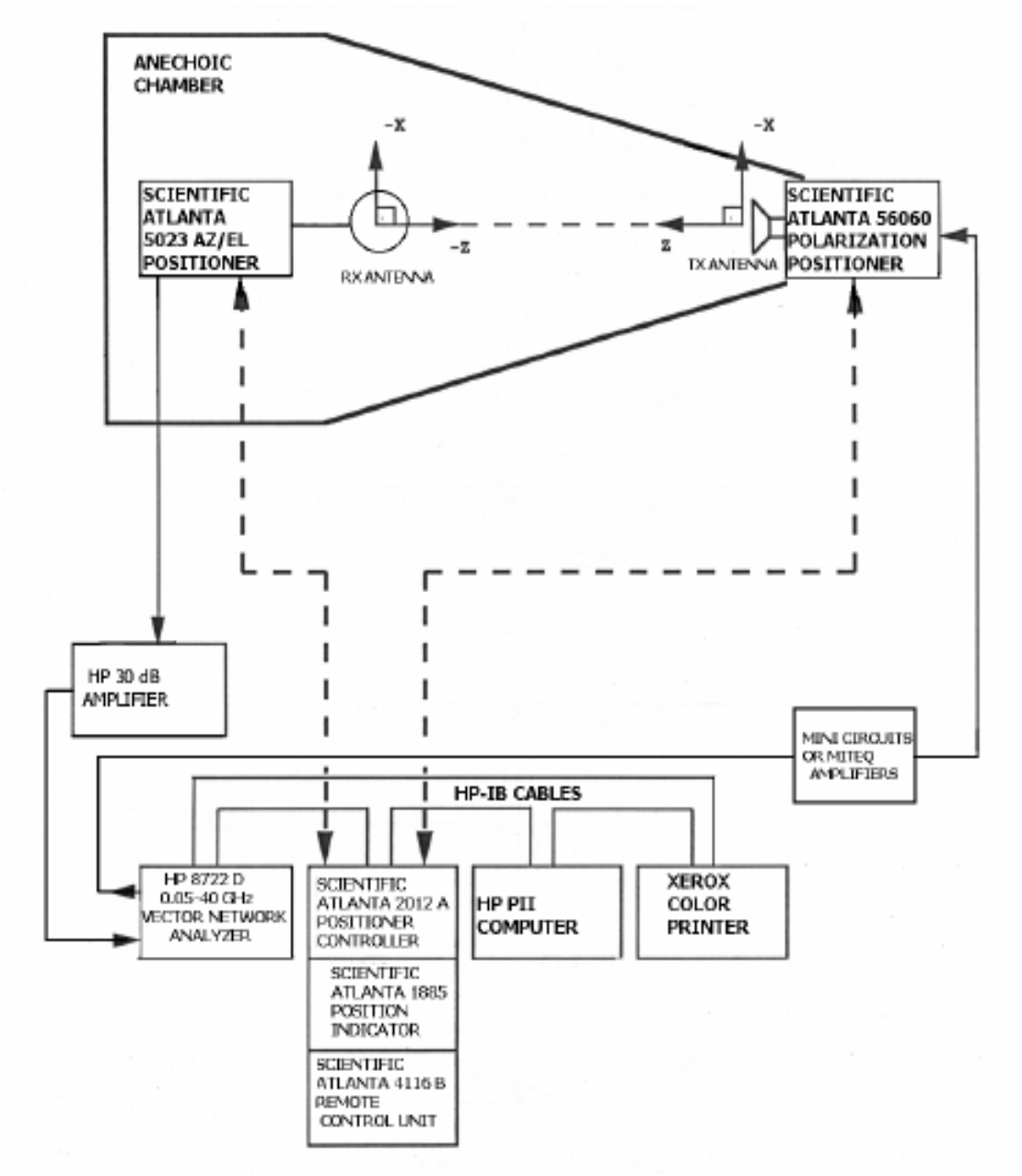

Figure A.2 Antenna Measurement Setup in Anechoic Chamber